

**Publication No. R78-18**

**Order No. 604**

**PB 284 507**

**Evaluation of Seismic Safety of Buildings**

**Report No. 12**

**ON INELASTIC RESPONSE SPECTRA  
FOR ASEISMIC DESIGN**

**by**

**SHIH-SHENG PAUL LAI**

**Supervised by**

**John M. Biggs**

**and**

**Erik H. Vanmarcke**

**July 1978**

**Sponsored by**

**National Science Foundation**

**Division of Advanced Environmental Research**

**and Technology**

**Grant ENV 76-19021**

**MIT**

**DEPARTMENT**

**OF**

**CIVIL**

**ENGINEERING**



**SCHOOL OF ENGINEERING**

**MASSACHUSETTS INSTITUTE OF TECHNOLOGY**

**Cambridge, Massachusetts 02139**

Additional Copies May Be Obtained from:

National Technical Information Service

U. S. Department of Commerce

5285 Port Royal Road

Springfield, Virginia 22161

BIBLIOGRAPHIC DATA SHEET		1. Report No. MIT-CE-R78-18	2.	3. Recipient's Accession No. 507
4. Title and Subtitle ON INELASTIC RESPONSE SPECTRA FOR ASEISMIC DESIGN (Evaluation of Seismic Safety of Buildings)				5. Report Date July 1978
7. Author(s) Shih-sheng Paul Lai, supervised by Erik H. Vanmarcke and John M. Biggs				6.
8. Performing Organization Name and Address Massachusetts Institute of Technology Dept. of Civil Engineering 77 Massachusetts Avenue Cambridge, Massachusetts 02139				8. Performing Organization Report No. R78-18; #604
9. Sponsoring Organization Name and Address National Science Foundation 1800 "G" Street, N.W. Washington, D.C. 20550				10. Project/Task/Work Unit No.
11. Contract/Grant No. NSF ENV 76-19021				13. Type of Report & Period Covered Research; 9/76 to present.
12. Supplementary Notes This is report No. 12 in a series began under NSF Grant ATA 74-06935.				14.
16. Abstracts The sources of variability in inelastic response spectra, namely, strong ground motion duration, ductility level, and viscous damping ratio, are investigated. From time history analysis, it is concluded that the Newmark inelastic response spectrum for elasto-plastic systems are unconservative for 5% damping, and conservative for 2% damping. By comparing the "inelastic response ratios," new inelastic response spectra are proposed. Based upon simulation studies, semi-empirical modifications to an elasto-plastic random vibration model are suggested. The resulting probabilistic predictions of the inelastic response are quite compatible with those obtained by time history analysis. Three steel moment-resisting frames are analyzed to assess the validity of the modal analysis-based inelastic frame design procedure. The results indicate that this design procedure of using the proposed inelastic response spectra yields better frame designs than those based upon the Newmark spectra. However, the procedure results in conservative design for interior columns and girders, and unconservative design for upper story exterior columns.				
17. Key Words and Document Analysis. 17a. Descriptors Aseismic Design. Earthquake Engineering. Dynamic Analysis. Frame Design. Inelastic Response Spectrum, Inelastic Response Ratio, Modal Analysis, Random Vibration, Steel Moment-Resisting Frame, Structural Frame, Shear Beam, Time History Analysis.				
17b. Identifiers/Open-Ended Terms				
17c. COSATI Field/Group 1313 Structural Engineering; 1302 Civil Engineering				
18. Availability Statement Release Unlimited		19. Security Class (This Report) UNCLASSIFIED		21. No. of Pages 155
1a		20. Security Class (This Page) UNCLASSIFIED		22. Price PCAP8 / MF / AD1



Massachusetts Institute of Technology  
Department of Civil Engineering  
Constructed Facilities Division  
Cambridge, Massachusetts 02139

Evaluation of Seismic Safety of Buildings

Report No. 12

ON INELASTIC RESPONSE SPECTRA  
FOR SEISMIC DESIGN

by

SHIH-SHENG PAUL LAI

Supervised by

John M. Biggs  
and  
Erik H. Vanmarcke

July 1978

Sponsored by National Science Foundation  
Division of Advanced Environmental Research  
And Technology. Grant ENV 76-19021



ABSTRACT

Sets of duration-dependent artificial strong ground motions are used to investigate the sources of variability in inelastic response spectra, namely, strong ground motion duration, ductility level, and viscous damping ratio. From time history analysis, it is concluded that the Newmark inelastic response spectra for elasto-plastic systems are unconservative for 5% damping, and conservative for 2% damping. By comparing the "inelastic response ratios," new inelastic response spectra are proposed for different ductility factors and damping ratios.

Based upon simulation studies, semi-empirical modifications to an elasto-plastic random vibration model are suggested. The resulting probabilistic predictions of the inelastic responses are quite compatible with those obtained by the time history analysis.

Three steel moment-resisting frames are analyzed to assess the validity of the modal analysis-based inelastic frame design procedure. The results indicate that this design procedure, based upon modal analysis using the proposed inelastic acceleration response spectrum, yields better frame designs than those based upon the Newmark inelastic spectrum. However, the procedure results in conservative design for interior columns and girders, and unconservative design for upper story exterior columns.

The results also indicate that the maximum story displacement predicted directly by the SRSS modal analysis using the inelastic displacement response spectrum is too conservative. The conservatism is more pronounced at top stories.



PREFACE

This is the twelfth report prepared under the research project entitled "Evaluation of Seismic Safety of Buildings," supported by National Science Foundation Grant ATA 74-06935 and its continuation Grant ENV 76-19021. This report is derived from a thesis written by Shih-sheng Paul Lai in partial fulfillment of the requirements for the degree of Master of Science in the Department of Civil Engineering at the Massachusetts Institute of Technology.

The purpose of the supporting project is to evaluate the effectiveness of the total seismic design process, which consists of steps beginning with seismic risk analysis through dynamic analysis and the design of structural components. The project seeks to answer the question: "Given a set of procedures for these steps, what is the actual degree of protection against earthquake damage provided?" Alternative methods of analysis and design are being considered. Specifically, these alternatives are built around three methods of dynamic analysis: (1) time-history analysis, (2) response spectrum modal analysis, and (3) random vibration analysis.

The formal reports produced thus far are:

1. Arnold, Peter, Vanmarcke, Erik H., and Gazetas, George, "Frequency Content of Ground Motions during the 1971 San Fernando Earthquake," M.I.T. Department of Civil Engineering Research Report R76-3, Order No. 526, January 1976.
2. Gasparini, Dario, and Vanmarcke, Erik H., "Simulated Earthquake Motion Compatible with Prescribed Response Spectra," M.I.T. Department of Civil Engineering Research Report R76-4, Order No. 527, January 1976.
3. Vanmarcke, Erik H., Biggs, J.M., Frank, Robert, Gazetas, George, Arnold, Peter, Gasparini, Dario A., and Luyties, William, "Comparison of Seismic Analysis Procedures for Elastic Multi-degree Systems," M.I.T. Department of Civil Engineering Research Report R76-5, Order No. 528, January 1976.
4. Frank, Robert, Anagnostopoulos, Stavros, Biggs, J.M., and Vanmarcke, Erik H., "Variability of Inelastic Structural Response Due to Real and Artificial Ground Motions," M.I.T. Department of Civil Engineering Research Report R76-6, Order No. 529, January 1976.

5. Haviland, Richard, "A Study of the Uncertainties in the Fundamental Translational Periods and Damping Values for Real Buildings," Supervised by Professors J.M. Biggs and Erik H. Vanmarcke, M.I.T. Department of Civil Engineering Research Report R76-12, Order No. 531, February 1976.
6. Luyties, William H. III, Anagnostopoulos, Stavros, and Biggs, John M., "Studies on the Inelastic Dynamic Analysis and Design of Multi-Story Frames," M.I.T. Department of Civil Engineering Research Report R76-29, Order No. 548, July 1976.
7. Gazetas, George, "Random Vibration Analysis of Inelastic Multi-Degree-of-Freedom Systems Subjected to Earthquake Ground Motions," Supervised by Professor Erik H. Vanmarcke, M.I.T. Department of Civil Engineering Research Report R76-39, Order No. 556, August 1976.
8. Haviland, Richard W., Biggs, John M., and Anagnostopoulos, Stavros A., "Inelastic Response Spectrum Design Procedures for Steel Frames," M.I.T. Department of Civil Engineering Research Report R76-40, Order No. 557, September 1976.
9. Gasparini, Dario A., "On the Safety Provided by Alternate Seismic Design Methods," Supervised by Professors J. M. Biggs and Erik H. Vanmarcke, M.I.T. Department of Civil Engineering Research Report R77-22, Order No. 573, July 1977.
10. Vanmarcke, Erik H., and Lai, Shih-sheng Paul, "Strong Motion Duration of Earthquakes," M.I.T. Department of Civil Engineering Research Report R77-16, Order No. 569, July 1977.
11. Robinson, James H. Jr., "Inelastic Dynamic Design of Steel Frames to Resist Seismic Loads," Supervised by Professors J. M. Biggs and Erik H. Vanmarcke, M.I.T. Department of Civil Engineering Research Report R77-23, Order No. 574, July 1977.

The project is supervised by Professors John M. Biggs and Erik H. Vanmarcke of the Civil Engineering Department. They have been assisted by Dr. Stavros Anagnostopoulos, a Research Associate in the Department. Research assistants, in addition to Mr. Lai, who contributed to the work reported herein were Peter Arnold, Robert Frank, William Luyties, Dario Gasparini, Richard Haviland, George Gazetas, James Robinson, and Ricardo Binder.

## TABLE OF CONTENTS

	Page
Title Page	1
Abstract	2
Preface	3
Table of Contents	5
List of Figures	8
List of Tables	11
CHAPTER 1 - INTRODUCTION	12
1.1 SCOPE	12
1.2 OUTLINE OF THESIS	14
CHAPTER 2 - MODELS FOR INELASTIC RESPONSE ANALYSIS (SDOF)	16
2.1 INTRODUCTION	16
2.2 TIME HISTORY ANALYSIS OF SDOF SYSTEMS	17
2.2.1 Basic Model Descriptions	17
2.2.2 Overshooting	20
2.3 RANDOM VIBRATION ANALYSIS OF SDOF SYSTEMS	21
2.3.1 Background	21
2.3.2 Statistical Parameters of Elastic Systems	22
2.3.3 Elasto-Plastic Random Vibration Model	25
2.4 SUMMARY	30
CHAPTER 3 - INELASTIC RESPONSE SPECTRA BASED ON TIME HISTORY ANALYSIS	32
3.1 INTRODUCTION	32
3.2 GENERATION OF ARTIFICIAL MOTIONS	35
3.3 EFFECTS OF STRONG GROUND MOTION DURATION	37
3.3.1 Effects on Inelastic Response Spectra	37
3.3.2 Cumulative Yielding Ductility	42

	Page
3.4 INELASTIC RESPONSE RATIOS	46
3.4.1 Definition	46
3.4.2 Results for 5% Damping	49
3.4.3 Results for 2% Damping	53
3.5 RESULTS BASED ON REAL STRONG GROUND MOTIONS	58
3.6 PROPOSED INELASTIC RESPONSE SPECTRA	62
3.6.1 5% Damping	62
3.6.2 2% Damping	72
3.7 SUMMARY	80
CHAPTER 4 - INELASTIC RESPONSE PREDICTED BY RANDOM VIBRATION	82
4.1 INTRODUCTION	82
4.2 MODIFICATIONS OF RANDOM VIBRATION MODEL	83
4.2.1 Transient Effect	83
4.2.2 Expected Inelastic Peak Displacement	85
4.3 RESULTING INELASTIC RESPONSE RATIOS	89
4.4 CONCLUSION	92
CHAPTER 5 - INELASTIC RESPONSE OF STRUCTURAL FRAMES	95
5.1 INTRODUCTION	95
5.2 INELASTIC RESPONSE OF SIMPLE SHEAR BEAM MODEL	97
5.2.1 Simple Shear Beam Model	97
5.2.2 Resulting Story Ductility and Displacement Distributions	99
5.3 DESCRIPTION OF BUILDING FRAMES INVESTIGATED	103
5.3.1 Basic Frames	103
5.3.2 Determination of Member Strength	108

	Page
5.4 INELASTIC DYNAMIC ANALYSIS FOR FRAMES	109
5.4.1 Program FRIEDA	109
5.4.2 Ductility Measures	110
5.5 RESULTS OF INELASTIC DYNAMIC ANALYSIS FOR FRAMES	117
5.5.1 Ductility Distribution	117
5.5.1.1 4-story Frame	118
5.5.1.2 10-story Frame	121
5.5.1.3 16-story Frame	127
5.5.1.4 Summary	130
5.5.2 MAXIMUM STORY DISPLACEMENT	130
5.5.2.1 4-story Frame	131
5.5.2.2 10-story Frame	133
5.5.2.3 16-story Frame	133
5.5.2.4 Summary	136
5.6 CONCLUSION	137
CHAPTER 6 - CONCLUSIONS AND RECOMMENDATIONS	139
6.1 Conclusions	139
6.2 Recommendations for Further Research	141
References	143
Appendix	146



## LIST OF FIGURES

FIGURE NO.	TITLE	PAGE
2.1	Basic Damped Mass - Spring System	18
2.2	Elasto-Plastic Force-Deformation Relationship	18
2.3	Energy Conversion for Overshooting	21
2.4	Typical Elastic Response Exceeding Threshold $\pm a$	24
2.5	Typical Elasto-Plastic Response	27
2.6	Up-Crossing of Barrier Level $d$ for Plastic Set	29
3.1	Newmark Elastic and Inelastic Response Spectra (5% Damping, $\mu = 5$ )	33
3.2	Intensity Envelopes for Artificial Strong Ground Motions	36
3.3	Typical Elastic Response of Artificial Ground Motion ( $\zeta = 0.05$ )	38
3.4	Mean Inelastic Displacement Responses for Different Strong Ground Motion Durations ( $\mu=5$ , $\zeta=0.05$ )	40
3.5	Mean Inelastic Acceleration Responses for Different Strong Ground Motion Durations ( $\mu=5$ , $\zeta=0.05$ )	41
3.6	Time Histories for Permanent Sets, Ductility Factors, Cumulative Yielding Ductilities ( $T=0.223, 1.048$ secs)	44
3.7	Newmark Inelastic Response Ratios for Acceleration (5% Damping)	47
3.8	Newmark Inelastic Response Ratios for Displacement (5% Damping)	48
3.9	Mean Inelastic Response Ratios for Acceleration (5% Damping)	51
3.10	Mean Inelastic Response Ratios for Displacement (5% Damping)	52
3.11	Newmark Inelastic Response Ratios for Acceleration (2% Damping)	54
3.12	Mean Inelastic Response Ratios for Acceleration (2% Damping)	56
3.13	Mean Inelastic Response Ratios for Displacement (2% Damping)	57
3.14	Mean Inelastic Response Ratios for Acceleration of Real Ground Motions (5% Damping)	60
3.15	Mean Inelastic Response Ratios for Displacement of Real Ground Motions (5% Damping)	61

FIGURE NO.	TITLE	PAGE
3.16	Proposed Inelastic Response Ratios for Acceleration (5% Damping)	63
3.17	Proposed Inelastic Response Ratios for Acceleration at Control Points (5% Damping)	64
3.18	Proposed Inelastic Response Ratios for Displacement (5% Damping)	66
3.19	Proposed Inelastic Response Ratios for Displacement at Control Points (5% Damping)	67
3.20	Proposed Inelastic Response Spectra (5% Damping, $\mu=2$ )	69
3.21	Proposed Inelastic Response Spectra (5% Damping, $\mu=4$ )	70
3.22	Proposed Inelastic Response Spectra (5% Damping, $\mu=5$ )	71
3.23	Proposed Inelastic Response Ratios for Acceleration (2% Damping)	73
3.24	Proposed Inelastic Response Ratios for Acceleration at Control Points (2% Damping)	74
3.25	Proposed Inelastic Response Ratios for Displacement (2% Damping)	76
3.26	Proposed Inelastic Response Ratios for Displacement at Control Points (2% Damping)	77
3.27	Proposed Inelastic Response Spectra (2% Damping, $\mu=2$ )	78
3.28	Proposed Inelastic Response Spectra (2% Damping, $\mu=5$ )	79
4.1	Power Spectral Density Functions for S=10,20,30,40 seconds	84
4.2	Comparison of Simulated and Theoretical Values for Average Amount of Inelastic Displacement Versus Threshold Levels $r$	87
4.3	Comparison of Simulated and Theoretical Values for $\delta^*/\sigma_y$ Versus Threshold Levels $r$	88
4.4	Inelastic Response Ratios for Displacement Predicted by Random Vibration ( $\zeta=0.05$ , S=20)	90
4.5	Relationship between Inelastic Response Ratios for Displacement and Acceleration	91
4.6	Inelastic Response Ratios for Acceleration Predicted by Random Vibration ( $\zeta=0.05$ , S=20)	93
5.1	Simple Shear Beam Model	98
5.2	Ductility Distributions for Simple Shear Beam Model	100
5.3	Maximum Relative Displacements of Simple Shear Beam Model ( $\zeta=0.05$ )	102

FIGURE NO.	TITLE	PAGE
5.4	4-story Building Plan	105
5.5	4-story Building Elevation (Redrawn from Ref. 18)	105
5.6	10-story Building Elevation (Redrawn from Ref. 18)	106
5.7	16-story Building Elevation (Redrawn from Ref. 18)	107
5.8	Definition for Rotation Ductility	112
5.9	Definition for Moment Ductility	112
5.10	Moment-Deformation Relationship for Columns	114
5.11	Maximum Ductility Factors for 4-story Building (Proposed Spectra, $\zeta=0.05$ )	119
5.12	Maximum Ductility Factors for 4-story Building (Newmark, $\zeta=0.05$ )	120
5.13	Maximum Column Ductility Factors for 10-story Building (Proposed Spectra, $\zeta=0.05$ )	123
5.14	Maximum Girder Ductility Factors for 10-story Building (Proposed Spectra, $\zeta=0.05$ )	124
5.15	Maximum Column Ductility Factors for 10-story Building (Newmark, $\zeta=0.05$ )	125
5.16	Maximum Girder Ductility Factors for 10-story Building (Newmark, $\zeta=0.05$ )	126
5.17	Maximum Column Ductility Factors for 16-story Building (Proposed Spectra, $\zeta=0.05$ )	128
5.18	Maximum Girder Ductility Factors for 16-story Building (Proposed Spectra, $\zeta=0.05$ )	129
5.19	Maximum Relative Story Displacements for 4-story Building	132
5.20	Maximum Relative Story Displacements for 10-story Building	134
5.21	Maximum Relative Story Displacements for 16-story Building	135

## LIST OF TABLES

TABLE NO.	DESCRIPTION	PAGE
3-1	Ductility Factors for Different Motion Durations	43
3-2	Seismic Parameters for the Set of Real Strong Ground Motions	59
3-3	Proposed Inelastic Response Ratios at Control Periods (5% Damping)	65
3-4	Proposed Inelastic Response Ratios at Control Periods (2% Damping)	75
5-1	Properties of the Simple Shear Beam Model	98
5-2	Rotational Ductilities vs. Moment Ductilities for 10-story Building	116
A-1	Modal Properties of Simple Shear Beam Model	147
A-2	Modal Properties of 4-story Frame	148
A-3	Modal Properties of 10-story Frame	148
A-4	Modal Properties of 16-story Frame	149
A-5	Moment Capacities for 4-story Frame (Proposed Spectra)	150
A-6	Moment Capacities for 10-story Frame (Proposed Spectra)	150
A-7	Moment Capacities for 16-story Frame (Proposed Spectra)	151
A-8	Moment Capacities for 4-story Frame (Newmark Spectra)	152
A-9	Moment Capacities for 10-story Frame (Newmark Spectra)	152

# CHAPTER 1

## INTRODUCTION

### 1.1 SCOPE

In aseismic engineering, it is often impractical, or at least uneconomical, to design a structure so that it will remain completely elastic. For years, researchers and designers have been trying to model the nonlinear behavior of structures. Various methods of differing complexity have been developed for the structural dynamic analysis. There are three main approaches currently used for seismic dynamic analysis, namely: a) time history analysis, b) random vibration analysis, and c) response-spectra-based modal analysis.

The time history analysis involves step-by-step time integration of the system motion equations for an ensemble of ground-motion accelerograms. Although the method is generally applicable, it is too expensive and time-consuming to be attractive for practical design. The random vibration analysis treats the earthquake ground motions as random processes. Based on random vibration theory, the probabilistic structural response can be directly predicted. Unfortunately, an exact random vibration solution for inelastic systems has not yet been derived. Hence the application of random vibration analysis to practical design has been limited.

The response-spectra-based modal analysis is considered by many to be the most practical approach. The structural response is computed for each normal mode of vibration. The total response is obtained by superimposing the responses of the contributing modes. Due to the use of modal superposition, the method is theoretically strictly limited to linear-elastic systems. However, because of its straightforward nature, the inelastic response-spectra-based modal analysis has been considered a potential method for inelastic structural design.

Studies (3, 12, 15, 18, 19) have been conducted to investigate the adequacy of this inelastic design procedure which is based on the modal analysis using inelastic response spectra. The general conclusion was that the inelastic design procedure would yield unconservative design. The unconservatism might come from the modal analysis itself, or the inelastic response spectrum used, the determination of member strength, the strong ground motion used for time history analyses, etc.

In this study, based on the widely accepted Newmark-Hall basic design spectrum (17), sets of strong ground motion duration-dependent artificial motions were generated. Inelastic response spectra of maximum absolute acceleration and maximum relative displacement were computed by the time history analyses using the sets of motions. Hence, the variabilities of inelastic response spectra on strong ground motion duration, ductility level, damping ratio, etc. were investigated. New inelastic response spectra for 2% and 5% damped elasto-plastic systems were proposed. Then the validities of the inelastic response-spectra-based inelastic design procedure were assessed. Also in this study the random vibration predictions of the inelastic response were evaluated. Based on the simula-

tion studies, the random vibration analysis was modified for single-degree-of-freedom elasto-plastic systems.

## 1.2 OUTLINE OF THESIS

Brief descriptions of the time history analysis for elasto-plastic single-degree-of-freedom (SDOF) systems are presented in Chapter 2. Background introductions of the random vibration model used in this study are also included.

In Chapter 3, the widely accepted Newmark approach of constructing inelastic response spectra from the elastic spectrum is presented. Brief descriptions of the input parameters for the generation of artificial motions are also included. This is followed by discussions on the effects of strong ground motion duration on the elasto-plastic SDOF responses. Inelastic response ratios are defined next. The results of elasto-plastic responses by time history analyses are presented in terms of the inelastic response ratios. These are compared with the results predicted by the Newmark approach. The results of inelastic responses based on a set of real ground motions are also reported and compared. Finally, inelastic response ratios for 5% and 2% damped elasto-plastic systems are proposed. The corresponding inelastic response spectra are presented.

Chapter 4 contains the modifications of the random vibration model used in this study. The inelastic response ratios predicted by the new random vibration model are presented.

In Chapter 5, brief descriptions of the modal analysis using the inelastic response spectrum are presented. A simple shear beam model is

tested with the new proposed inelastic response spectra. This is followed by brief descriptions of the structural frames used in this study. The inelastic-frame design procedure based on modal analysis using the inelastic-acceleration response spectrum is outlined. The method of time history inelastic dynamic analysis for frames used in this study is briefly discussed. Relationship between the rotational ductility and the moment ductility is investigated. Results of inelastic dynamic analyses for frames designed by the modal analysis using inelastic response spectra are reported and compared. Finally, conclusions drawn from the discussion in this Chapter are summarized.

Chapter 6 contains conclusions reached from this study and recommendations for further research.

# CHAPTER 2

## MODELS FOR INELASTIC RESPONSE ANALYSIS (SDOF)

### 2.1 INTRODUCTION

In this Chapter, brief descriptions of the time history analysis for elasto-plastic single-degree-of-freedom (SDOF) systems are presented. This contains the recurrence formulas, time integration scheme used, and notes on the overshooting problem. The time history model will be used to compute the inelastic responses. The resulting inelastic response spectra for acceleration and displacement are presented in Chapter 3.

Background introductions to some pertinent statistical parameters of elastic SDOF systems by random vibration analysis are also included. This is followed by detailed descriptions of the elasto-plastic random vibration model used in this study. Based on the model, the probabilistic predictions of elasto-plastic response of SDOF systems can be approximately assessed.

## 2.2 TIME HISTORY ANALYSIS OF SDOF SYSTEMS

### 2.2.1 Basic Model Descriptions

The conventional simple elasto-plastic spring-mass-dashpot system was used for the computation of single-degree-of-freedom time history response. The model consists of a mass  $M$ , an idealized elasto-plastic spring with stiffness  $K$ , and a viscous damper with damping  $C$  as shown in Fig. 2.1. The basic motion equation is:

$$M\ddot{U} + C\dot{U} + KU = -M\ddot{y}_s \quad (2-1)$$

where  $U$  = relative horizontal displacement of the mass

$\ddot{y}_s$  = horizontal ground acceleration.

Step-by-step time integration of the differential motion equation was employed to obtain elasto-plastic response. Anagnostopoulos (1), in his doctoral dissertation, compared different numerical integration schemes. He concluded that "the constant velocity method", though simple, was numerically stable for the computations of structural response. The only restriction was that the integration time interval should be kept below  $1/5 - 1/10$  of the natural period of the system. Since the shortest natural period of interest was 0.1 sec, 0.02sec has been selected as the integration time interval in this study.

The fundamental recurrence formulas for the constant velocity method of time integration are: (Biggs, 5):

$$\dot{U}^{(s)} = \frac{U^{(s+1)} - U^{(s-1)}}{2\Delta t} \quad (2-2)$$

$$\ddot{U}^{(s)} = \frac{1}{\Delta t^2} (U^{(s+1)} - 2U^{(s)} + U^{(s-1)}) \quad (2-3)$$

where superscript  $s$  represents time step  $s$ .

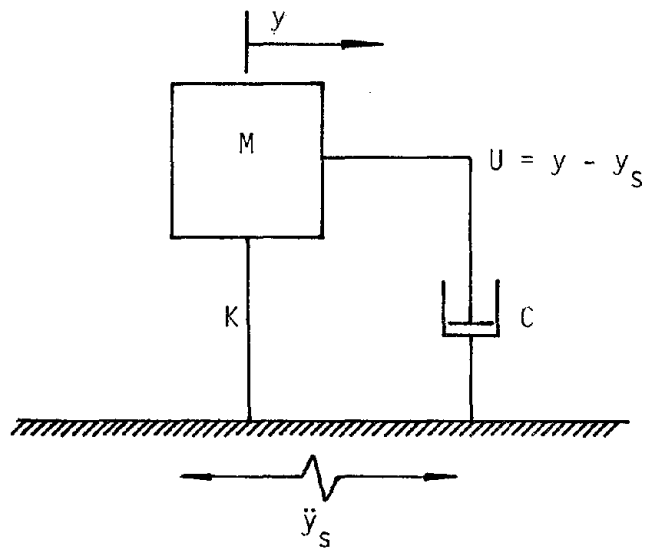


FIG. 2.1 - BASIC DAMPED MASS-SPRING SYSTEM

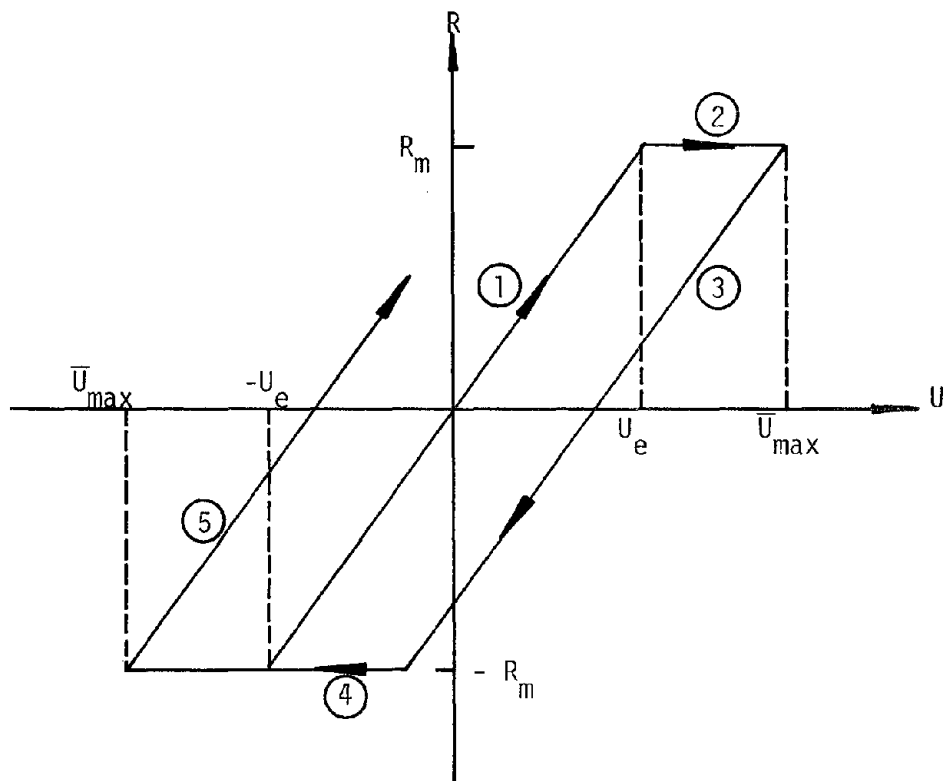


FIG. 2.2 - ELASTO-PLASTIC FORCE-DEFORMATION RELATIONSHIP

The well-known force-deformation relationship for elasto-plastic systems is shown in Fig. 2.2. Yielding behavior can be modelled for five stages. Relative acceleration of time step  $s$  for each of the stages can be expressed as a function of relative displacements in time step  $s$  and  $s-1$  as follows:

a) stage 1 - elastic

$$\ddot{U}(s) = \frac{-M\ddot{y}_s^{(s)} - KU(s) - C(U(s) - U^{(s-1)})/\Delta t}{M + C \Delta t/2} \quad (2-4-a)$$

b) stage 2 - positive plastic

$$\ddot{U}(s) = \frac{-M\ddot{y}_s^{(s)} - R_m - C(U(s) - U^{(s-1)})/\Delta t}{M + C \Delta t/2} \quad (2-4-b)$$

c) stage 3 - positive rebound

$$\ddot{U}(s) = \frac{-M\ddot{y}_s^{(s)} - R_m + K(\bar{U}_{\max} - U(s)) - C(U(s) - U^{(s-1)})/\Delta t}{M + C \Delta t/2} \quad (2-4-c)$$

d) stage 4 - negative plastic

$$\ddot{U}(s) = \frac{-M\ddot{y}_s^{(s)} + R_m - C(U(s) - U^{(s-1)})/\Delta t}{M + C \Delta t/2} \quad (2-4-d)$$

e) stage 5 - negative rebound

$$\ddot{U}(s) = \frac{-M\ddot{y}_s^{(s)} + R_m + K(\bar{U}_{\max} - U(s)) - C(U(s) - U^{(s-1)})/\Delta t}{M + C \Delta t/2} \quad (2-4-e)$$

where  $\bar{U}_{\max}$  is the maximum relative displacement when the elasto-plastic system starts to rebound as shown in Fig. 2.2.

### 2.2.2 Overshooting

Due to the finite small time interval, the problem of overshooting will always arise during time integration. This means that when the elasto-plastic system starts to yield, the computed spring force will exceed the maximum resisting force  $R_m$  of the spring. The amount of this overshoot resisting force is  $(U_2 - U_1)K$ , as shown in Fig. 2.3.

Several approaches have been proposed to improve the overshooting problem. The usual way is to decrease the integration time interval. However, this is very expensive to implement. Luyties et al. (15) suggested that to balance the overshoot deformation, an input force be applied to the system in the next time step.

In this study, a new simple scheme has been implemented. The correcting scheme is based on the argument that the strain energy due to elastic action when the resisting force in the spring exceeds  $R_m$  should be dissipated by inelastic deformation  $\Delta U$ . As shown in Fig. 2.3:

$$\frac{1}{2} (U_2 - U_1)^2 \cdot K = R_m \Delta U .$$

Therefore:

$$\Delta U = \frac{(U_2 - U_1)^2}{2U_e} \quad (2-5)$$

$$U_3 = U_2 + \Delta U$$

where  $U_e$  = yielding displacement of the elasto-plastic system

$U_2$  = uncorrected displacement

$U_3$  = corrected displacement.

Numerical examples have been tested for this correcting scheme. The results are quite compatible with those obtained by reducing time integration intervals. Hence, it can be concluded that the new approach to improving the overshooting problem is quite satisfactory.

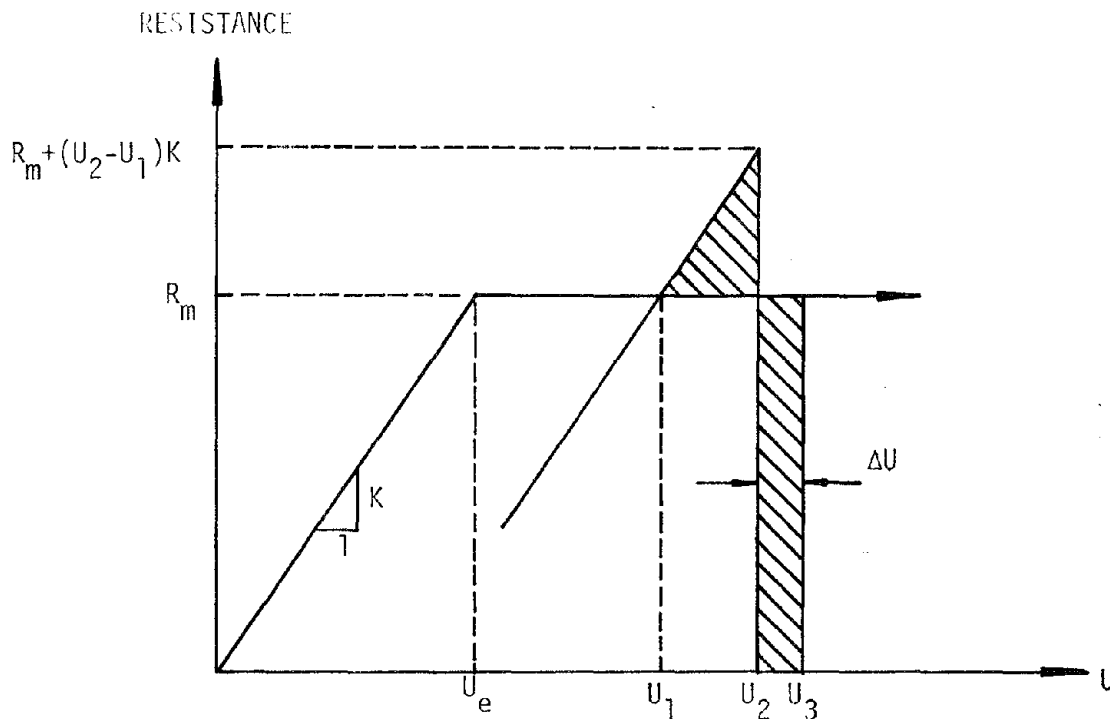


FIG. 2.3 - ENERGY CONVERSION FOR OVERSHOOTING

## 2.3 RANDOM VIBRATION ANALYSIS OF SDOF SYSTEMS

### 2.3.1 Background

As mentioned in Chapter 1, time history analysis is generally too expensive to implement. Besides, one does not grasp the statistical sense of structural behavior. In view of the fact that a seismic activity is indeed a random phenomenon, the random vibration analysis seems to be a more desirable approach.

Unfortunately, to the author's knowledge, exact random vibration solution of elasto-plastic single-degree-of-freedom oscillating systems has not been derived. Several approximate approaches for small inelastic deformations have been suggested. But most of the models are extremely difficult to incorporate. Vanmarcke and Veneziano (24) suggested

an approximate stochastic model for inelastic response of elasto-plastic oscillators. The mean, variance, and probability distribution of the inelastic response can be approximately predicted by the model.

In this section, brief descriptions of the statistical parameters of a simple linear elastic oscillating system are presented. This is followed by detailed discussions of the elasto-plastic model proposed by Vanmarcke et al., which was used in this study.

### 2.3.2 Statistical Parameters of Elastic Systems

It is a well-known fact that strong ground motion--in fact, any periodic function, can be expressed in terms of a series of sinusoidal waves as follows:

$$X(t) = \sum_{i=1}^n A_i \sin(\omega_i t + \phi_i) \quad (2-6)$$

where  $A_i$  is the amplitude and  $\phi_i$  is the phase angle of the  $i^{\text{th}}$  contributing sinusoid with frequency  $\omega_i$ . The power spectral density function (PSD),  $G_x(\omega)$ , which reveals the information of relative importance of sinusoids, is defined as:

$$G_x(\omega_i)\Delta\omega = A_i^2/2 \quad (2-7)$$

From random vibration theory (Crandall and Mark, 8), when a linear elastic system is subjected to a stochastic ground motion, the spectral density function of relative displacement  $G_y(\omega)$  can be directly expressed in terms of the input PSD as follows:

$$G_y(\omega) = |H(\omega)|^2 G_x(\omega) \quad (2-8)$$

$$|H(\omega)|^2 = \frac{1}{(\omega^2 - \omega_n^2)^2 - 4\zeta^2 \omega_n^2 \omega^2}$$

where  $H(\omega)$  is the so-called "transfer function," and  $\zeta$  is the damping ratio of the system. The variance of the response,  $\sigma_y^2$ , equals the total area under  $G_y(\omega)$ ;

$$\sigma_y^2 = \int_0^{\infty} G_y(\omega) d\omega = \int_0^{\infty} G_x(\omega) |H(\omega)|^2 d\omega \quad (2-9)$$

Vanmarcke (22) has derived an approximate formula for  $\sigma_y^2$ :

$$\begin{aligned} \sigma_y^2 &= \int_0^{\infty} G_x(\omega) |H(\omega)|^2 d\omega \\ &\approx \frac{G_y(\omega_n)}{\omega_n^3} \left( \frac{\pi}{4\zeta} - 1 \right) + \frac{1}{\omega_n^4} \int_0^{\omega_n} G_y(\omega) d\omega \end{aligned} \quad (2-10)$$

The moment of the PSD, i.e.,  $\lambda_1$ , and the bandwidth measure  $q$  can also be evaluated:

$$\lambda_1 = \int_0^{\infty} \omega^1 G_y(\omega) d\omega \quad (2-11)$$

$$q = \sqrt{1 - \lambda_1^2 / \lambda_0 \lambda_2} \quad (2-12)$$

Fig. 2.4 shows a typical elastic response of a lightly damped linear-elastic system subjected to zero-mean stationary random process of ground shaking. It has been observed that the exceedances of a given level of threshold  $\pm a$  tend to arrive in clumps. (Karnopp and Scharon, 13). A clump is defined as a series of barrier impacts occurring every half-cycle of the system transient response. The observation suggests that the consecutive peaks of the response tend to be highly correlated. Hence, the expected value of the random number of successive exceedances,  $N_a$ , for response threshold  $a$  can be approximately expressed as: (Vanmarcke, 21,24)

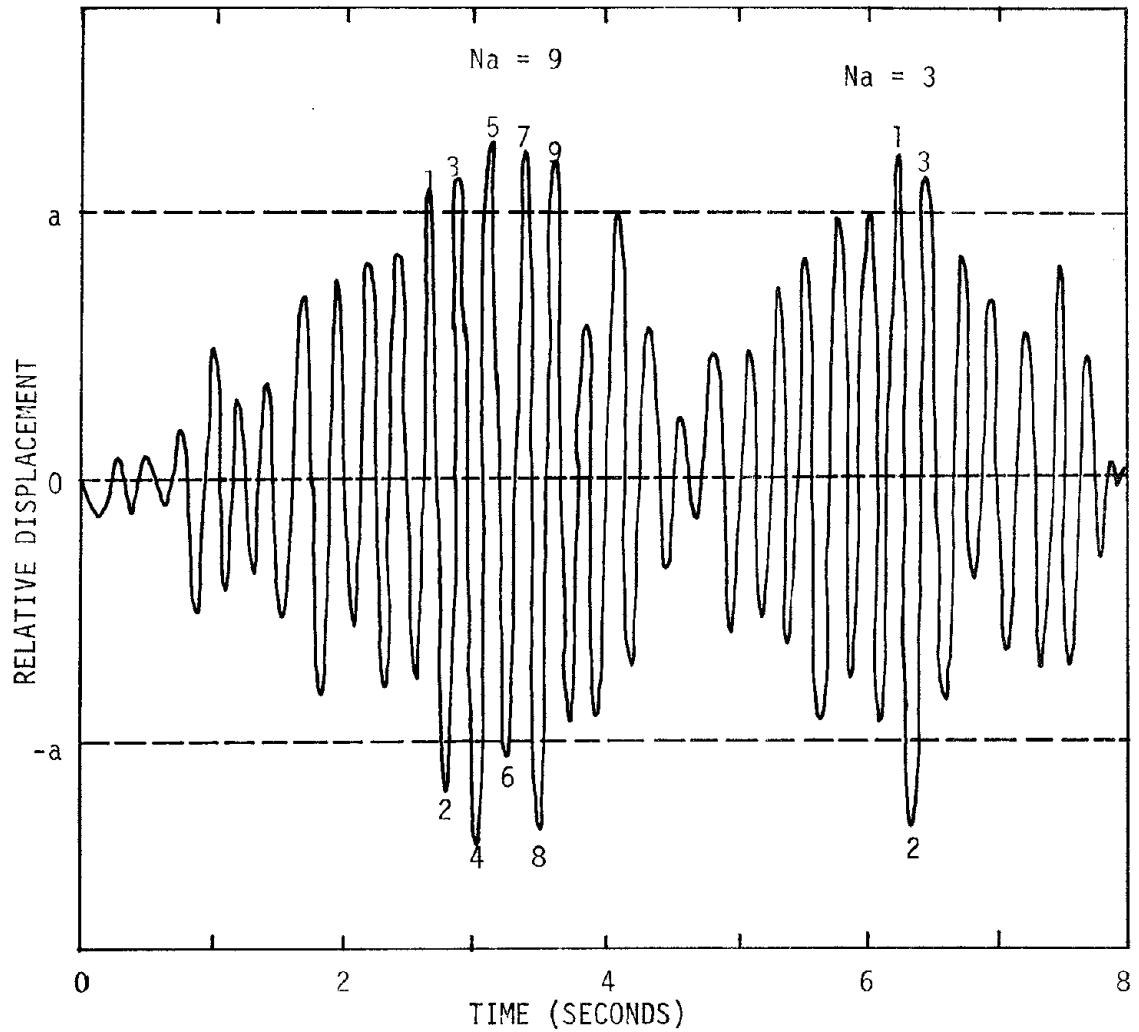


FIG. 2.4 - TYPICAL ELASTIC RESPONSE OF EXCEEDING THRESHOLD  $\pm a$

$$E[Na] = [1 - \exp(-\sqrt{\pi/2} r q)]^{-1} \quad (2-13)$$

where  $r = a/\sigma_y$  is the normalized factor of the threshold level  $a$  divided by the standard deviation of the response. As will be shown later,  $r$  is a very important parameter in predicting the inelastic response.

The mean rate of up-crossings of the response threshold  $a$ ,  $v_a$ , is expressed as follows:

$$\begin{aligned} v_a &= \frac{1}{2\pi} (\lambda_2/\lambda_0)^{1/2} \exp(-a^2/2\sigma_y^2) \\ &= v_0 \exp(-r^2/2) \end{aligned} \quad (2-14)$$

where  $v_0 = \frac{1}{2\pi}(\lambda_2/\lambda_0)^{1/2}$  = mean rate of zero crossings. The average number of clumps per unit time has been approximately derived as:

$$\begin{aligned} \mu_a &= \frac{2v_a}{E[Na][1 - \exp(-r^2/2)]} \\ &= \frac{2v_a [1 - \exp(-\sqrt{\pi/2} r q)]}{\exp(r^2/2) - 1} \end{aligned} \quad (2-15)$$

Based on the above-mentioned statistical parameters for an elastic system, detailed descriptions of the elasto-plastic random vibration model used in this study are presented next.

### 2.3.3 ELASTO-PLASTIC RANDOM VIBRATION MODEL

As shown in Fig. 2.2, the elasto-plastic SDOF system behaves linear elastically between plastic actions. Based on the work by Karnopp and Scharon (13), Vanmarcke (21) argued that the elasto-plastic response could be divided into two components: a component of permanent set and an equivalent elastic response component as illustrated in Fig. 2.5. He further suggested that the nonlinear effect could be modelled as a first threshold passage problem for the associated linear elastic system. The yielding level  $U_e$  of the elastoplastic system was taken to be the threshold response  $a$  as indicated in Fig. 2.5.c.

It has been stated previously that for elastic systems, the exceedances of a threshold tend to arrive in clumps. Vanmarcke observed that yield level crossings of the elasto-plastic response also would arrive in clumps. From simulation studies of white noise Gaussian excitations, Yanev (26) concluded that for high thresholds the rate of zero crossings  $\nu_0$  of the elasto-plastic systems should approximately remain the same as for the associated elastic systems. Hence, the time between clumps for elasto-plastic systems can be approximately assumed to have an exponential distribution with mean  $1/\nu_a$ .

Karnopp & Scharon (13) have derived the expected amount of inelastic deformation, denoted as  $\delta$  (an absolute value), for a single crossing of the yield level  $U_e$ . This was based on the principle of conservation of energies. When an elasto-plastic system starts to yield, the kinetic energy  $M\dot{U}^2/2$  will be dissipated by yielding action  $R_m D$ .  $D$  is the plastic deformation as illustrated in Fig. 2.5.b for a single excursion of the yielding deformation  $U_e$ . Hence

$$R_m D = \frac{1}{2} M \dot{U}^2$$

$$E[D] = \frac{M}{2R_m} E[\dot{U}^2] = \frac{M}{2KU_e} E[\dot{U}^2] = \frac{1}{2\omega_n^2 U_e} E[\dot{U}^2]$$

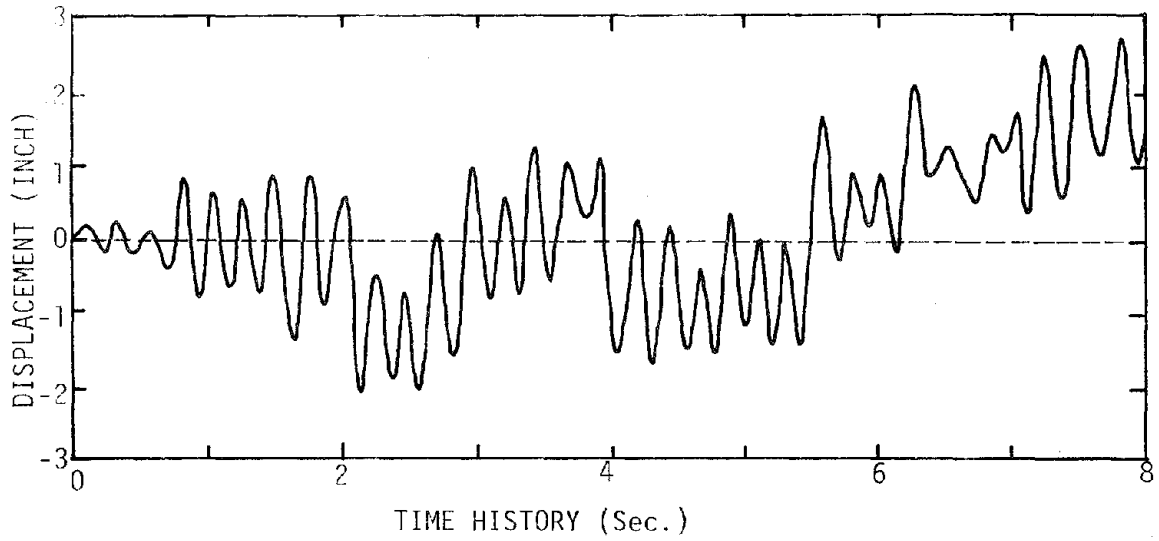
For high thresholds,  $E[\dot{U}^2]$  can be replaced by  $\omega_n^2 \sigma_y^2$  (13). This leads to:

$$E[D] = \delta = \frac{\sigma_y^2}{2U_e} = \frac{\sigma_y}{2r} \quad (2-16)$$

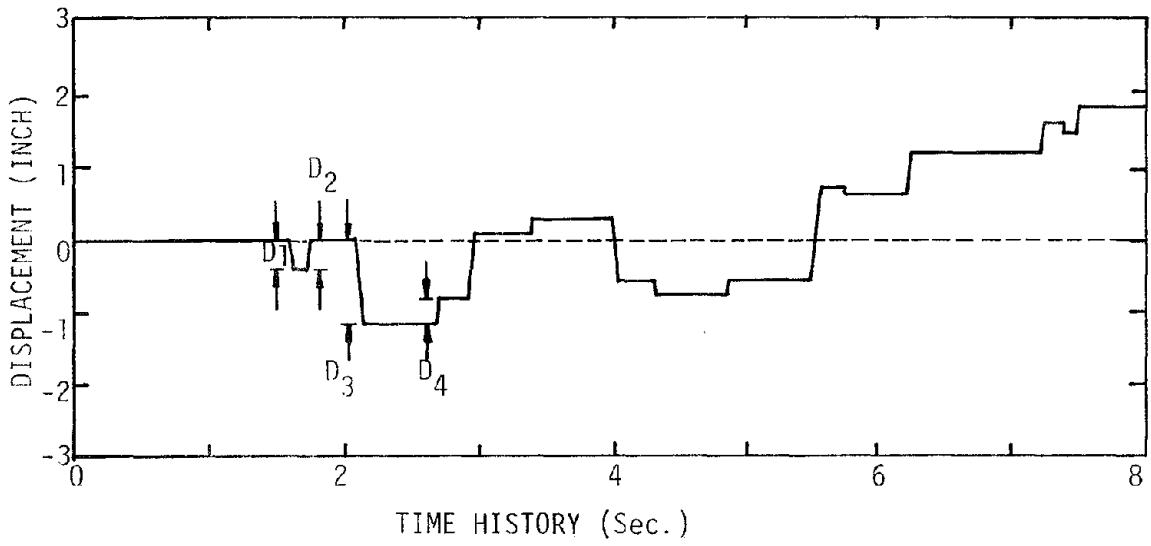
For a lower threshold,  $E[\dot{U}^2]$  may itself depend on  $r$  (11).

Hence,  $E[D] = \delta = f(r) \sigma_y$ . (2-17)

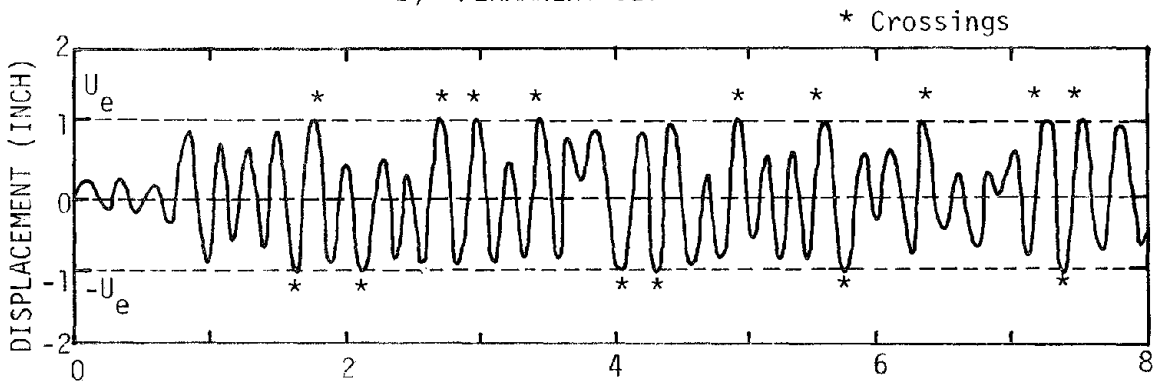
Based on simulation studies and time history analysis, a new semi-empir-



a) TOTAL ELASTO-PLASTIC DEFORMATION



b) PERMANENT SET



c) ELASTIC COMPONENT OF RESPONSE

FIG. 2.5 - TYPICAL ELASTO-PLASTIC RESPONSE

ical function of  $r$ ,  $f(r)$ , is suggested in this study and will be presented in detail in Chapter 4.

It is assumed that the random number of plastic deformation contributions has a Poisson distribution with mean  $\mu_a S$  (21, 22, 24). The probability density function for threshold  $d$  is  $f_D(d) = (2\delta)^{-1} \exp(-|d|/\delta)$ . Thus, the mean and variance for the random process of the total inelastic deformation  $D(S)$  can be expressed as follows:

$$\begin{aligned} E[D(S)] &= \mu_a S E[D_i] = 0 \\ \text{Var}[D(S)] &= \mu_a S (\text{Var}[D_i] + E^2[D_i]) = 2\mu_a S \delta^2 \end{aligned} \quad (2-18)$$

where  $D(S) = \sum_i D_i$ ,  $D_i$  is the contribution of inelastic deformation due to a single excursion.  $\mu_a$  is the average number of clumps per unit time. The peak inelastic deformation  $D_p$  will be less than or equal to the threshold  $d$ , if there is no crossing existing in period  $S$ . Hence,

$$P[D_p \leq d] = \exp \left[ - \int_0^S v_d(t) dt \right] \quad (2-19)$$

where  $v_d(t) = \mu_a P_d(t)$  = mean rate of up-crossing threshold  $d$  in time  $t$ .  $P_d(t)$  = probability of a plastic set resulting in an upcrossing of response threshold  $d$  in time  $t$ .

As shown in Fig. 2.6, an up-crossing of the barrier level  $d$  will occur, provided that  $D_i > d - D(t)$ .  $D(t)$  is the permanent set at time  $t$ , while  $D_i$  is the contribution of inelastic deformation. Therefore,

$$P_d(t) = 2 \int_{-\infty}^d P[D_i > d-x] f_D(x) dx \quad (2-20)$$

Since

$$P[D_i > d-x] = \int_{d-x}^{\infty} (2\delta)^{-1} \exp(-|x|/\delta) dx = 1/2 e^{-|d-x|/\delta},$$

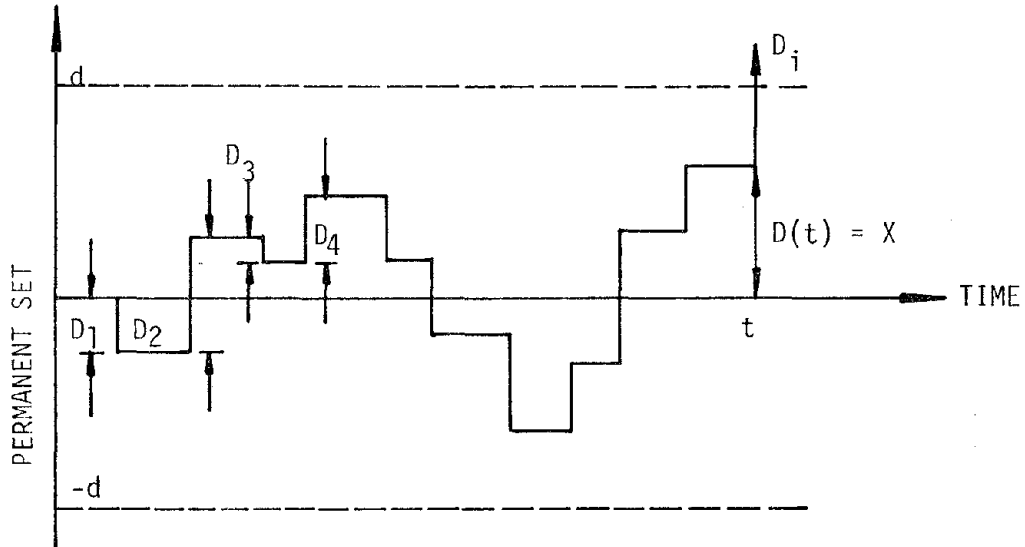


FIG. 2.6 - UP-CROSSING OF BARRIER LEVEL  $d$   
FOR PLASTIC SET

this leads to

$$\begin{aligned}
 P_d(t) &= e^{-d/\delta} \int_{-\infty}^d e^{x/\delta} f_D(x) dx \\
 &= e^{-d/\delta} E [e^{x/\delta}].
 \end{aligned} \tag{2-21}$$

From applied probability theory, the exponential transformation (or  $s$  transformation) of any PDF  $f(x)$  can be expressed as (9):

$$\begin{aligned}
 f_x^T(s) &= E [e^{-sx}] = \int_{-\infty}^{\infty} e^{-sx} f_x(x) dx \\
 &= e^{-sE(x) + s^2\sigma_x^2/2}
 \end{aligned} \tag{2-22}$$

Here,  $E[x] = 0$ ,  $\sigma_x^2 = 2\mu_a t \delta^2$  (Eq. 2-18), and  $s = -1/\delta$ .

Substituting these values into Eqs. (2-22 and 2-21),

$$P_d(t) \approx e^{-d/\delta} e^{\mu_a t} \tag{2-23}$$

Eq. (2-19) now becomes

$$\begin{aligned} P [D_p \leq d] &= \exp \left[ - \int_0^S \mu_a e^{-d/\delta} e^{\mu_a t} dt \right] \\ &= \exp \left[ (1 - e^{\mu_a S}) e^{-d/\delta} \right] \end{aligned} \quad (2-24)$$

This result is given in Ref. 22.

Finally, one arrives at the expected total inelastic peak displacement  $d$  with probability  $P$  of not being exceeded:

$$d = \delta \left\{ \ln[1 - \exp(\mu_a S)] - \ln(-\ln P) \right\} \quad (2-25)$$

Based on Eq. (2-25), the probabilistic predictions of inelastic action in terms of ductility factors or maximum inelastic displacement can be approximately assessed.

#### 2.4 SUMMARY

A strong ground motion can be expressed either in the time domain or in the frequency domain. In the time domain, the motion can be represented as an acceleraogram. The structural response can be computed by time integration analysis as described in Sec. 2.2. In the frequency domain, the strong motion is expressed as a power spectral density function. As mentioned in the previous section, the probabilistic structural response can be predicted.

In a given excitation and a particular damping value, it has been common practice to plot the single-degree-of-freedom response versus the undamped natural period of the system. The plot is the widely-used response spectrum. Based on the time history model described in this Chapter, variabilities of the inelastic response spectra for acceleration and

displacement can be investigated. Results are presented in the next Chapter. Probabilistic predictions of the inelastic response by the random vibration model described in Sec. 2.3 will be discussed further in Chapter 4.

# CHAPTER 3

## INELASTIC RESPONSE SPECTRA BASED ON TIME HISTORY ANALYSIS

### 3.1 INTRODUCTION

The use of a "response spectrum" to characterize the maximum structural response has been well established in aseismic engineering. The Applied Technology Council (3) has recommended that the shape of a design response spectrum should be proportional to the shape based on site seismic parameters. The parameters, i.e., maximum ground acceleration, velocity, and displacement, are determined by an appropriate site response study. In this study, the assessment of general validity of the response-spectra-based design procedure was the major objective. Hence, no attempt was made to cope with local geological conditions.

To best represent a variety of site conditions, Newmark and Hall (17) suggested a maximum ground acceleration value of 1.0G, maximum ground velocity of 48 in/sec, and maximum ground displacement of 36 inches. They also suggested that for 5% damping coefficient the amplification factors of 2.6, 1.9, and 1.4 for acceleration, velocity, and displacement should be used. Fig. 3.1 shows the resulting basic design response spectrum for 5% damping.

An approximate procedure to construct the inelastic response spectra for displacement and acceleration from the basic elastic design spectrum

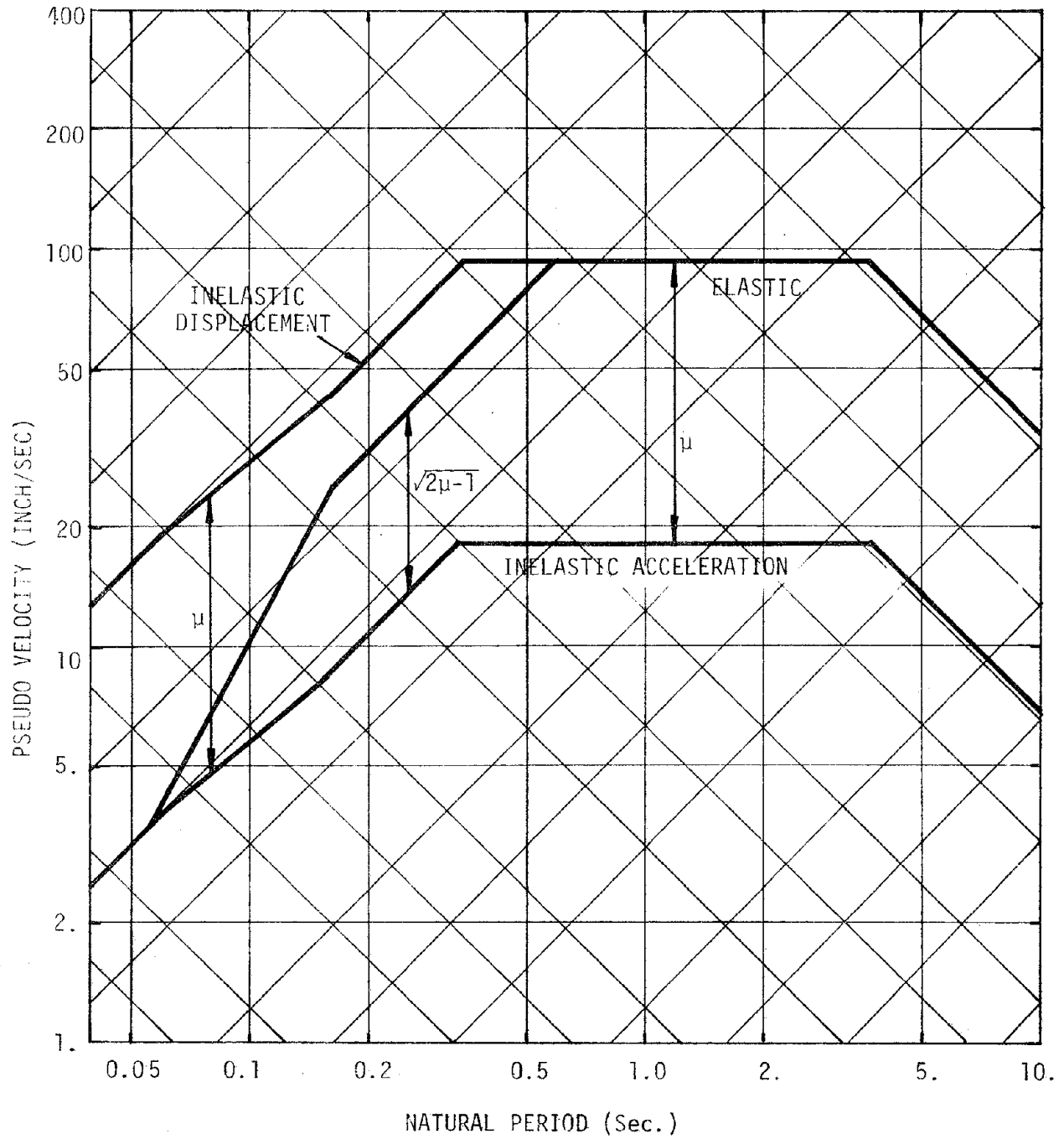


FIG. 3.1 - NEWMARK ELASTIC AND INELASTIC RESPONSE SPECTRA  
(5% DAMPING,  $\mu = 5$ )

has been proposed by Newmark and Hall (17). Brief descriptions of the procedure are presented herein.

As illustrated in Fig. 3.1, for intermediate and high natural period ranges (i.e., the velocity and displacement amplification regions), the inelastic acceleration response spectrum equals the elastic response spectrum divided by the ductility ratio  $\mu$ . The inelastic displacement response spectrum is the same as the elastic spectrum in these ranges. In the intermediate low natural period range (i.e., the acceleration amplification region), the inelastic acceleration response spectrum equals the elastic spectrum divided by  $(2\mu-1)^{1/2}$ . This was derived based on the principle of energy conservation. In the same range, the inelastic displacement response spectrum is equal to the elastic spectrum times  $\mu/(2\mu-1)^{1/2}$ . For the very low natural period range, the system is very stiff, and the inelastic acceleration response is equal to the elastic one. The inelastic displacement equals the elastic response times the ductility factor. In summary, the Newmark approach assumes the inelastic acceleration and displacement spectra differ by the ductility ratio  $\mu$  for all natural periods, as shown in Fig. 3.1. More elaborate discussion of the procedure is reported in references 16 and 17.

One of the objectives of this study is to investigate the variabilities of inelastic acceleration and displacement response spectra on strong ground motion duration, ductility demand, damping ratio, etc. Furthermore, the assessment of validity of the above-mentioned Newmark procedure of constructing inelastic response spectra directly from the elastic spectrum is also desired. In making this assessment, 50 natural periods equally spaced between 0.1 sec and 10 sec on the logarithmic scale were used. Based on the Newmark basic design response spectrum, a series of

strong ground motion duration-dependent artificial motions were generated. Brief descriptions of the generation of artificial motions are presented in the following section.

### 3.2 GENERATION OF ARTIFICIAL MOTIONS

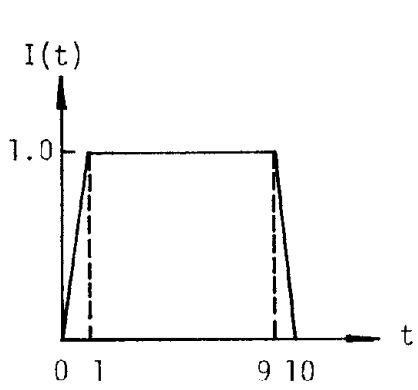
The program SIMQKE (10, 14) was used to generate a series of duration-dependent artificial strong ground motions for the subsequent inelastic response analyses. With the input of a "target" response spectrum, which is the Newmark basic elastic design spectrum of 5% damping, as mentioned previously, the program computes the corresponding power spectral density function. By generating randomly based phase angles and employing Eq. (2-6), artificial strong ground motions can be generated.

In order to simulate the transient character of actual ground shakings, the program has incorporated an intensity envelope function  $I(t)$ . Eq. (2-6) then becomes,

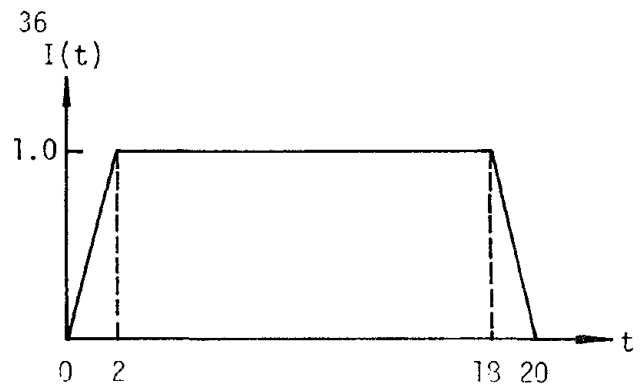
$$X(t) = I(t) \sum_{i=1}^n A_i \sin(\omega_i t + \phi_i) \quad (3-1)$$

Several authors have proposed different types of intensity functions, namely: exponential, trapezoidal, compound, etc. Due to its simple nature and distinctively defined strong motion portion, the trapezoidal intensity envelope function was used.

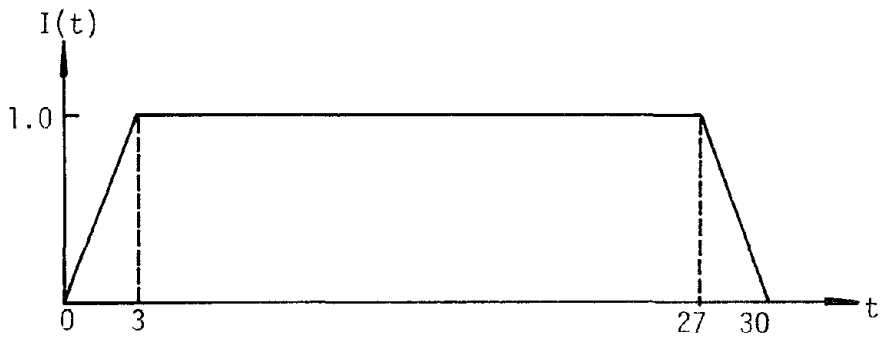
Four sets of artificial motions with varying strong ground motion durations, i.e., 10, 20, 30 and 40 seconds, were generated. Each set consists of five different artificial strong ground motions. The corresponding intensity envelopes of different strong ground motion durations are shown in Fig. 3.2. The maximum acceleration for all motions is 1.0 G.



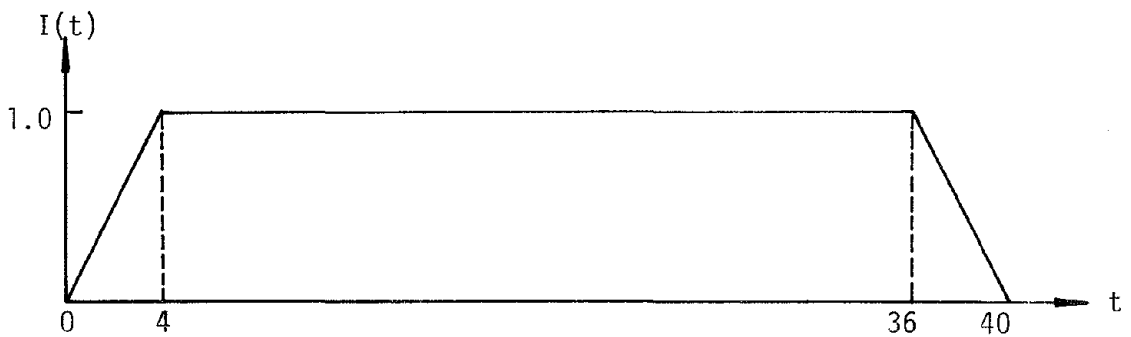
a)  $S = 10$  secs.



b)  $S = 20$  secs.



c)  $S = 30$  secs.



d)  $S = 40$  secs.

FIG. 3.2 - INTENSITY ENVELOPES FOR ARTIFICIAL STRONG GROUND MOTIONS

A typical resulting elastic response of an artificial motion is shown in Fig. 3.3. Notice that it matches the target response spectrum quite satisfactorily.

With different strong motion durations, the corresponding power spectral density functions will vary. As mentioned in Chapter 2, the power spectral density function is the basis for random vibration analysis. The PSD's computed by this program are presented in Chapter 4.

### 3.3 EFFECTS OF STRONG GROUND MOTION DURATION

#### 3.3.1 Effects on Inelastic Response Spectra

Strong ground motion duration has long been considered an important parameter in seismic engineering. The response of very lightly damped linear systems or strength-degrading nonlinear systems depends significantly on the duration of ground shaking. Different definitions for the strong motion duration have been proposed (23); however, no single measure of the duration is in common usage in earthquake engineering. In this section, the variabilities of inelastic response spectra on strong ground motion duration are investigated.

In matching the Newmark elastic design response spectrum, duration-dependent artificial motions were generated as described in section 3.2. 50 SDOF systems with natural periods ranging from 0.1 to 10.0 seconds have been considered in this study. The elasto-plastic responses corresponding to four ductility levels, i.e.,  $\mu = 2, 3, 4$  and  $5$ , are of interest herein. Hence, by varying the resistance function for each system, the elasto-plastic responses corresponding to a given ductility level can be calculated based on the time history model described in Chapter 2.

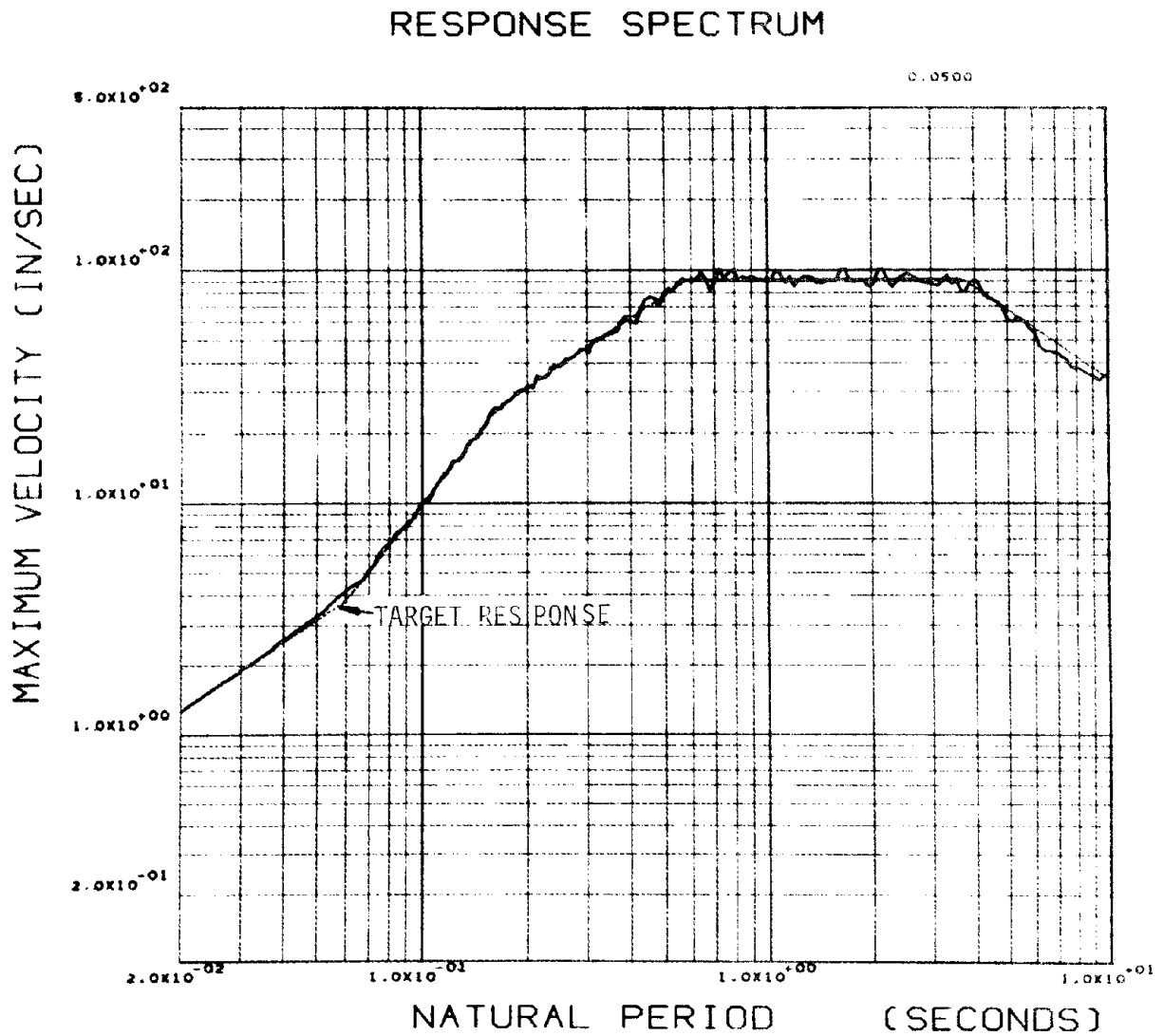


FIG. 3.3 - TYPICAL ELASTIC RESPONSE OF ARTIFICIAL GROUND  
MOTION ( $\zeta = 0.05$ )

The mean elasto-plastic response of SDOF systems can then be computed for each set of artificial motions.

Figs. 3.4 and 3.5 show the mean inelastic displacement and acceleration responses for different strong ground motion durations ( $\mu=5$ ). In easy comparison, the Newmark elastic responses and inelastic response spectra for  $\mu=5$  are also shown in the figures.

As shown in the figures, for each of the 50 natural periods considered, the mean inelastic response of relative displacement or absolute acceleration does vary with different strong motion durations. However, there is no unique trend with respect to the variations of strong ground motion duration. Hence, it can be concluded that for a given ductility level, the inelastic responses for maximum relative displacement and maximum absolute acceleration are not significantly dependent on strong ground motion duration.

However, one must be cautious to interpret the conclusion. The above-mentioned conclusion is true only when the duration-dependent artificial motions were matching the same target response. In other words, the conclusion is valid only when the ground motions have approximately the same level of elastic response spectra.

As mentioned earlier, it has been recognized that the strong ground motion duration is a very important parameter in earthquake engineering. Intuitively, one would expect the motion duration to be closely related to nonlinear structural response. This leads to the question of whether the usual way of measuring structural inelastic behavior by the peak ductility factor is adequate. Further discussions concerning the adequacy of  $\mu$  are presented in the following paragraphs.

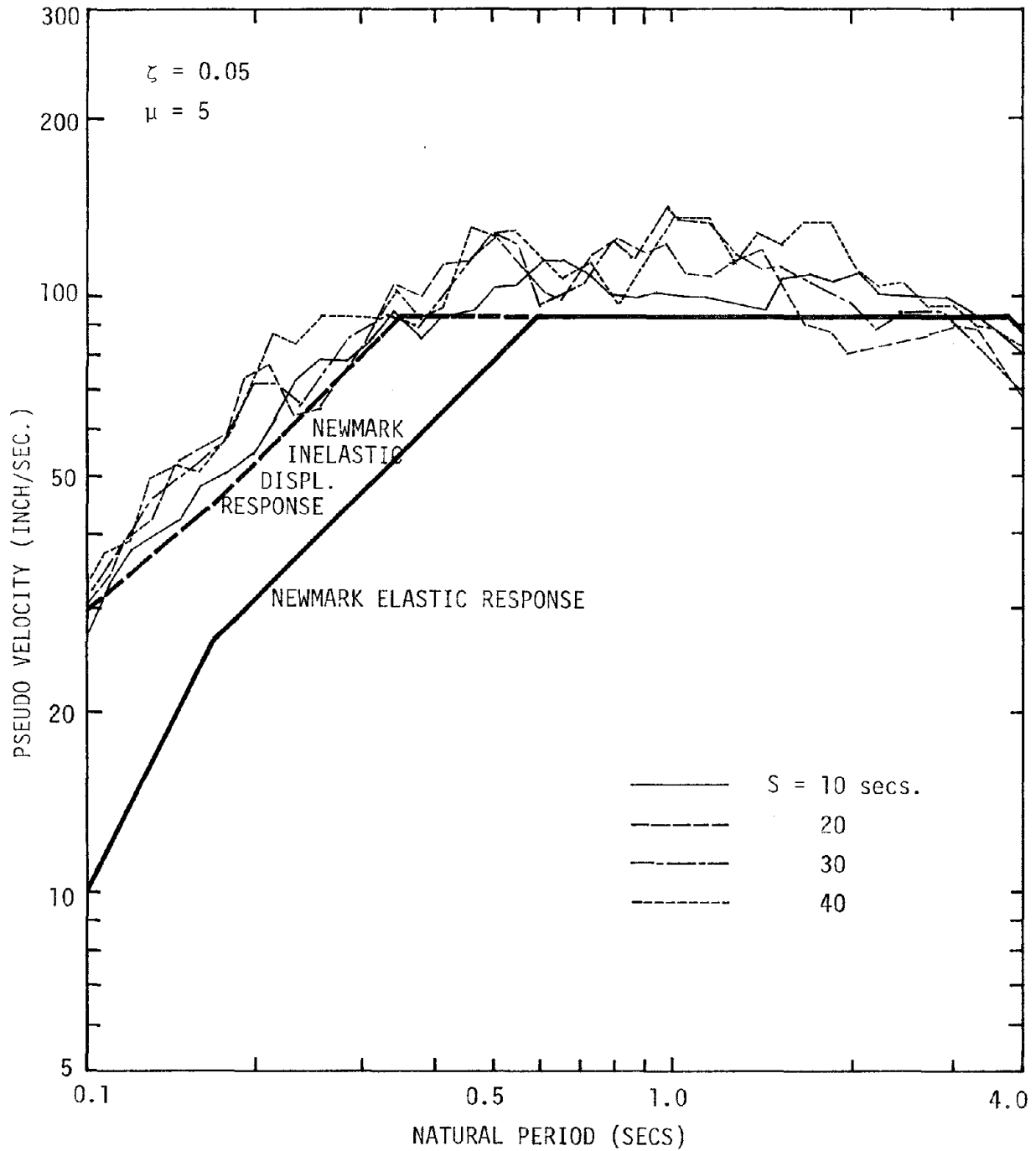


FIG. 3.4 - MEAN INELASTIC DISPLACEMENT RESPONSES FOR DIFFERENT STRONG GROUND MOTION DURATIONS ( $\mu = 5$ ,  $\zeta = 0.05$ )

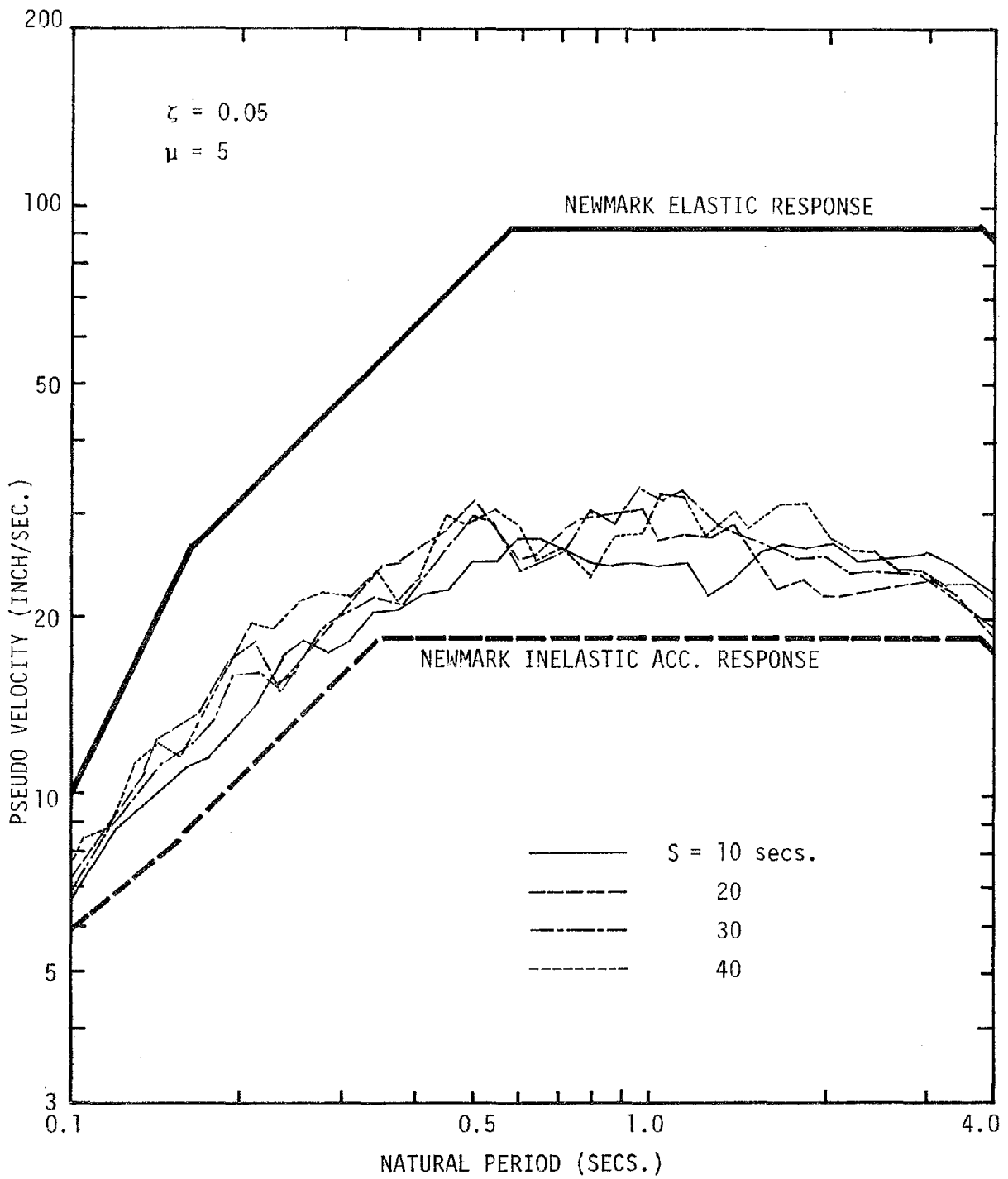


FIG. 3.5 - MEAN INELASTIC ACCELERATION RESPONSES FOR DIFFERENT STRONG GROUND MOTION DURATIONS ( $\mu = 5$ ,  $\zeta = 0.05$ )

### 3.3.2 Cumulative Yielding Ductility

The traditional way of evaluating inelastic behavior of a system is by computing the peak ductility factor  $\mu$ . The peak ductility factor is defined as the maximum relative displacement response divided by the yielding displacement of the system. As depicted earlier, the inelastic responses are not significantly related to strong ground motion duration. However, one would intuitively expect the inelastic structural response to be closely dependent on the motion duration, at least when dealing with the damage of the system. This suggests that the conventional ductility factor, though it reveals the information of peak deformation, may not be a pertinent measure for long-term structural damage. In view of this postulation, a new inelastic behavior measure has been tested. The results are reported herein.

The new measure "cumulative yielding ductility," denoted by  $\eta$ , is defined as:

$$\eta = \frac{\sum |D_i|}{U_e} + 1 \quad (3-2)$$

where  $D_i$  = individual plastic deformation as described in section 2.3.3, and  $U_e$  = yield displacement of the elasto-plastic system. The information of total amount of plastic actions (in absolute value) can be obtained by using the cumulative yielding ductility  $\eta$ .

A series of systems subjected to artificial strong ground motions was studied. For illustration purposes, only two systems are presented herein. The first elasto-plastic system has a natural period of 0.233 sec, maximum spring resistance  $R_m = 365$  kips, yield displacement  $U_e = 0.503$  in. When subjected to a 40-second artificial motion, the inelastic responses can be computed by time history analysis. The resulting maximum relative

displacement is 3.2 inches. This corresponds to a peak ductility factor of 6.37. Plots of the permanent sets and the peak ductility factors vs. time are shown in Figs. 3.6-a,b. Note that the peak ductility factor remains the same from approximately 10 seconds to 32 seconds. This suggests that the risk of the yielding displacement of the system to exceed a certain threshold of response remains the same in that period. However, extensive plastic actions took place in the period, as shown in Fig. 3.6-a. Hence, it illustrates the inadequacy of using the peak ductility factor as the only measure for inelastic structural behavior.

Fig. 3.6-c shows the relationship of the cumulative yielding ductility vs. time. As shown in the figure, the cumulative yielding ductility is clearly dependent on the motion duration. In fact, it is almost linearly related to the strong ground motion duration. Values of the corresponding  $\mu$ 's and  $\eta$ 's for selective time steps are tabulated in Table 3-1.

TABLE 3-1 DUCTILITY FACTORS FOR DIFFERENT MOTION DURATIONS

NATURAL PERIOD (Secs)	RESISTING FUNCTION (Kips)	YIELD DISPLACENT. (Inches)	TYPE OF DUCTILITY	MOTION DURATION (Secs)			
				10	20	30	40
0.233	365	0.503	$\mu$	1.72	4.24	4.24	6.37
			$\eta$	3.82	21.00	37.19	58.0
1.048	122	3.402	$\mu$	3.83	7.62	7.62	8.44
			$\eta$	3.84	13.93	24.50	38.00

The second system considered has natural period 1.048 seconds,  $R_m = 122$  kips,  $U_e = 3.402$  inches. When subjected to the same  $s = 40$  second artificial motion, the inelastic responses can also be computed by time

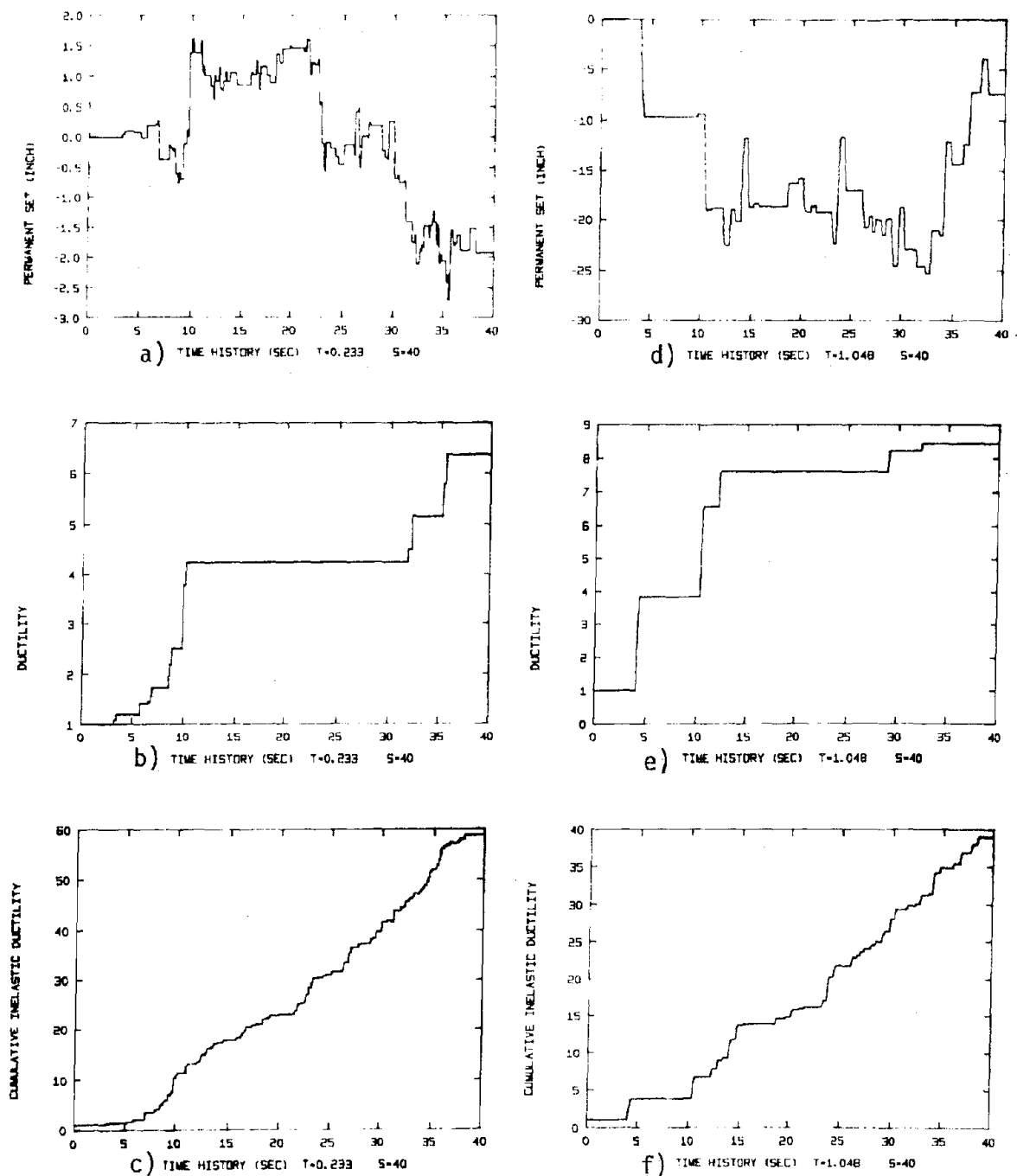


FIG. 3.6 - TIME HISTORIES FOR PERMANENT SETS, DUCTILITY FACTORS, CUMULATIVE YIELDING DUCTILITIES (T = 0.223, 1.048 SECS.)

history analysis. Results versus time are plotted in Figs. 3.6-d,e,f. At the end of the motion, the peak ductility factor  $\mu$  equals 8.44, whereas the cumulative yielding ductility  $\eta$  equals 38.0. As shown in the figures, the peak ductility factor does not closely relate to the variations of motion duration, while the cumulative yielding ductility does. Values of the  $\mu$ 's and  $\eta$ 's versus selective motion periods are also listed in Table 3-1 for comparison.

All the other systems tested have the same trend. Hence, the analyses suggest that the cumulative yielding ductility  $\eta$  is a potential measure for plastic behavior. It can reveal information as to duration dependency for the energy dissipation of plastic action. The traditional ductility factor, however, can only indicate the maximum deformation of elasto-plastic systems.

No attempt was made to apply the new measure to real ground motions. Unlike artificial motions, which have distinctive intensity contents, real ground motions have much greater variations in intensity, and strong portions of ground shaking are difficult to define. However, if one incorporates a definition of equivalent strong ground motion duration like the one suggested by Vanmarcke and Lai (23), the new cumulative yielding ductility can be directly employed to measure inelastic responses.

In summary, the study indicates that the cumulative yielding ductility  $\eta$  is a useful measure of structural damage. The traditional ductility factor  $\mu$  can reveal only information on maximum responses; hence, can assess only the risk of sudden failure of structures.

### 3.4 INELASTIC RESPONSE RATIOS

#### 3.4.1 Definition

As mentioned in section 3.2, all the artificial motions were generated to have elastic responses matching the Newmark target response spectrum. Inevitably, the elastic response of artificial motions will deviate from the target. Hence, the inelastic response spectra are affected. In view of this undesirable situation, new measures of "inelastic response ratios" are proposed to evaluate the elasto-plastic behavior of SDOF systems.

"Inelastic Response Ratio" is defined as the ratio of elastic response versus inelastic response of an elasto-plastic system. Therefore, inelastic acceleration response ratio is the ratio between elastic and inelastic acceleration responses of a system. The inelastic displacement response ratios can similarly be defined. Dealing with the inelastic response ratios directly, the effect of elastic response deviating from the Newmark target response can be filtered out.

Newmark's relationship between the elastic and inelastic responses for different ductility levels can be expressed in terms of the new inelastic response ratios. Fig. 3.7 shows the Newmark inelastic acceleration ratios for 5% damping elasto-plastic systems. Note that when the undamped natural period is longer than 0.6 seconds (approximately), the inelastic acceleration response ratio just equals the ductility factor  $\mu$ . When the natural period is in the range from 0.167 to 3.5 seconds (or longer, depending on the ductility level), the inelastic acceleration response ratio equals  $(2\mu-1)^{1/2}$  as shown in the figure.

Similarly, inelastic displacement response ratios for the Newmark approach are shown in Fig. 3.8. As expected, when the natural period

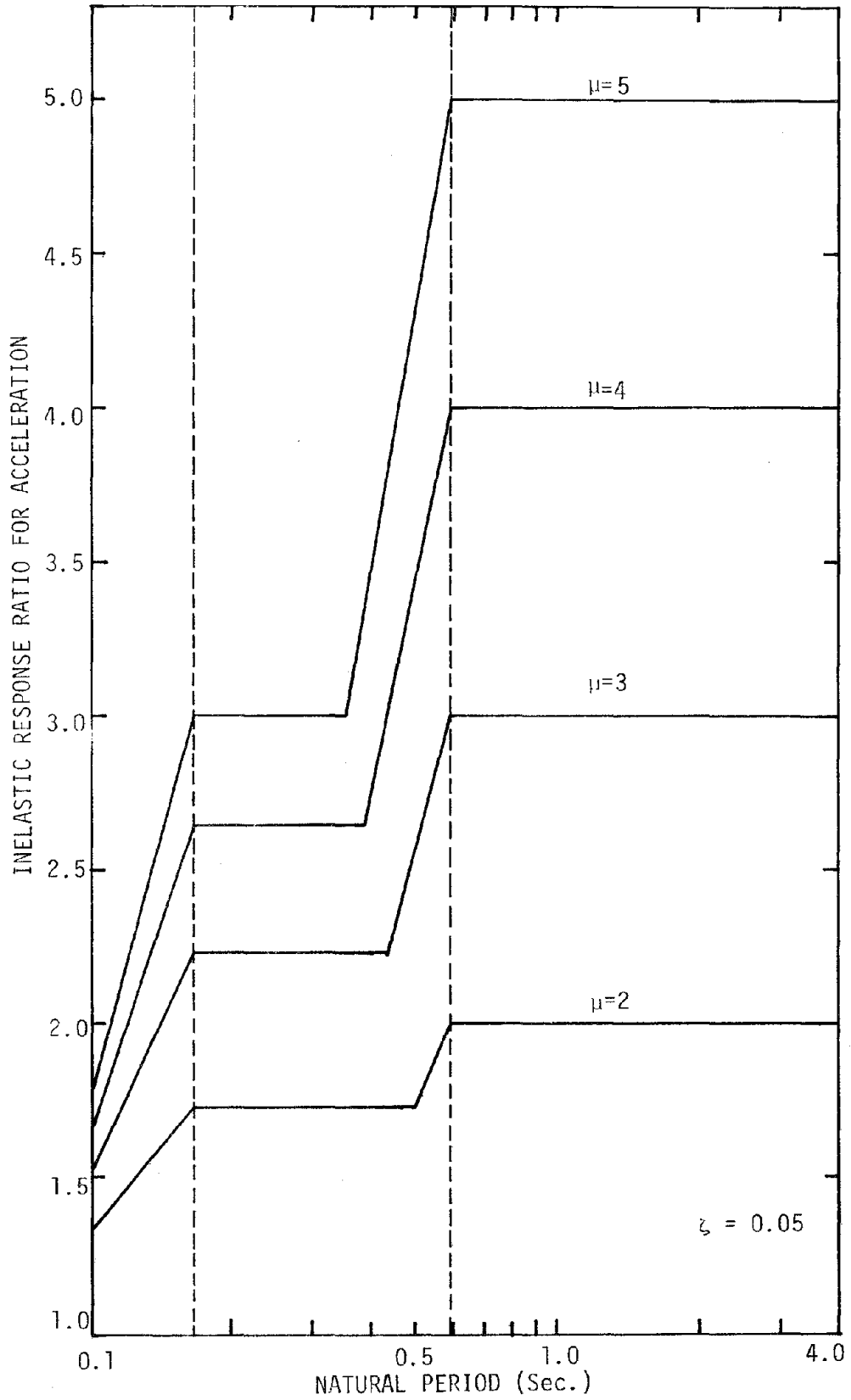


FIG. 3.7 - NEWMARK INELASTIC RESPONSE RATIO FOR ACCELERATION  
(5% DAMPING)

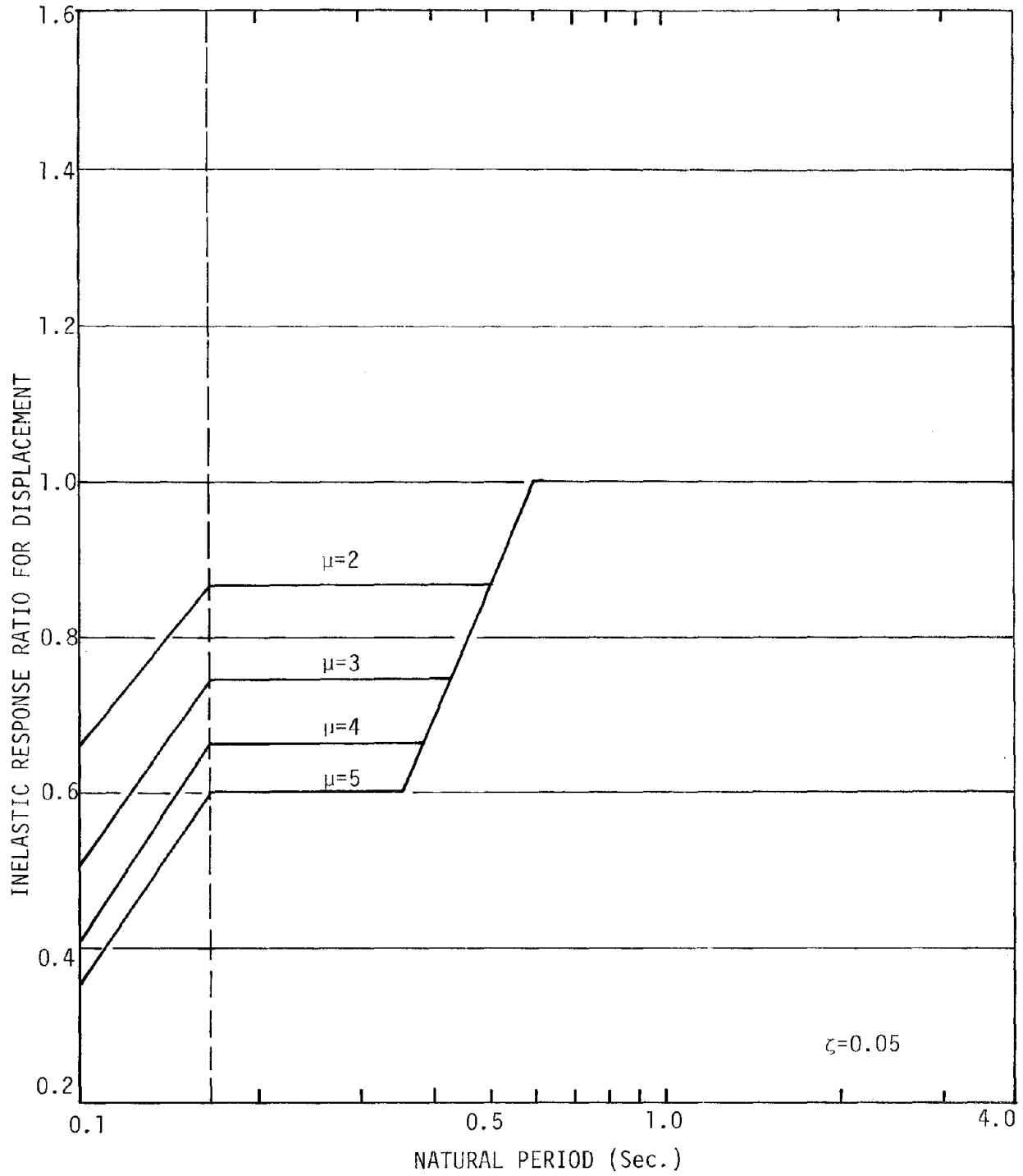


FIG. 3.8 - NEWMARK INELASTIC RESPONSE RATIO FOR DISPLACEMENT (5% DAMPING)

of the elasto-plastic system is longer than 0.6 seconds, the ratio equals one regardless of the ductility factor. When the natural period lies in the range from 0.167 to 3.5 seconds (or longer, again depending on the ductility), the inelastic displacement response ratio equals  $(2\mu-1)^{1/2}/\mu$ .

As will be shown later in this chapter, the inelastic response ratios are very powerful measures in evaluating the variabilities of inelastic response spectra, especially when the comparison with Newmark's spectra is desired.

#### 3.4.2 Results for 5% Damping

As concluded in section 3.3.1, for time history analysis of elasto-plastic systems, the strong ground motion duration has no significant effect on the results, either in terms of maximum absolute acceleration or of maximum relative displacement. However, one must be aware that the argument is valid only when the duration-dependent strong ground motions have approximately the same level of elastic responses.

Because of the lack of dependency of the inelastic responses on duration, it was decided to compute the mean of the inelastic response ratios for all the generated motions. This means a total of 20 artificial motions, regardless of the different strong motion durations, which are included to arrive at the mean responses.

The resulting mean inelastic acceleration response ratios for  $\mu=2, 3, 4$  and  $5$ , of 5% damped elasto-plastic systems are shown in Fig. 3.9. The ratios are generally lower than those shown in Fig. 3.7, and the differences are more pronounced with increasing ductility level. For example, in the low natural period range, when  $\mu=2$ , new inelastic acceleration

response ratios are on the average 15% lower than those corresponding to the Newmark approach. When  $\mu=3$ , it's 20% lower, for  $\mu=4$ , 25% lower, for  $\mu=5$ , 30% lower. When the natural periods are longer than 0.7 seconds, the new inelastic acceleration response ratios are smaller than those of Newmark by 8% for  $\mu=2$ , 15% for  $\mu=3$ , 21% for  $\mu=4$ , and 32% for  $\mu=5$ .

Fig. 3.10 shows the results of mean inelastic displacement response ratios for 5% damped elasto-plastic systems. The calculated mean inelastic displacement response ratios match nicely with those of Newmark for  $\mu=2$ . However, when  $\mu$  increases, the discrepancies become more pronounced. For example, the computed ratios are 12% on the average lower than Newmark for  $\mu=3$ , 20% lower for  $\mu=4$ , 25% lower for  $\mu=5$  in the shorter natural period range, while in the longer natural period range the mean inelastic displacement ratios are a little lower than those of Newmark for  $\mu=3$ , 11% for  $\mu=4$ , and 18% lower for  $\mu=5$ .

Based on the principle of energy conservation, i.e., the kinetic energy of elastic action exceeding yield level  $U_e$  will be dissipated in terms of plastic action, it can be concluded that the elasto-plastic deformation shall be equal to or greater than the associated linear elastic deformation. However, as shown in Fig. 3.10, when natural periods are longer than 2.0 seconds, the inelastic displacement response ratios become higher than one. Since the ratio is defined as elastic response versus inelastic response, this suggests the maximum deformation of the elasto-plastic system is smaller than that of the associated elastic system. This appears to be in contradiction to the principle of energy conservation. The discrepancy has been pointed out by Veletsos et al. (25), "the principle of conservation of energies is valid only under very restrictive conditions."

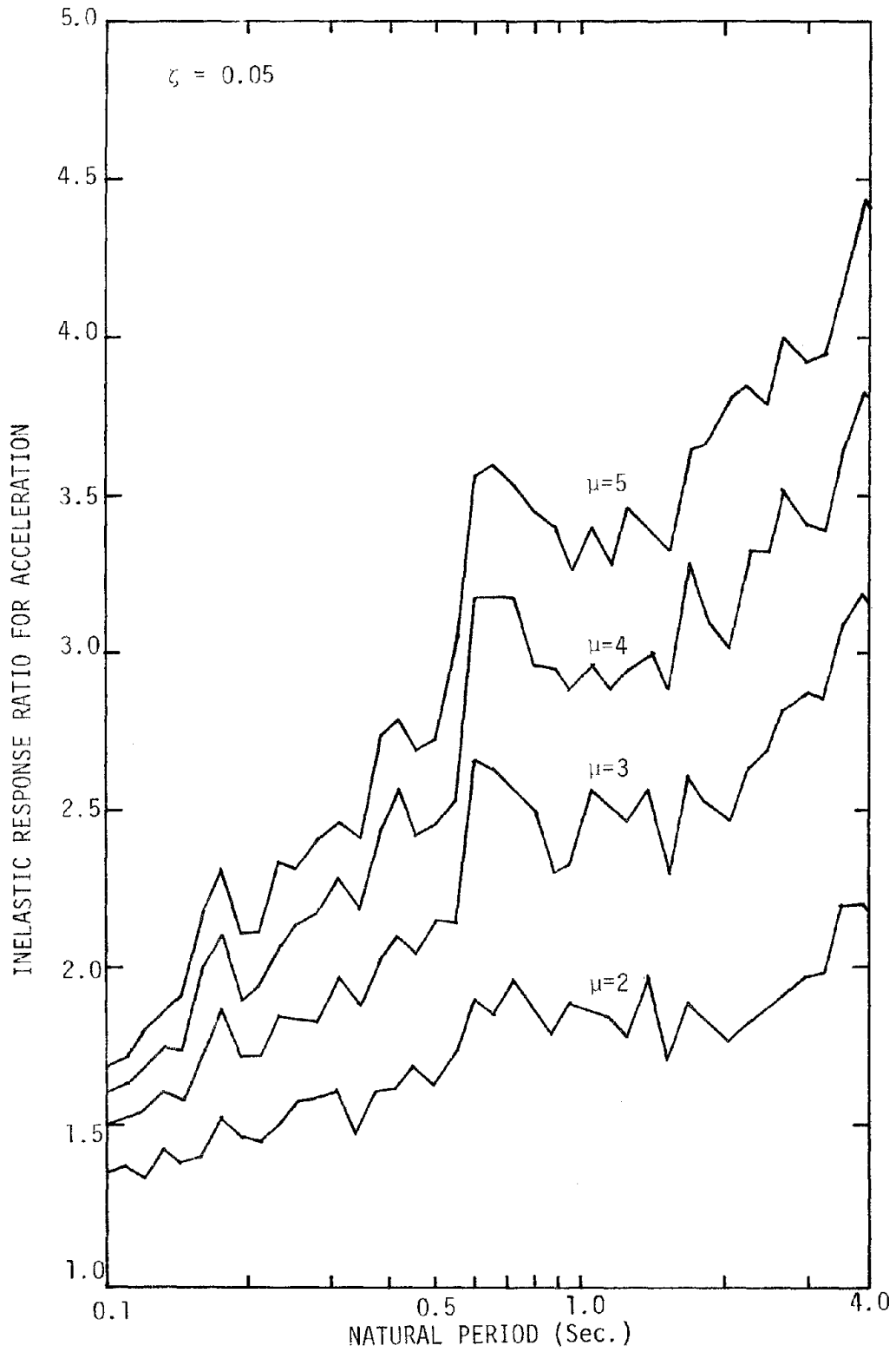


FIG. 3.9 - MEAN INELASTIC RESPONSE RATIO FOR ACCELERATION (5% DAMPING)

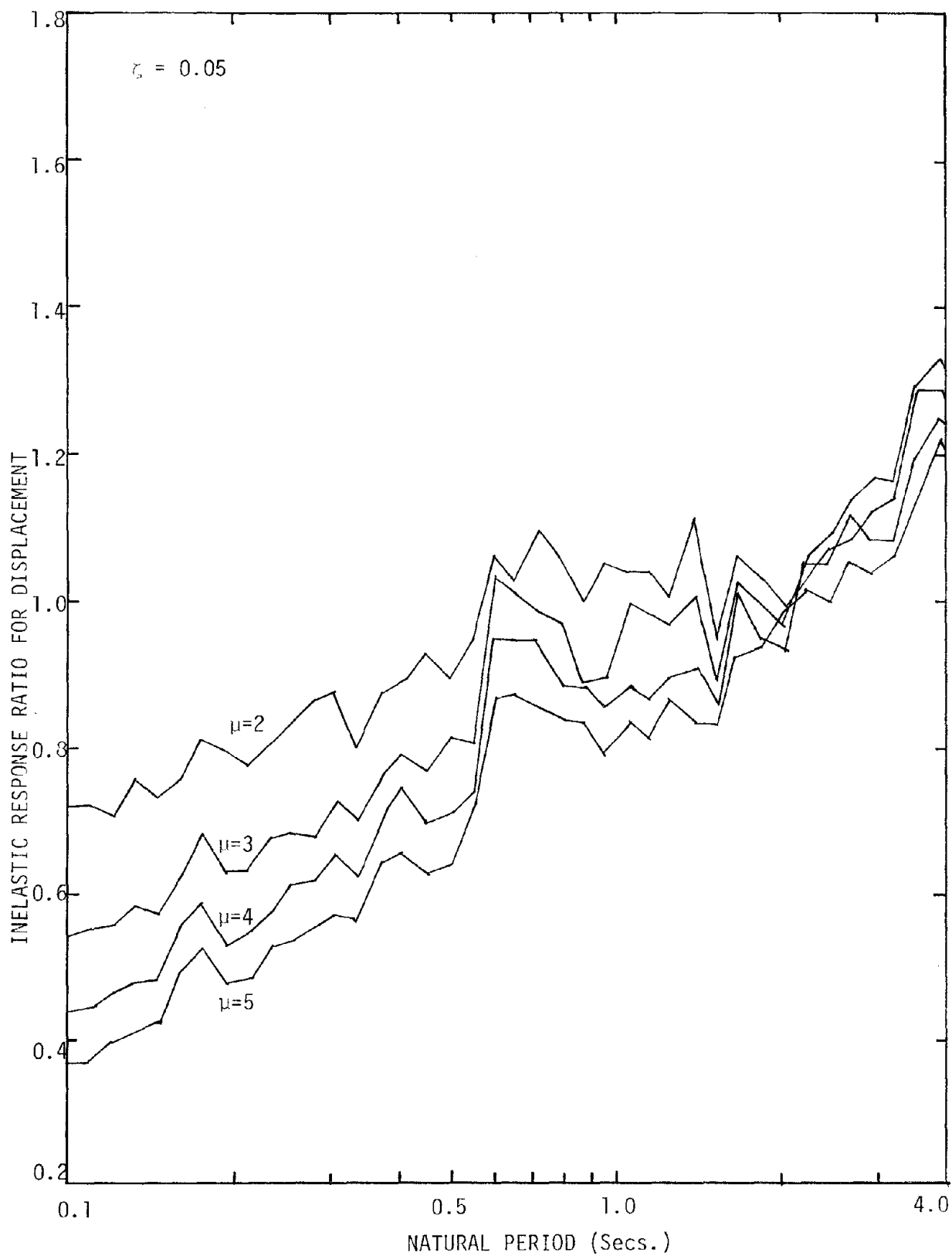


FIG. 3.10 - MEAN INELASTIC RESPONSE RATIO FOR DISPLACEMENT (5% DAMPING)

The above-mentioned discussions can be concluded as follows:

- 1) The mean inelastic response ratios for acceleration and displacement based on the time history analyses are generally smaller than those of the Newmark approach for all ductility levels. This suggests that the Newmark prediction of elasto-plastic response is unconservative by a factor of 1.1 ~ 1.6.
- 2) The discrepancy between the time history inelastic response result and that predicted by the Newmark approach is more pronounced with increasing ductility.
- 3) In the natural period range from 0.5 to 3.0 seconds, which is the range where the fundamental periods of most structures may lie, the underprediction for inelastic acceleration of Newmark's approach is most severe.
- 4) When natural period is longer than 2.0 seconds, the maximum elasto-plastic displacement is smaller than that of the associated linear-elastic system. This suggests that the principle of energy conservatism does not hold in that natural period range.

#### 3.4.3 Results for 2% Damping

For welded steels, prestressed concrete structures, and some vital piping problems, the damping ratios are generally in the range of 2%. Hence, the variabilities of inelastic response spectra are also of interest for this study.

Because of changes in the amplification factors for 2% damping, the Newmark basic elastic design spectrum changes. Hence, different Newmark inelastic response ratios result. Since the changes are small, only the corresponding Newmark inelastic acceleration response ratios for 2% damping are shown in Fig. 3.11. Notice that the inelastic acceleration response ratio is equal to the ductility level when the natural period is longer than 0.5 second, approximately, instead of 0.6 second, as in the

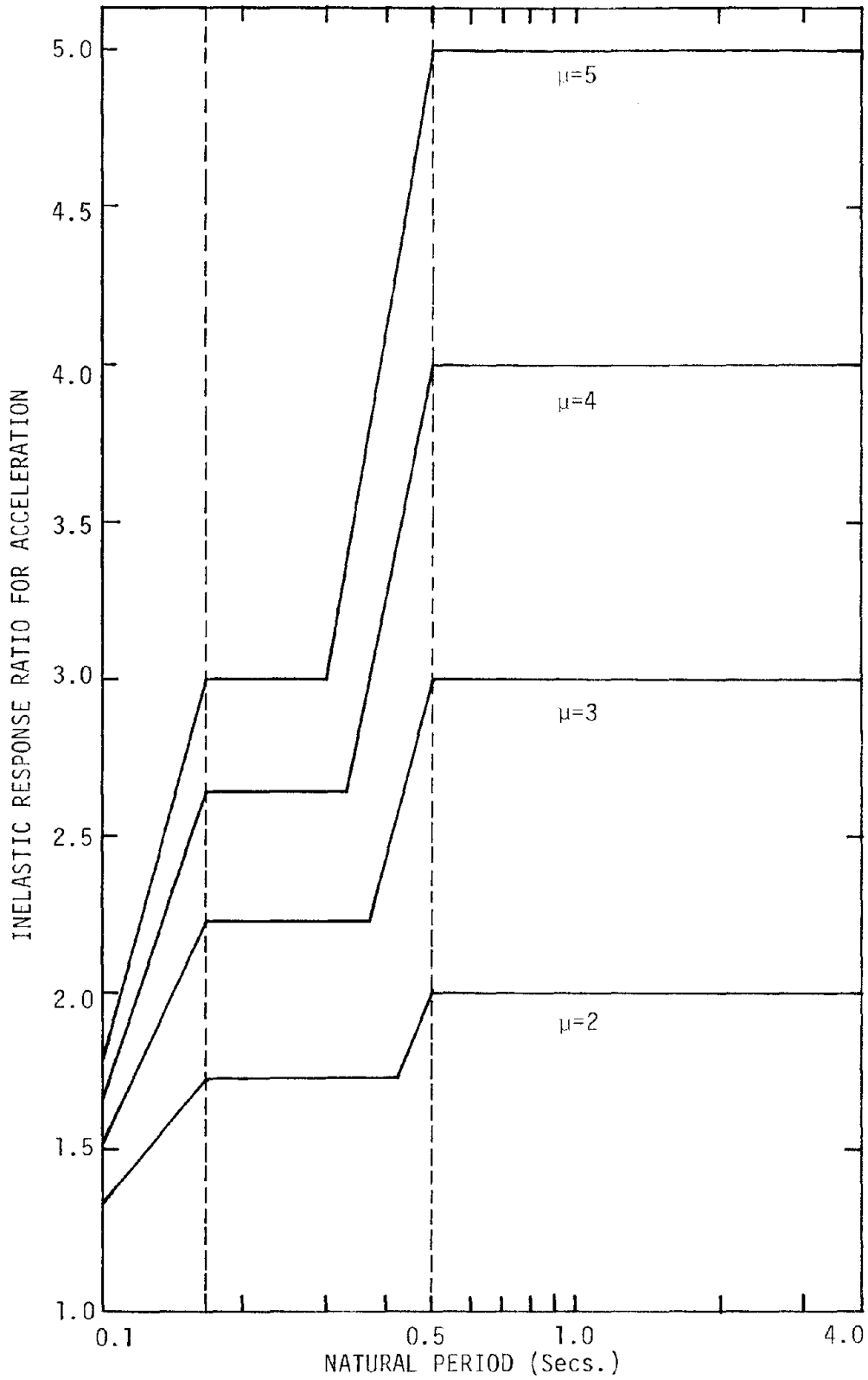


FIG. 3.11 - NEWMARK INELASTIC RESPONSE RATIO FOR ACCELERATION (2% DAMPING)

case of 5% damping. When the natural period is longer than 0.5 second, the inelastic displacement response ratio equals one.

Since the 20 artificial motions generated based on 5% damping also match well with the Newmark target response for 2% damping, no attempt was made to generate new motions. For the 20 artificial strong ground motions, the mean inelastic response ratios can be computed by time history analyses. The results of mean inelastic acceleration response ratios are shown in Fig. 3.12. Contrary to the results for 5% damping, the mean inelastic acceleration response ratios for 2% damping are generally higher than those from the Newmark approach. For example, in the high period range (i.e., longer than 0.5 second), the time history analyses resulted in inelastic acceleration ratios on the average 15% higher than those of the Newmark approach for  $\mu=2$ , 11% higher for  $\mu=3$ , 8% higher for  $\mu=4$ , and just a little higher for  $\mu=5$ . In the low natural period range, the mean inelastic acceleration response ratios match quite satisfactorily with the corresponding Newmark inelastic response ratios for all ductility levels.

Fig. 3.13 shows the mean inelastic displacement response ratios of the time history results for 2% damping. The general trend is the same as for 5% damping. In the high natural period range, the inelastic displacement response ratios are ranging approximately above the 1.2 value. This again suggests that the elasto-plastic response is smaller than the elastic response of the system. The physical interpretation of this interesting situation to the actual inelastic design procedure of structural frames will be presented in Chapter 5. In the low natural period range, the mean inelastic displacement response ratios are generally 20% higher than those from the Newmark approach.

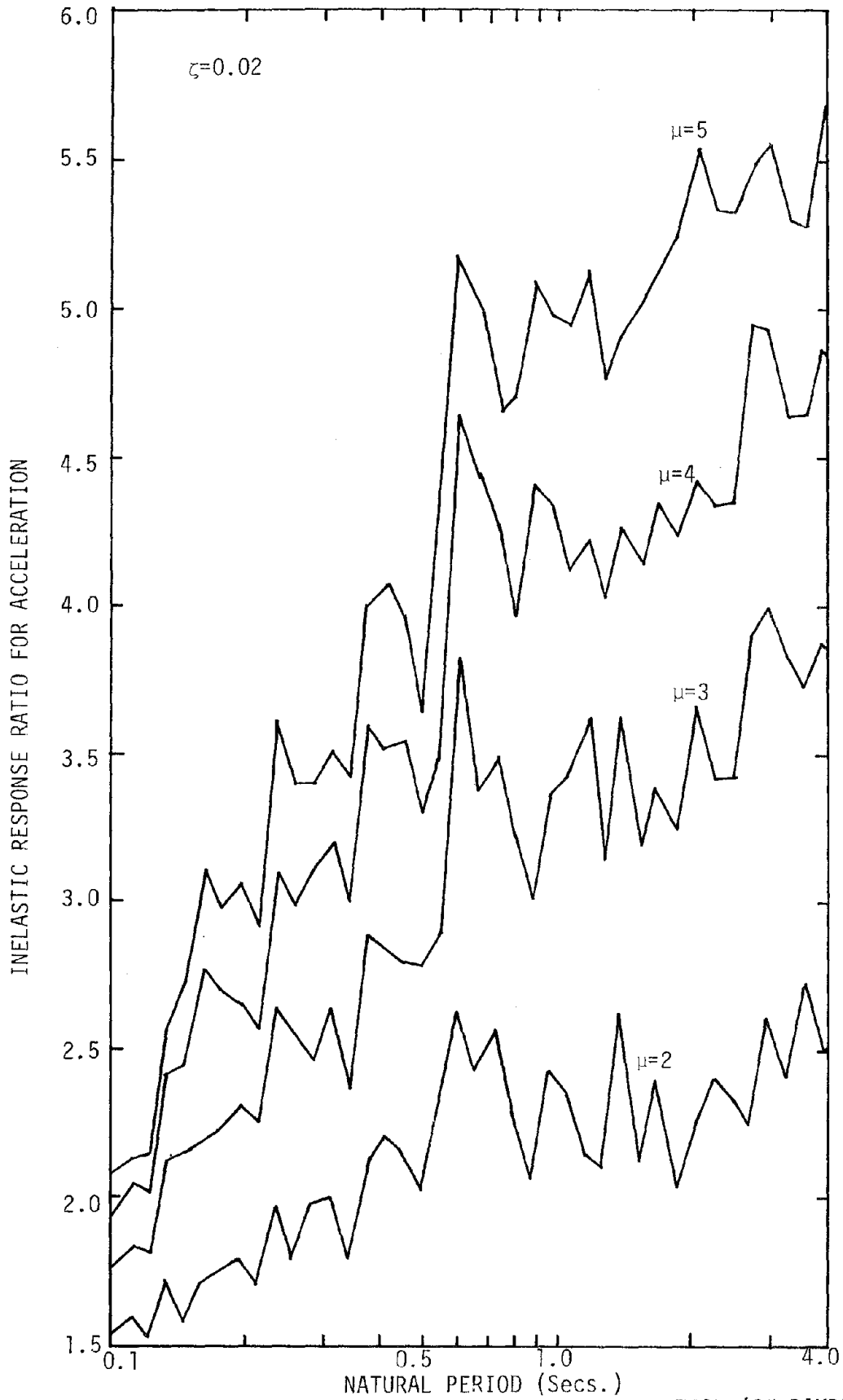


FIG. 3.12 - MEAN INELASTIC RESPONSE RATIO FOR ACCELERATION (2% DAMPING)

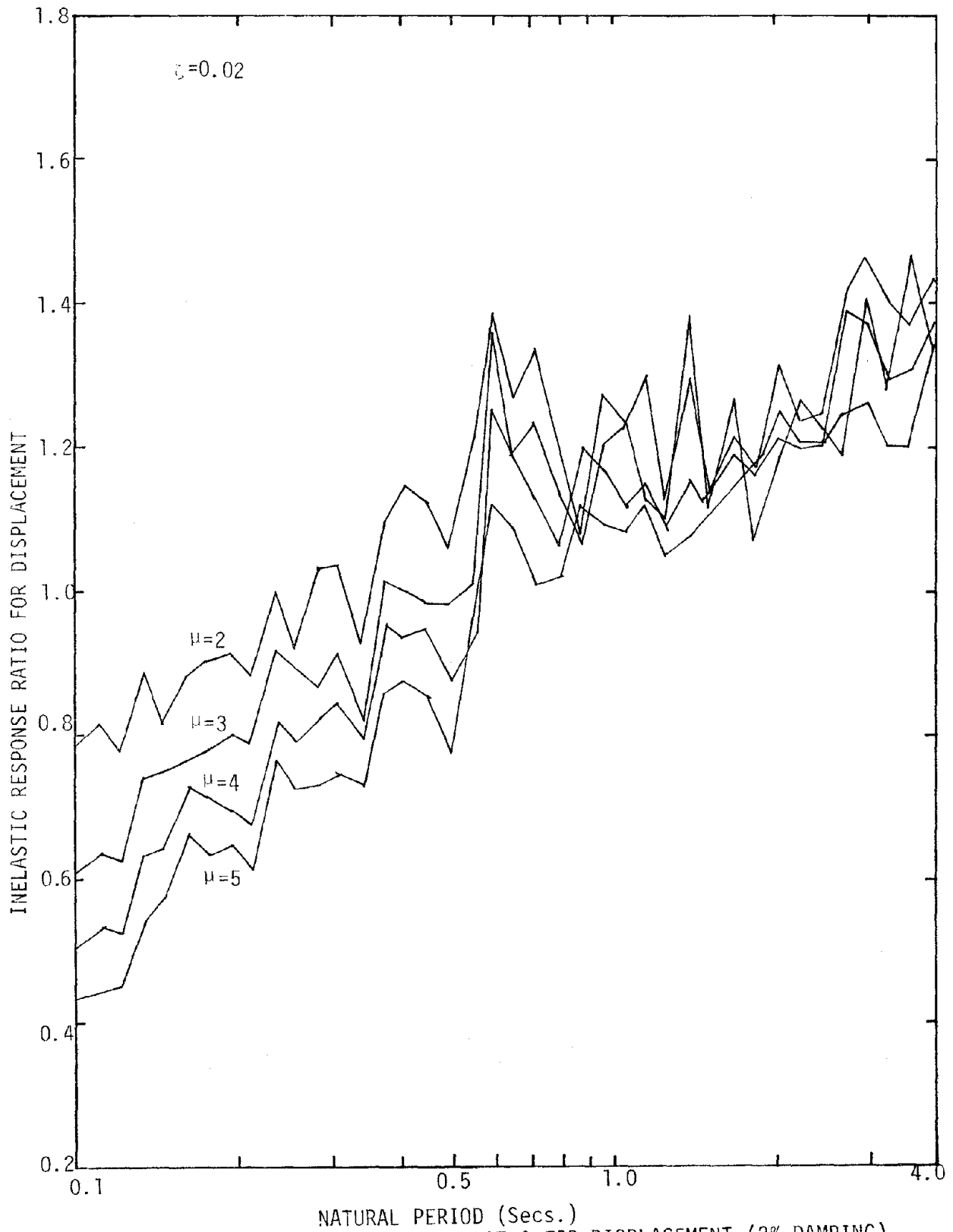


FIG. 3.13 - MEAN INELASTIC RESPONSE RATIO FOR DISPLACEMENT (2% DAMPING)

The above-mentioned results for 2% damped systems can be concluded as follows:

- 1) The mean inelastic acceleration and displacement response ratios based on time history analyses are generally higher than those from the Newmark approach. This suggests that the Newmark predictions of inelastic acceleration and displacement for 2% damped elasto-plastic systems are conservative.
- 2) With increasing ductility level, the discrepancy between the time history analysis based inelastic acceleration response ratios and that predicted by the Newmark approach becomes smaller. The inelastic displacement response ratio, however, shows no significant variation from varying ductility levels.
- 3) For higher natural period, the maximum elasto-plastic displacement is smaller than that of the associated linear-elastic system. This again indicates that the principle of energy conservation is not valid for high natural period ranges.

### 3.5 RESULTS BASED ON REAL STRONG GROUND MOTIONS

In this section, the results of the previous section are compared with the time history analyses inelastic responses, using a set of real strong ground motions. The Caltech identification numbers, values of maximum ground acceleration, velocity and displacement, and record duration of motions are tabulated in Table 3.2 (6). The motions were selected to have strong ground motion durations compatible with those of artificial motions. The definition for strong ground motion duration used herein is based on the following equation: (Vanmarcke and Lai, 23).

$$S_0 = [2 \ln (2 S_0/T_0)] (I_0/A_{\max}^2) \quad S_0 \geq T_0 \quad (3-3)$$

TABLE 3-2 SEISMIC PARAMETERS FOR THE SET OF REAL STRONG GROUND MOTIONS

CIT No.	EARTHQUAKE	$A_{\max}$ (G's)	$V_{\max}$ (in/sec)	$D_{\max}$ (inch)	RECORD DURATION (sec)	$S_0$ (sec)
A004-2	KERN COUNTY	0.179	6.97	3.622	54.4	10.72
B024-2	LOWER CALIF.	0.183	4.567	1.457	90.24	10.19
C048-2	SAN FERNANDO	0.134	9.41	5.433	59.6	22.88
T286-2	BORREGO VALLEY	0.047	2.402	1.299	71.34	20.24

where  $S_0$  = equivalent strong ground motion duration,  $T_0$  = predominant period of the earthquake motion,  $I_0$  = Arias Intensity = integral of the squared accelerations,  $A_{\max}$  = peak ground acceleration. The corresponding equivalent strong ground motion durations for the set of real earthquakes are also listed in Table 3-2. All motions were normalized to have the same peak ground acceleration of 1.0 G.

The mean inelastic response ratios for acceleration and displacement for 5% damped elasto-plastic systems are shown in Figs. 3.14 and 3.15. In comparison with the results shown in Figs. 3.9 and 3.10, it can be concluded that the results based on real ground motions are quite compatible with the results of artificial motions. Hence, the conclusions mentioned in the previous sections can be applied to real ground motions with confidence.

The elasto-plastic responses of other real ground motions were also computed. The resulting inelastic response ratios have the same general trend as the set reported. However, since most real ground motions have shorter strong ground motion durations (23), in the higher natural period range the system considered will be subjected to only one cycle or less

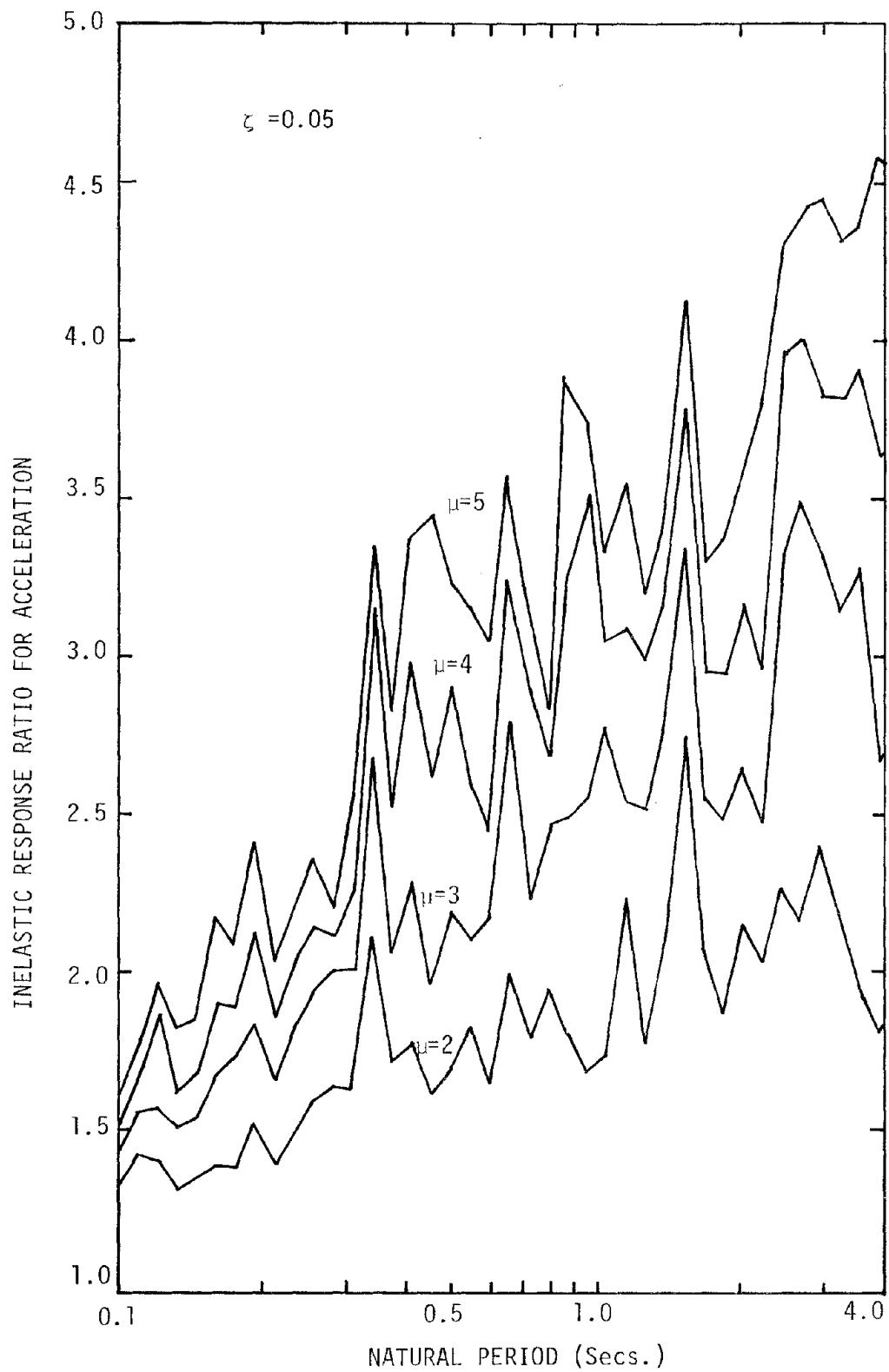


FIG. 3.14 - MEAN INELASTIC RESPONSE RATIO FOR ACCELERATION OF REAL GROUND MOTIONS (5% DAMPING)

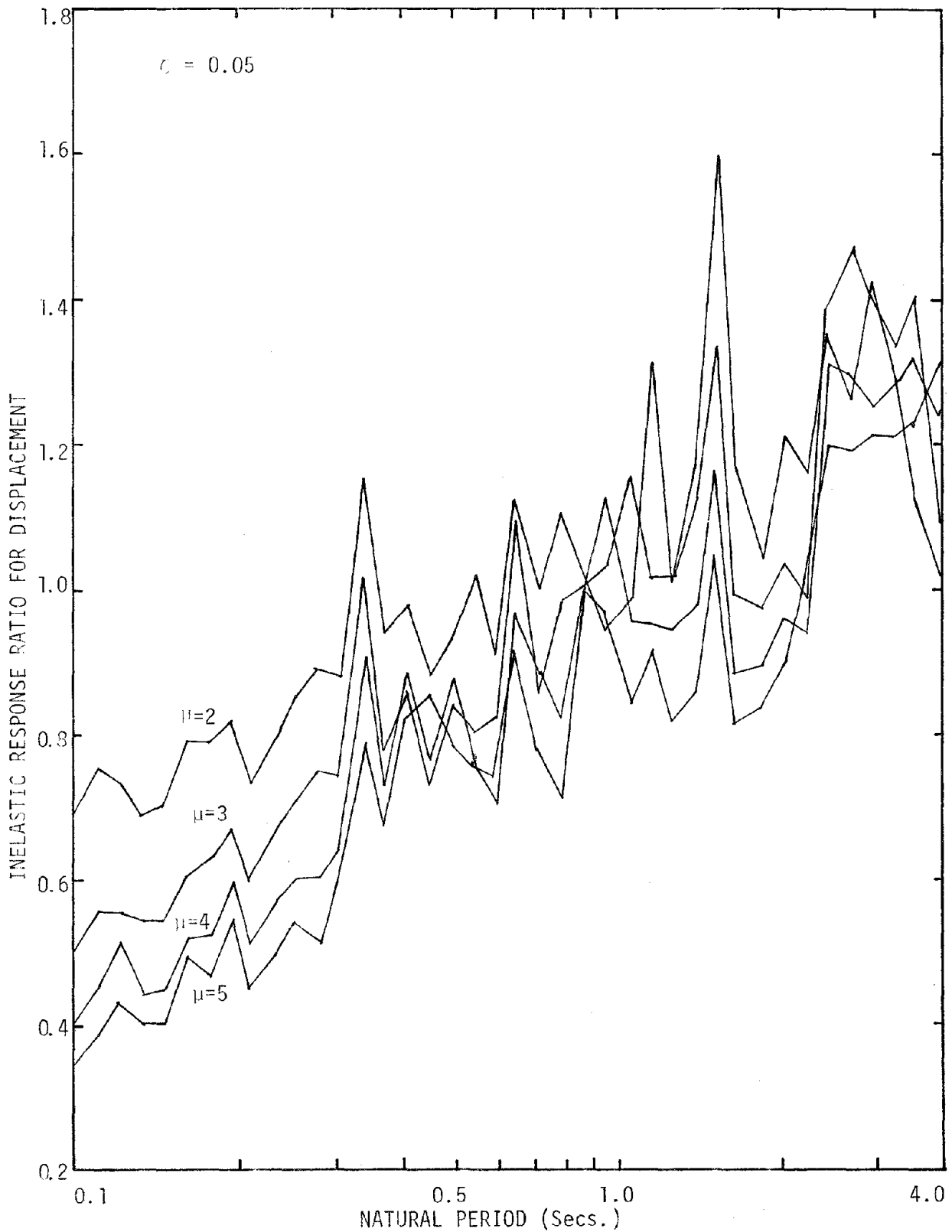


FIG. 3.15 - MEAN INELASTIC RESPONSE RATIO FOR DISPLACEMENT OF REAL GROUND MOTIONS (5% DAMPING)

of strong ground shaking. The resulting inelastic response may be misleading. Therefore, results for those motions are not included in this report.

### 3.6 PROPOSED INELASTIC RESPONSE SPECTRA

#### 3.6.1 5% Damping

Based on the results of time history analyses for elasto-plastic systems, new inelastic response ratios for acceleration and displacement can be proposed. For simplicity, all the inelastic response ratios were assumed to have linear relationship with the undamped natural periods on the logarithmic scale between a number of control periods. The control periods, denoted as a, b, c and d, were selected as 0.1, 0.5, 0.7, and 4.0 seconds. The linear regression of minimum squared error was used as a guide, but the final lines were selected by eyeball fitting.

Fig. 3.16 shows the proposed inelastic acceleration response ratios for different ductility levels of 5% damped elasto-plastic systems. The values of inelastic acceleration ratios at the control periods are tabulated in Table 3.3. For convenient interpolation, the inelastic acceleration response ratios are plotted versus the ductility levels for different control periods in Fig. 3.17.

The same line fitting procedures were used for proposing inelastic displacement response ratios. Fig. 3.18 shows the resulting proposed inelastic displacement response ratios for different ductility levels of 5% damped elasto-plastic systems. Note that at control period d, the inelastic displacement ratios are all equal to one, regardless of the different ductility levels. Between control periods b and c, the proposed displacement ratios are rather conservative compared with the actual

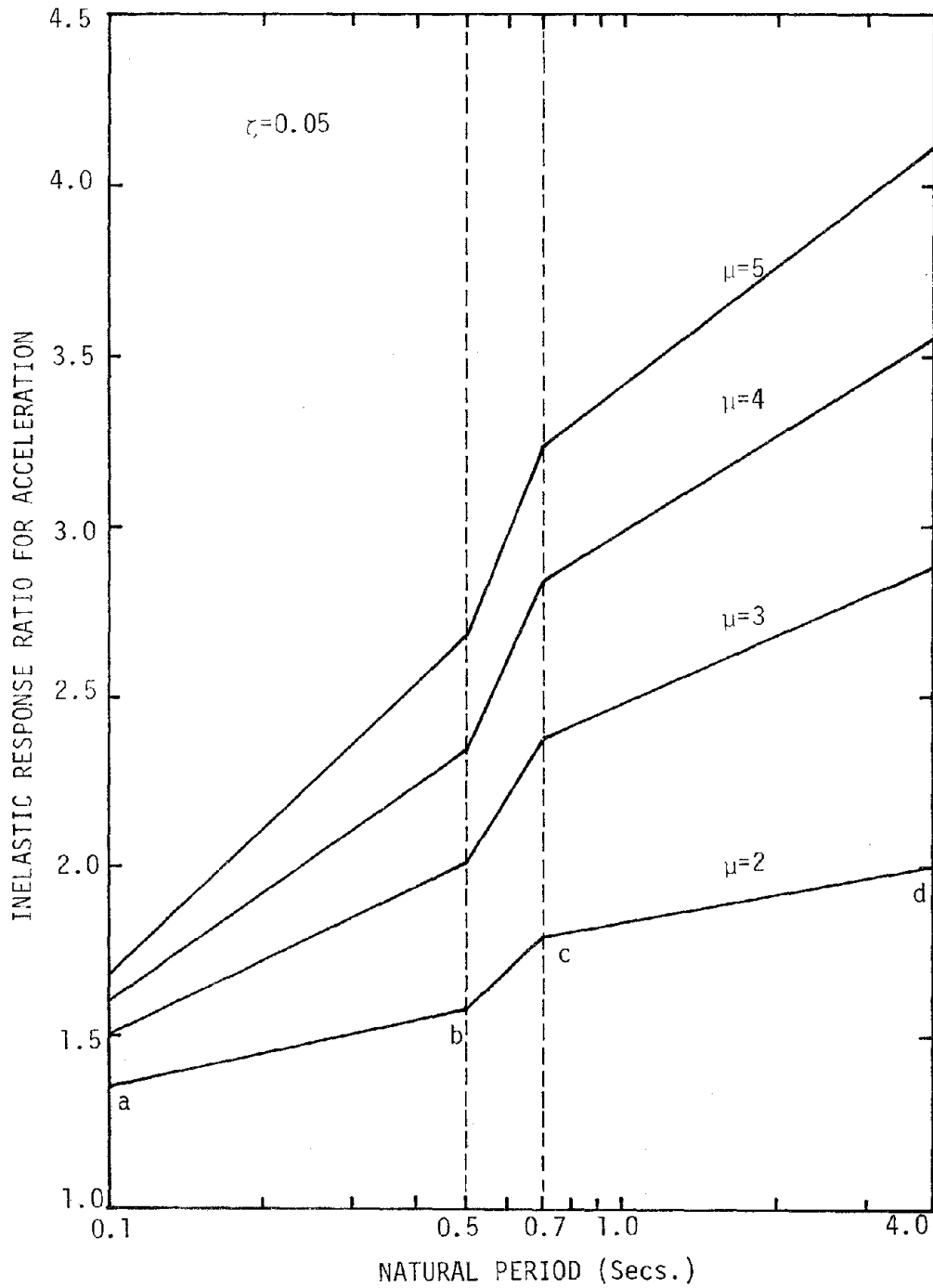


FIG. 3.16 - PROPOSED INELASTIC RESPONSE RATIO FOR ACCELERATION  
(5% DAMPING)

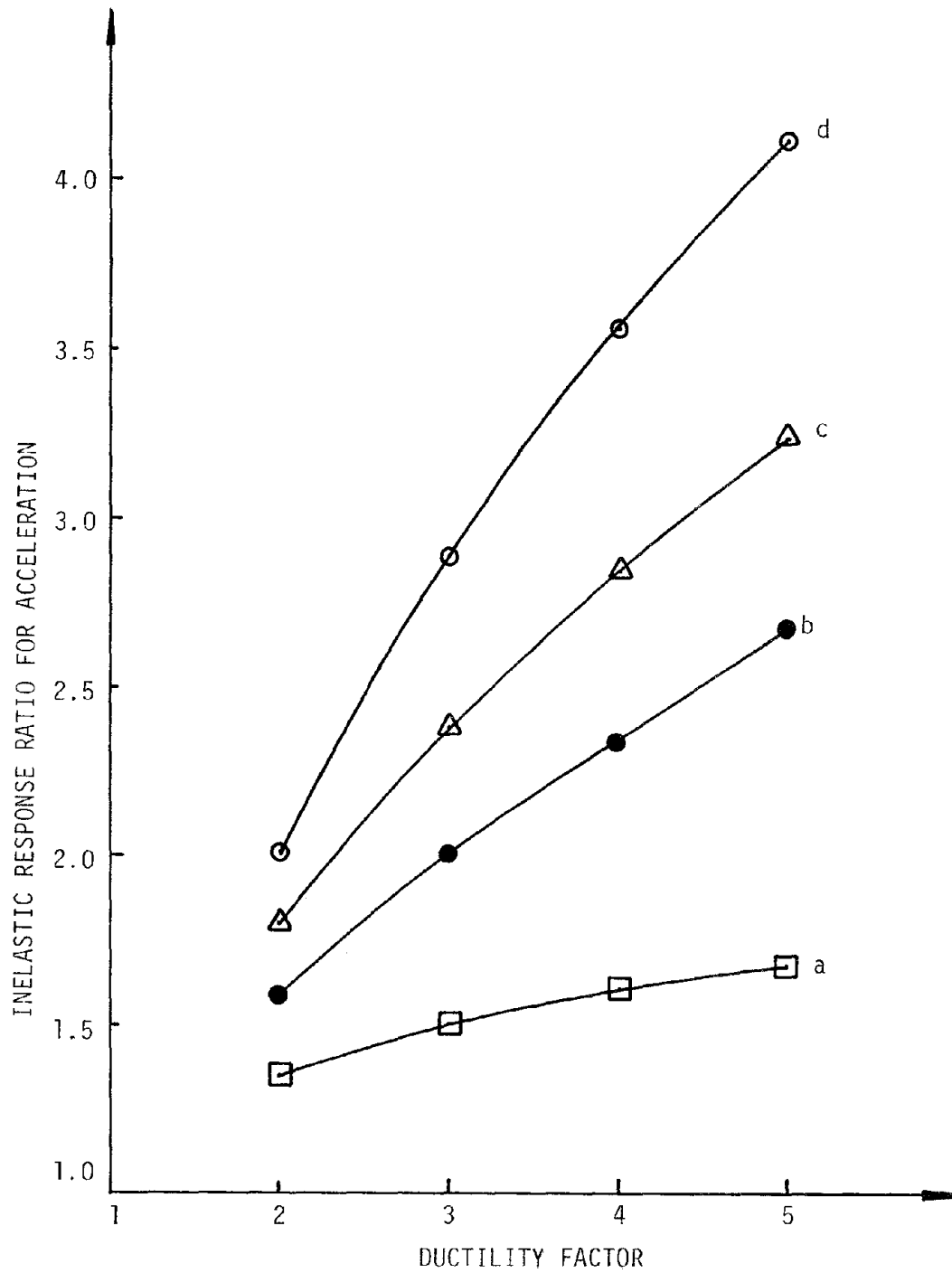


FIG. 3 .17 - PROPOSED INELASTIC RESPONSE RATIO FOR ACCELERATION AT CONTROL POINTS (5% DAMPING)

TABLE 3-3 PROPOSED INELASTIC RESPONSE RATIOS AT CONTROL PERIODS (5% DAMPING)

TYPE OF RATIO	INELASTIC ACCELERATION RESPONSE RATIOS				INELASTIC DISPLACEMENT RESPONSE RATIOS			
	a	b	c	d	a	b	c	d
$\mu = 2$	1.35	1.58	1.80	2.00	0.72	0.90	1.00	1.00
$\mu = 3$	1.50	2.01	2.38	2.88	0.54	0.79	0.89	1.00
$\mu = 4$	1.60	2.34	2.84	3.55	0.44	0.71	0.81	1.00
$\mu = 5$	1.68	2.68	3.24	4.11	0.37	0.65	0.75	1.00

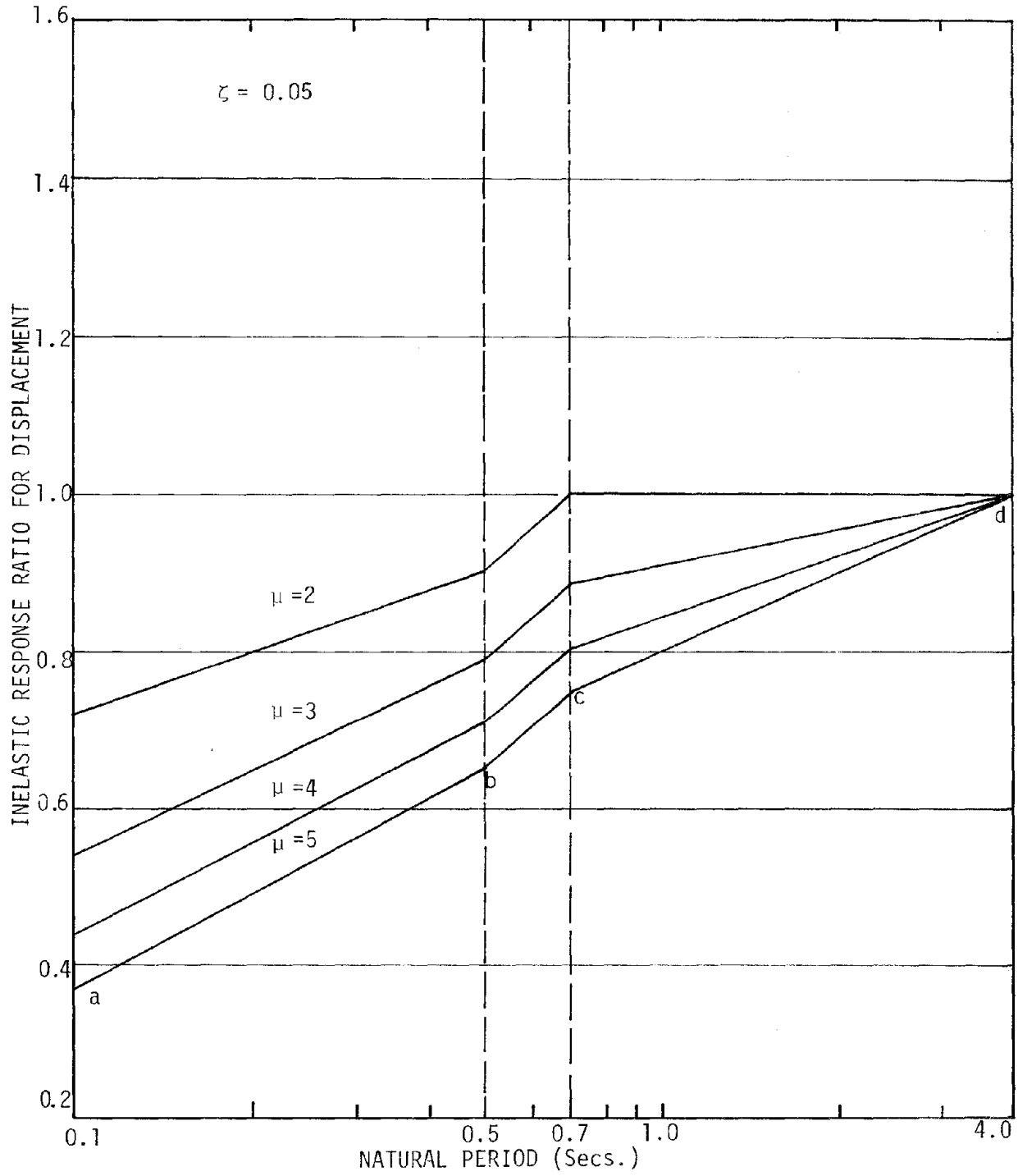


FIG. 3.18 - PROPOSED INELASTIC RESPONSE RATIO FOR DISPLACEMENT (5% DAMPING)

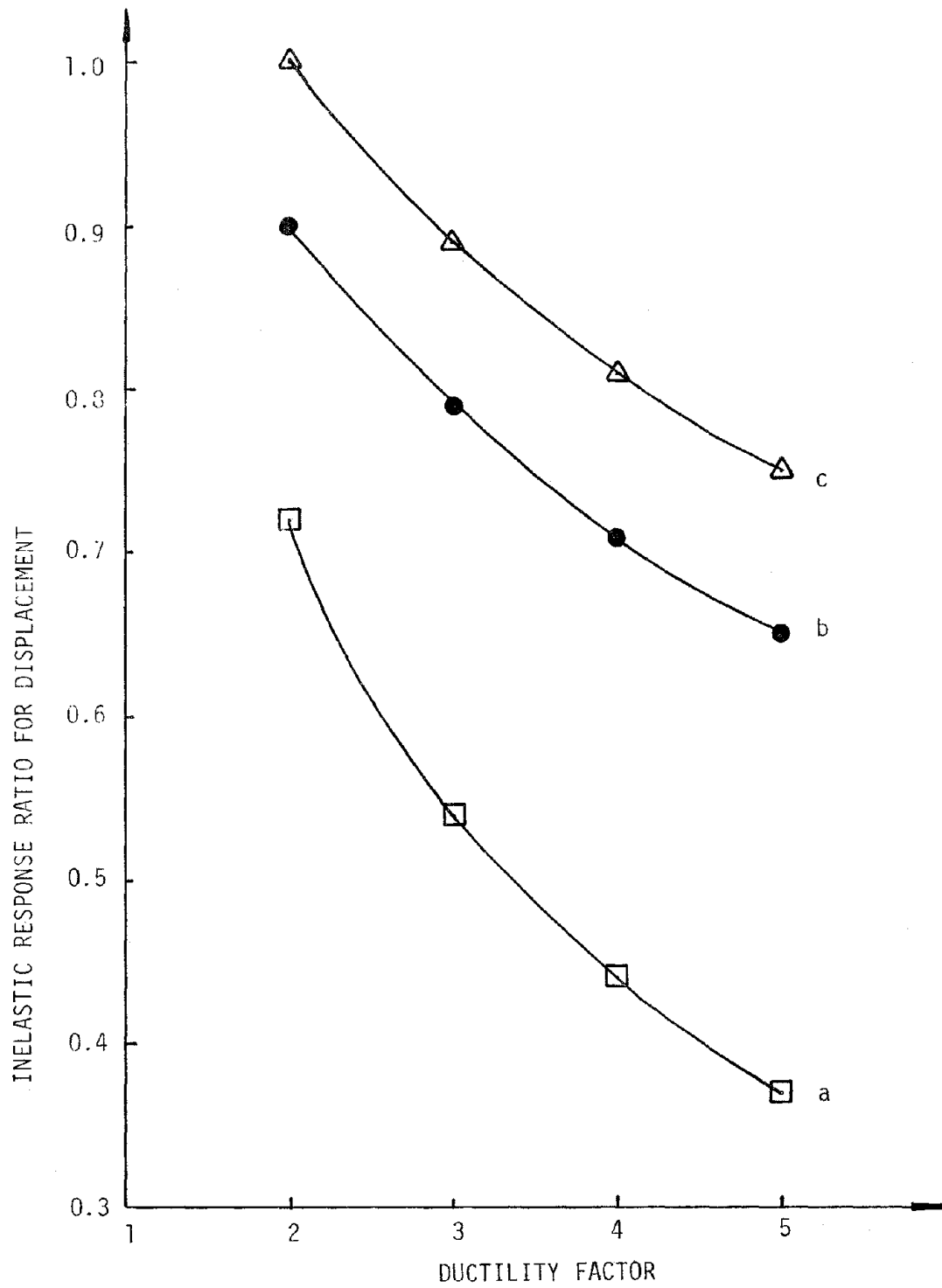


FIG. 3.19 - PROPOSED INELASTIC RESPONSE RATIO FOR DISPLACEMENT AT CONTROL POINTS (5% DAMPING)

mean values. The values of inelastic displacement response ratios at control periods are also tabulated in Table 3.3. In addition, the ratios are plotted versus the ductility levels at different control periods in Fig. 3.19.

Based on the proposed new inelastic response ratios, one can also calculate the corresponding inelastic response spectra. Figs. 3.20, 3.21 and 3.22 show the resulting inelastic response spectra for  $\mu=2$ , 4 and 5 respectively. The Newmark elastic and inelastic response spectra are also shown in the figures for easy comparison. As shown in Fig. 3.20, the proposed inelastic displacement response spectrum for  $\mu=2$  is almost the same as Newmark's. For inelastic acceleration response spectra, the proposed one predicts a little higher response than Newmark's. However, the difference is more pronounced with increasing ductility. For example, as shown in Fig. 3.22, the proposed inelastic response spectra are much greater than those of Newmark ( $\mu=5$ ). In the intermediate natural period range, the proposed inelastic displacement responses are greater than those of the Newmark approach by 33%, while the proposed inelastic acceleration responses are even 68% greater than those of the Newmark responses.

In summary, the new proposed inelastic response spectra predict greater elasto-plastic responses than the Newmark spectra. The inelastic response spectra for  $\mu=4$  and 5% damping as shown in Fig. 3.21 will be the basis for inelastic response spectra-based modal analyses presented in Chapter 5.

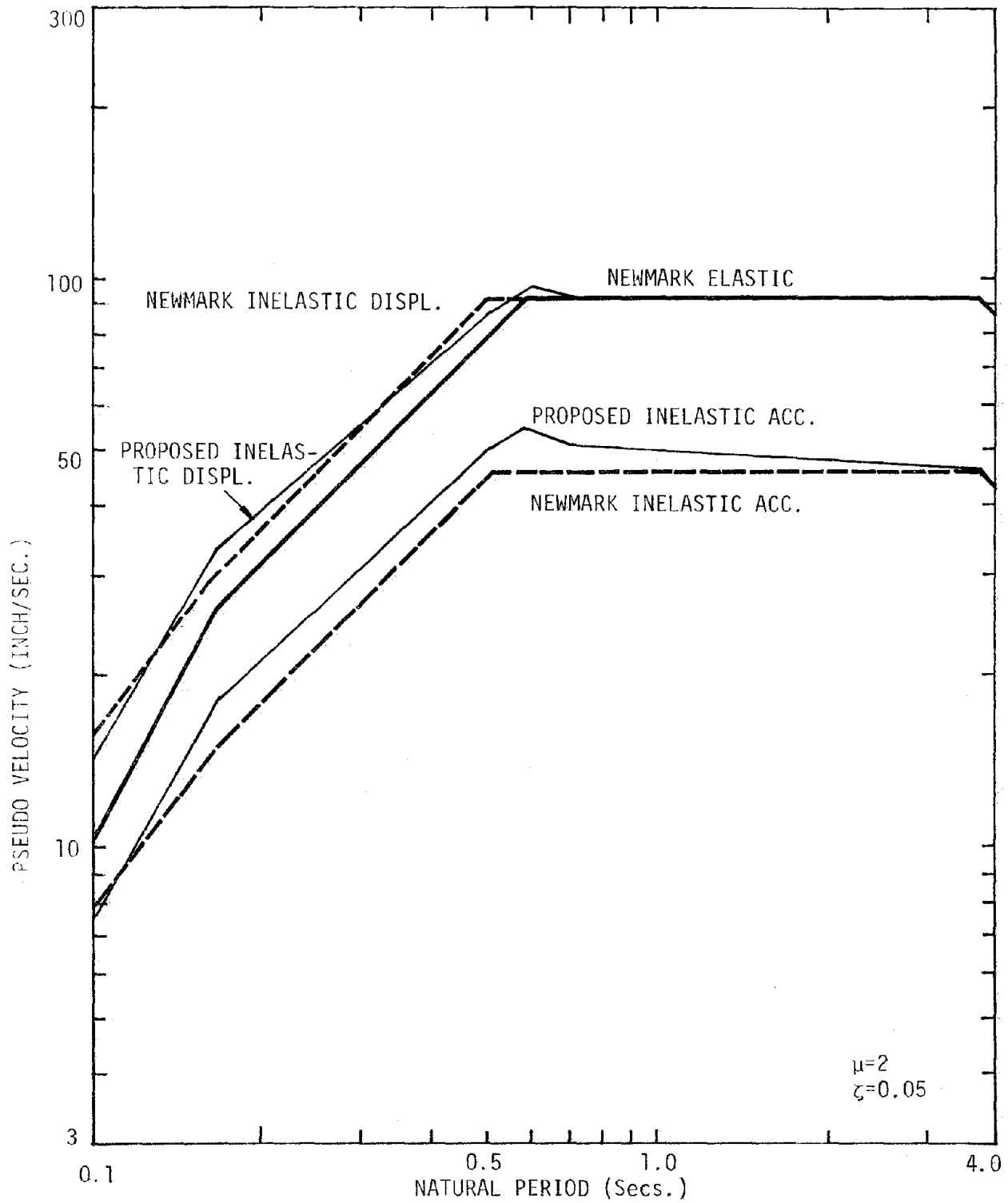


FIG. 3.20 - PROPOSED INELASTIC RESPONSE SPECTRA (5% DAMPING,  $\mu=2$ )

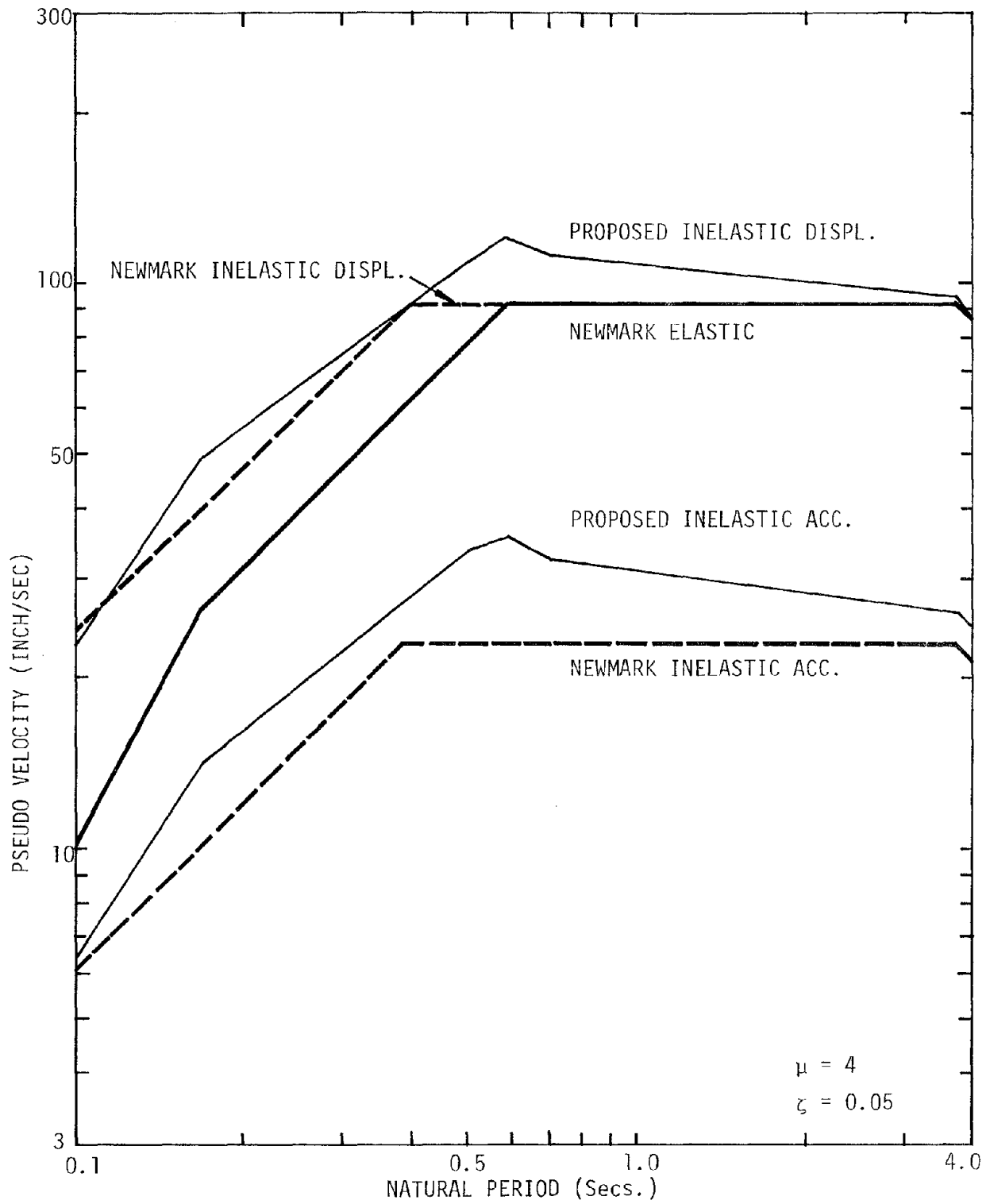


FIG. 3.21 - PROPOSED INELASTIC RESPONSE SPECTRA (5% DAMPING,  $\mu = 4$ )

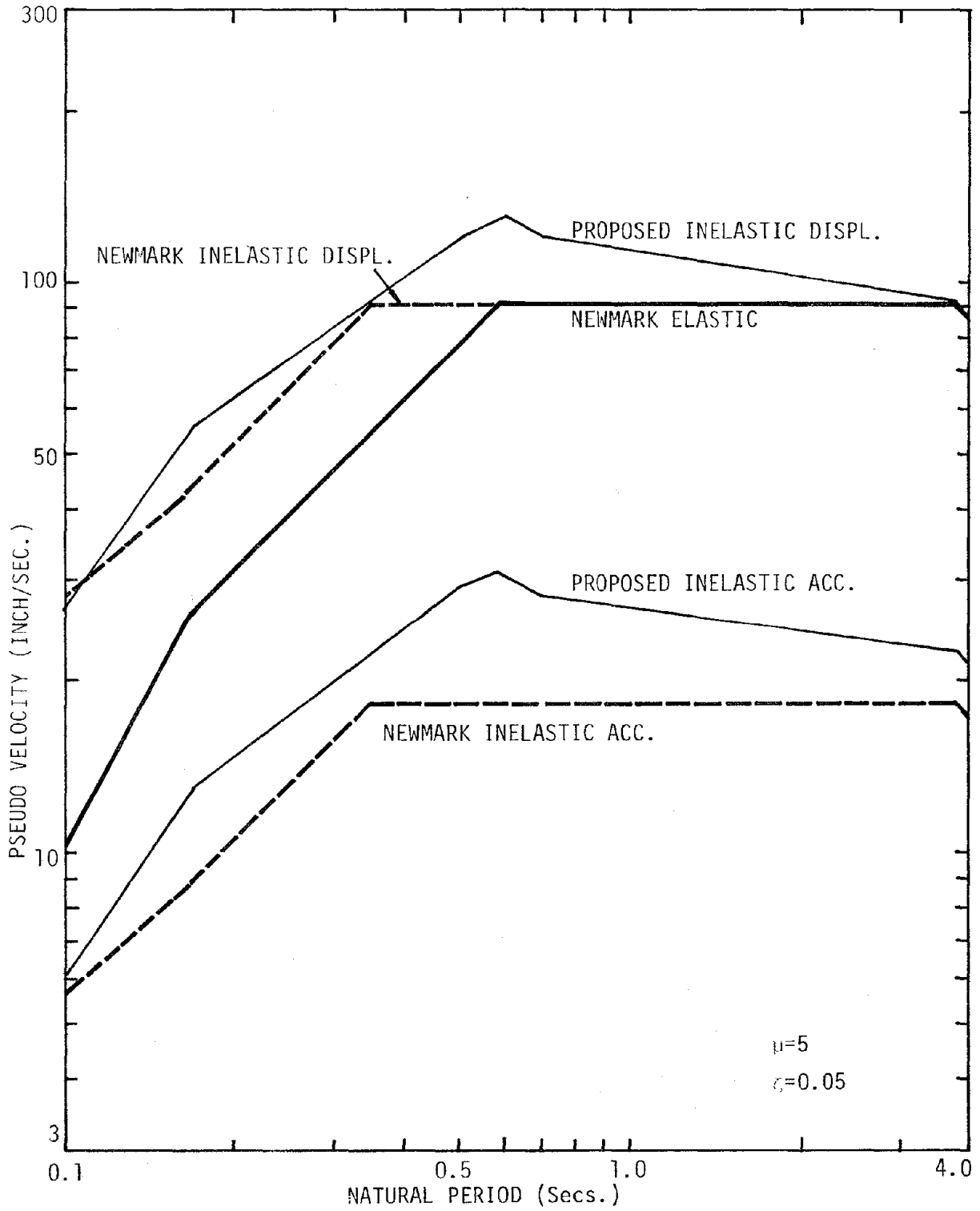


FIG. 3.22 - PROPOSED INELASTIC RESPONSE SPECTRA (5% DAMPING,  $\mu=5$ )

### 3.6.2 2% Damping

The same line fitting procedures have been applied to proposed new inelastic response ratios for 2% damped systems. Fig. 3.23 shows the proposed inelastic acceleration response ratios for 2% damped elasto-plastic systems. The control natural periods were kept the same as in the case of 5% damping. In comparison with the Newmark inelastic acceleration response ratios for 2% damping as in Fig. 3.11, the proposed ratios are generally greater than those of the Newmark approach, especially in the high natural period range. The values of the inelastic acceleration response ratios at control periods are tabulated in Table 3-4. For easy interpolation, the inelastic acceleration response ratios are plotted versus the ductility levels for different control periods in Fig. 3.24.

The proposed inelastic displacement response ratios for 2% damped elasto-plastic systems are shown in Fig. 3.25. Note that in the intermediate and high natural period range, the displacement ratios are greater than one. In fact, the ratios equal 1.2. This indicates that the principle of energy conservation is not valid in higher period ranges as mentioned earlier in section 3.4.3. The values of the inelastic displacement response ratios at the control periods are tabulated also in Table 3-4. The ratios are plotted versus the ductility levels at different control periods in Fig. 3.26.

The corresponding inelastic response spectra for  $\mu=2,5$  of 2% damped elasto-plastic systems are shown in Figs. 3.27 and 3.28, respectively. The Newmark elastic and inelastic response spectra are also shown in the figures for easy comparison. In the high natural period

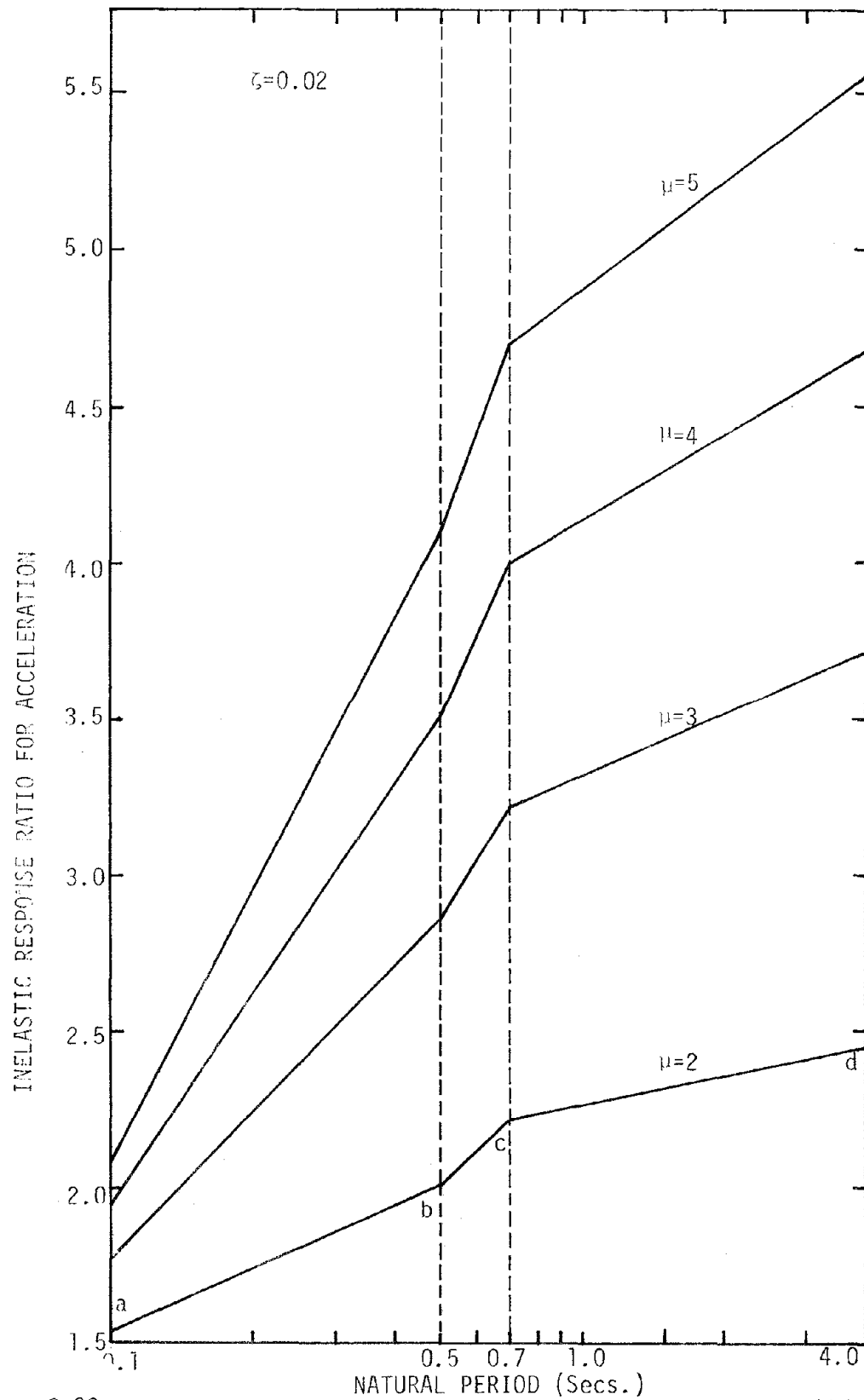


FIG. 3.23 - PROPOSED INELASTIC RESPONSE RATIO FOR ACCELERATION (2% DAMPING)

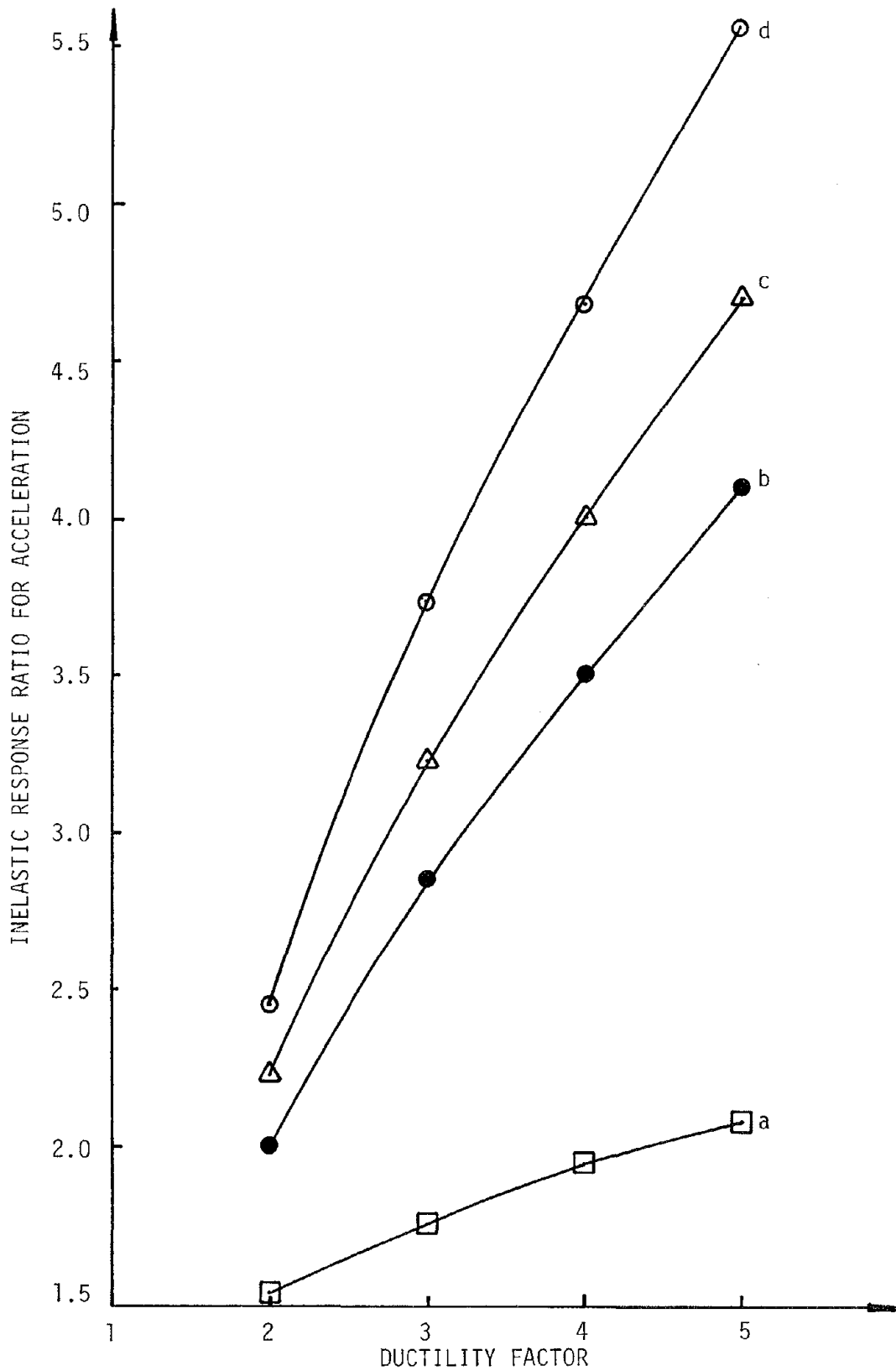


FIG. 3.24 - PROPOSED INELASTIC RESPONSE RATIO FOR ACCELERATION AT CONTROL POINTS (2% DAMPING)

TABLE 3-4 PROPOSED INELASTIC RESPONSE RATIOS AT CONTROL PERIODS (2% DAMPING)

TYPE OF RATIO	INELASTIC ACCELERATION RESPONSE RATIO				INELASTIC DISPLACEMENT RESPONSE RATIO			
	a	b	c	d	a	b	c	d
$\mu = 2$	1.53	2.00	2.22	2.45	0.79	1.08	1.20	1.20
$\mu = 3$	1.76	2.85	3.22	3.72	0.61	0.98	1.10	1.20
$\mu = 4$	1.94	3.50	4.00	4.68	0.51	0.91	1.03	1.20
$\mu = 5$	2.07	4.10	4.70	5.56	0.43	0.86	0.98	1.20

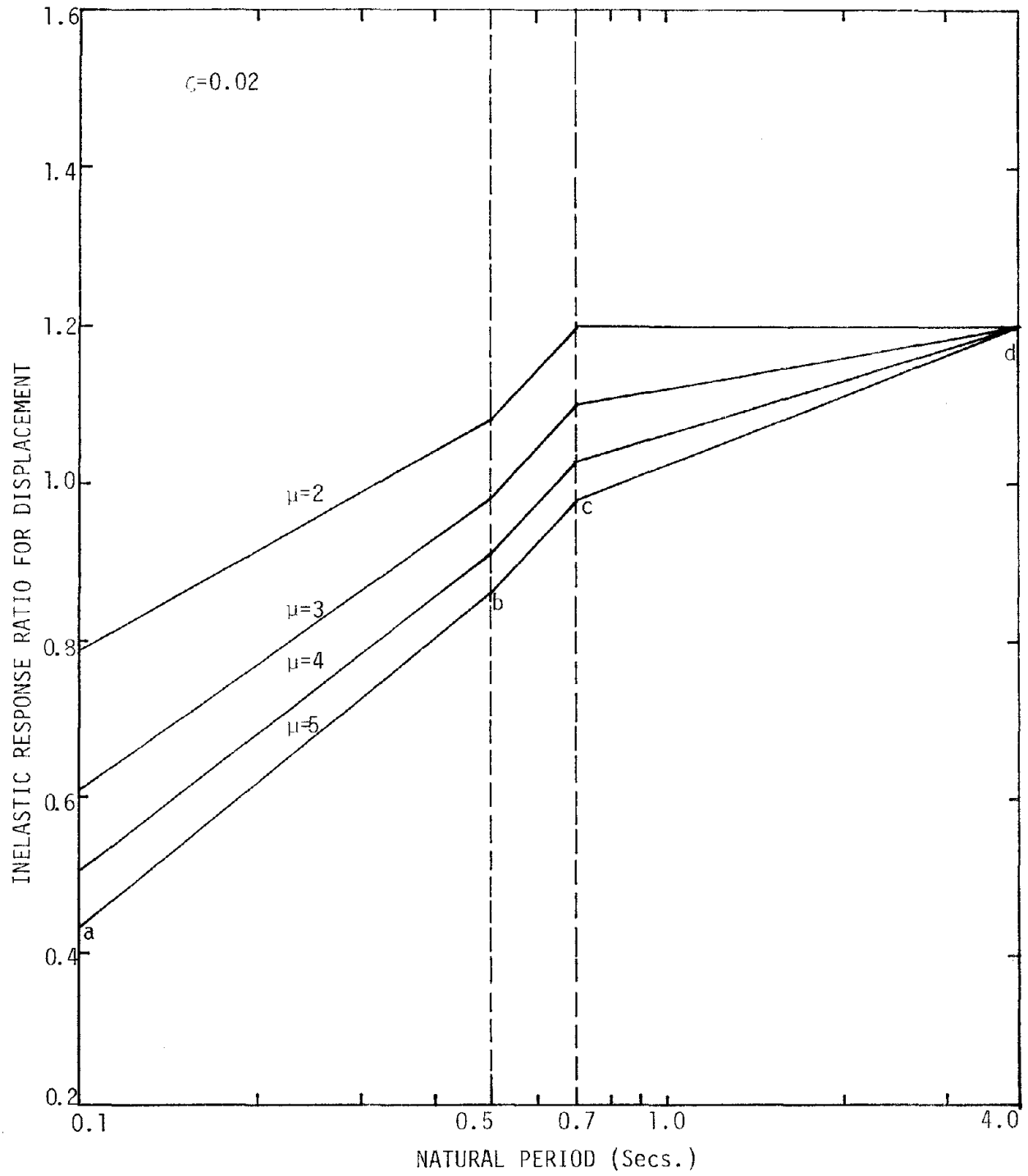


FIG. 3.25 - PROPOSED INELASTIC RESPONSE RATIO FOR DISPLACEMENT  
(2% DAMPING)

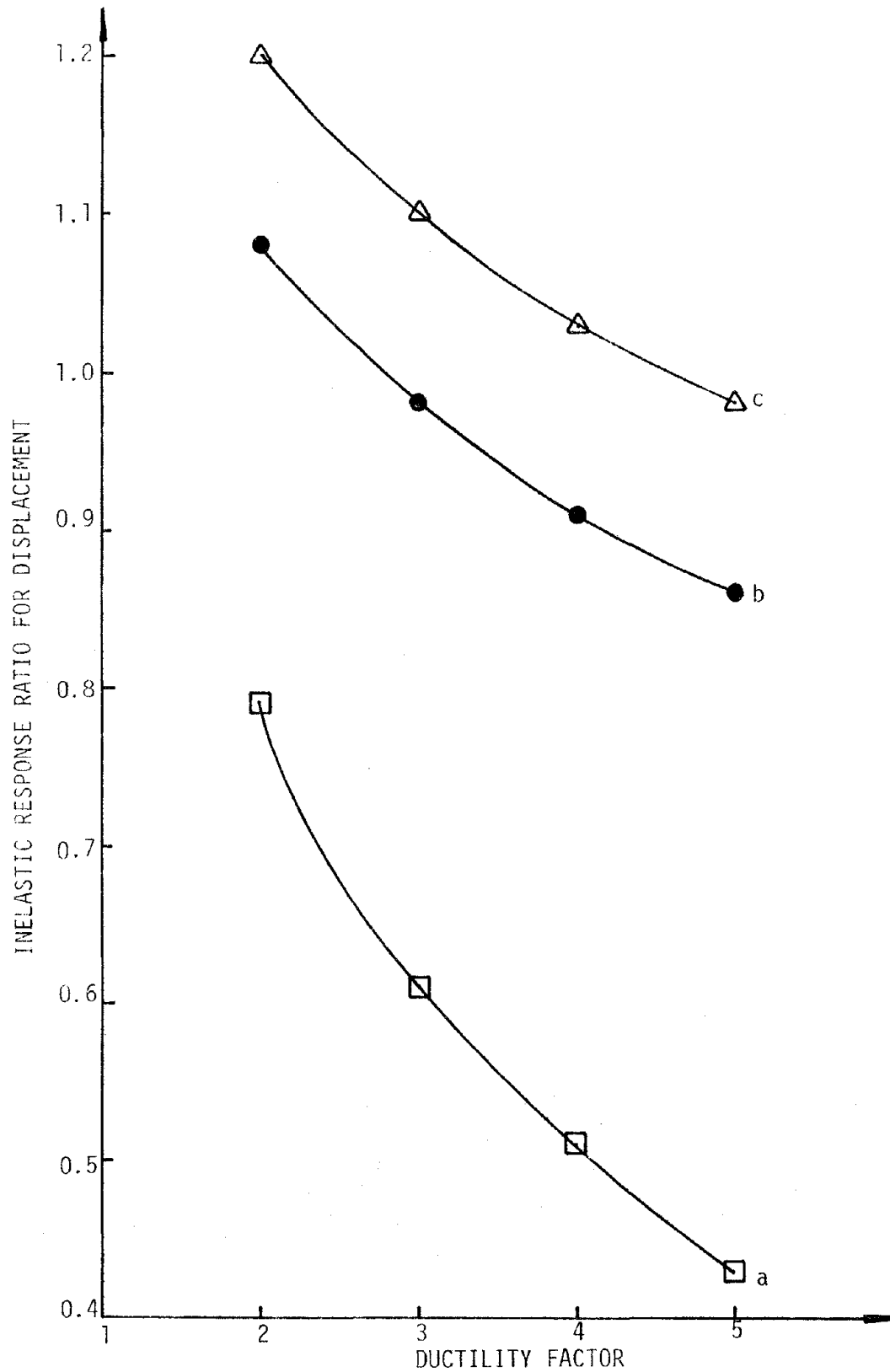


FIG. 3.26 - PROPOSED INELASTIC RESPONSE RATIO FOR DISPLACEMENT AT CONTROL POINTS (2% DAMPING)

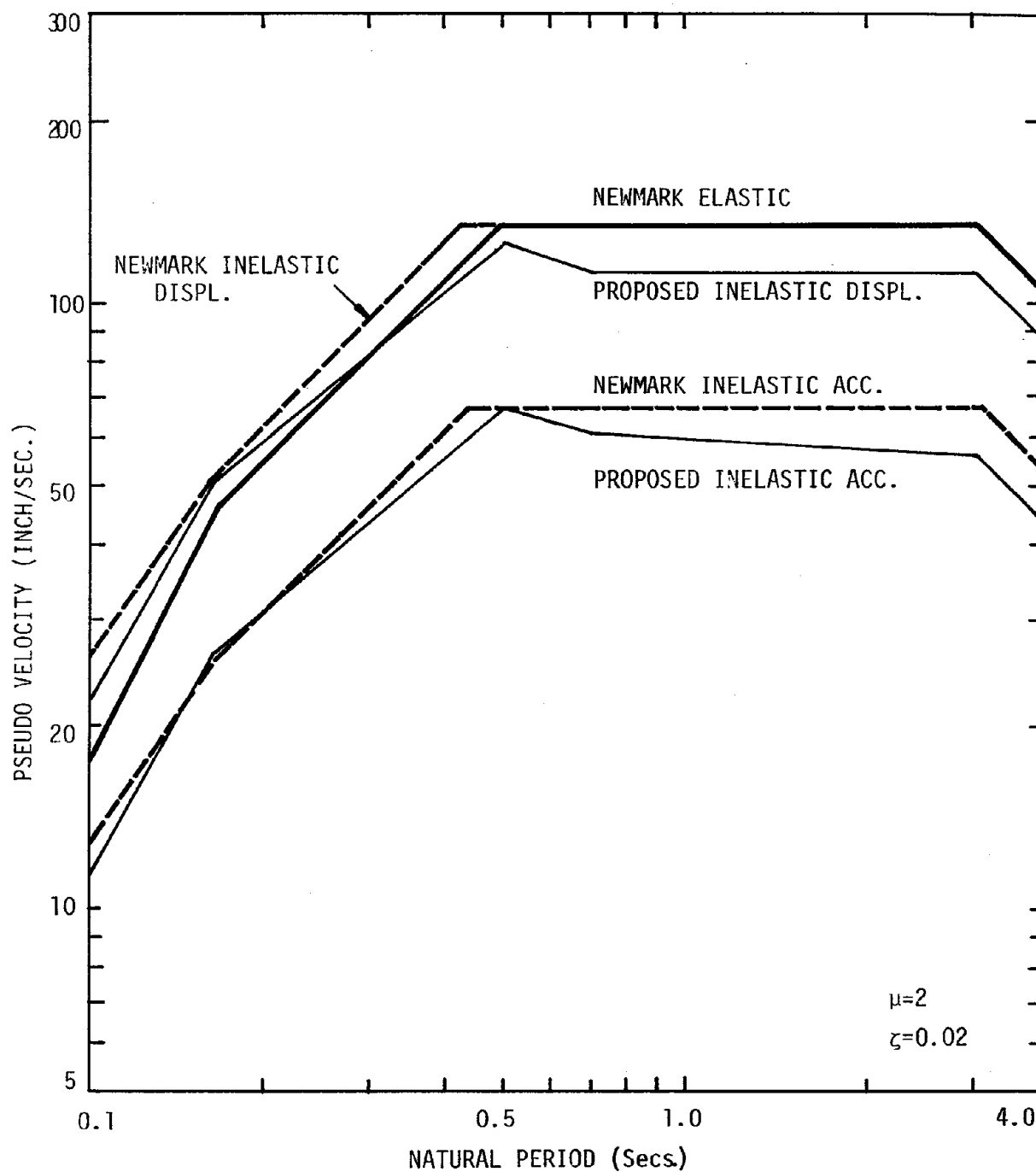


FIG. 3.27 - PROPOSED INELASTIC RESPONSE SPECTRA  
(2% DAMPING,  $\mu = 2$ )

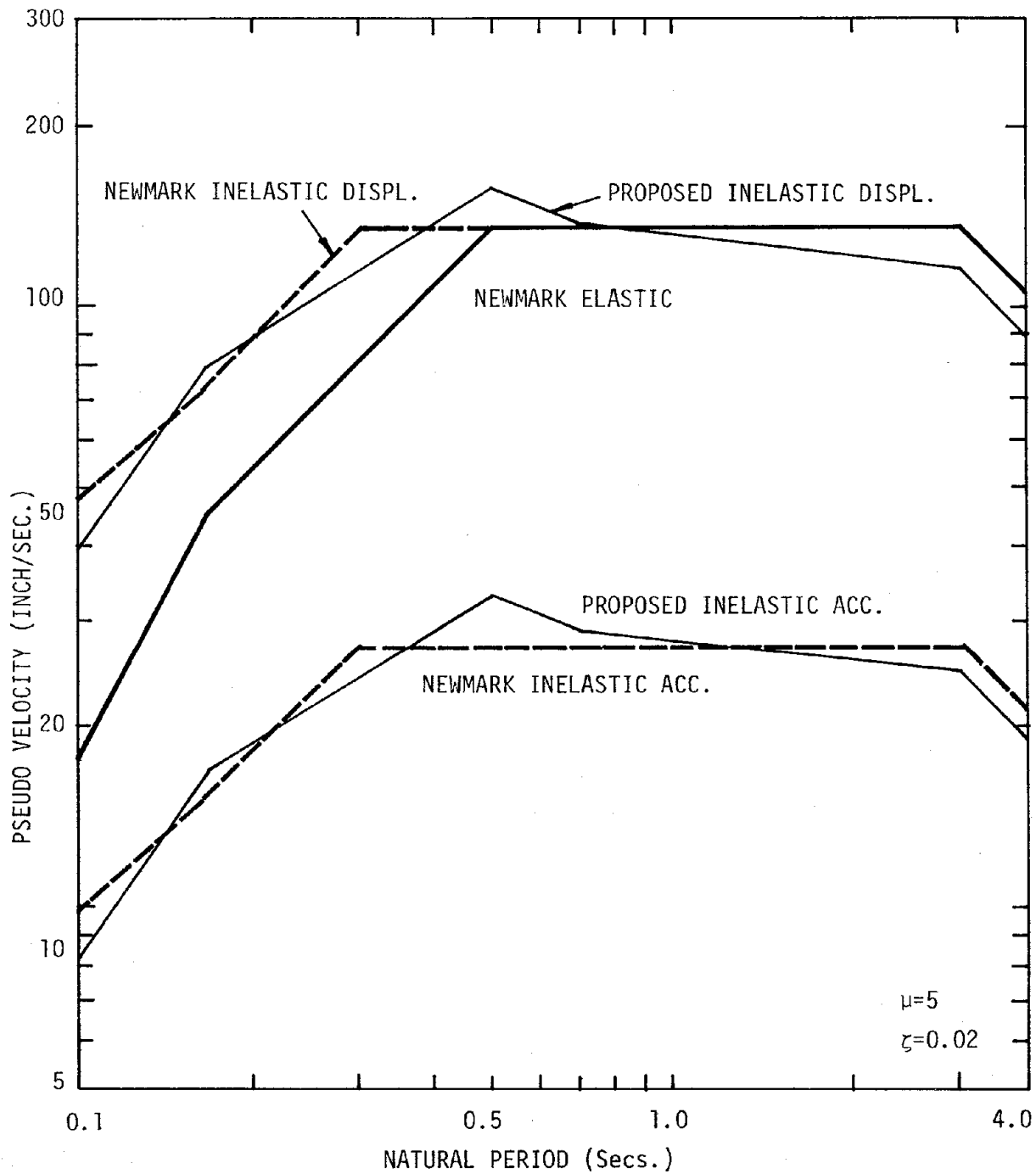


FIG. 3.28 - PROPOSED INELASTIC RESPONSE SPECTRA  
(2% DAMPING,  $\mu = 5$ )

range, the discrepancies between the proposed and the Newmark spectra are more pronounced for  $\mu=2$ . In the low natural period range, the proposed inelastic response spectra match those of Newmark nicely.

In summary, the proposed inelastic response spectra are generally smaller than those of the Newmark approach. This suggests that the Newmark inelastic response spectra predict conservative elasto-plastic responses for 2% damped systems. The conservatism will increase with the decrease in ductility level.

### 3.7 SUMMARY

Sets of duration-dependent artificial strong ground motions were generated. Time history analyses for a series of elasto-plastic SDOF systems subjected to artificial motions were performed. From the results, it can be concluded that the inelastic responses are not significantly dependent on strong ground motion duration. However, the conclusion is valid only when the artificial motions have approximately the same level of elastic response. It has also been shown that the conventional ductility factor is not a pertinent measure for structural damage. The newly proposed "cumulative yielding ductility," on the other hand, is a potential measure, for it reveals the strong motion duration dependency of inelastic action.

Results in terms of "inelastic response ratios" of the inelastic responses calculated by time history analyses and those predicted by the Newmark approach were compared. It can be concluded that the Newmark prediction of inelastic response is unconservative for 5% damped elasto-plastic systems, and is conservative for 2% damped systems. Hence, new

inelastic response spectra for acceleration and displacement have been proposed. The new spectra will be the basis for response-spectra-based modal analysis of structural frames in Chapter 5.

# CHAPTER 4

## INELASTIC RESPONSE PREDICTED BY RANDOM VIBRATION

### 4.1 INTRODUCTION

As mentioned in Chapter 2, it is possible to predict the peak displacement of elasto-plastic systems using random vibration theory. Fig. 4.1 shows four power spectral density functions corresponding to the Newmark basic design response spectrum for 5% damping. Each PSD function relates to a different strong ground motion duration, i.e.,  $S = 10, 20, 30, 40$  seconds respectively. These PSD's will be the basis for the analyses in this Chapter.

One objective of the analyses is to calculate the average amount of elasto-plastic deformation  $\delta$ . As shown in Eq. (2-16),  $\delta$  is a function of  $r$  and  $\sigma_y$ .  $r$  is the ratio between the yielding level  $U_e$  and the standard deviation  $\sigma_y$  of the response of associated elastic systems. For high thresholds, based on Karnopp-Scharton (13) and confirmed by Yanev's simulation studies (26) for white noise Gaussian excitation,  $\delta$  takes the following form:

$$\delta = \frac{\sigma_y^2}{2U_e} = \frac{\sigma_y}{2r} . \quad (4-1)$$

All previous analyses concerning random vibration applied to SDOF elasto-plastic systems by Vanmarcke and associates (21, 22, 24, 26), and to MDOF systems by Gazetas (11) were based on Eq. (4-1).

However, in this study, from the simulation studies based on the results of time history analysis, Eq. (4-1) is found to be valid only when the system "r value" is greater than 2. This means the relationship is true only when the system has a high yielding level  $U_e$  or a high resistance function  $R_m$ , compared with the response of the associated linear system. As will be shown later, for the range of ductilities of interest, i.e.,  $\mu = 2 \sim 5$ , the implied value of r will generally be less than 2. In fact, it may lie anywhere between 0.2 and 2, and it is often close to the lower value. Note that Eq. (4-1) tends to predict very high values of  $\delta$  when r approaches zero. Therefore, a new relationship of  $\delta$  versus r is needed, and it will be determined in a semi-empirical way in this chapter.

## 4.2 MODIFICATIONS OF RANDOM VIBRATION MODEL

### 4.2.1 Transient Effect

When the natural period of the system is long, the steady-state solution presented in Chapter 2 will never be approached. This is especially true when the damping of the system is relatively small. The response variance will build up from zero to the maximum value near the end of the motion duration. Vanmarcke (22) has suggested an "equivalent stationary response duration  $S_0$ ," which is a fraction of the input strong ground motion duration:

$$S_0 = S \cdot \exp [-2(m-1)] \quad (4.2)$$

where

$$m = \frac{\sigma_y^2(S)}{\sigma_y^2(S/2)}$$

$$= \frac{1 - e^{-2\zeta\omega_n S}}{1 - e^{-\zeta\omega_n S}}$$

In the limit, when  $\zeta\omega_n S$  approaches  $\infty$ ,  $m = 1$ , and  $S_0 = S$ ; when  $\zeta\omega_n S = 0$ ,

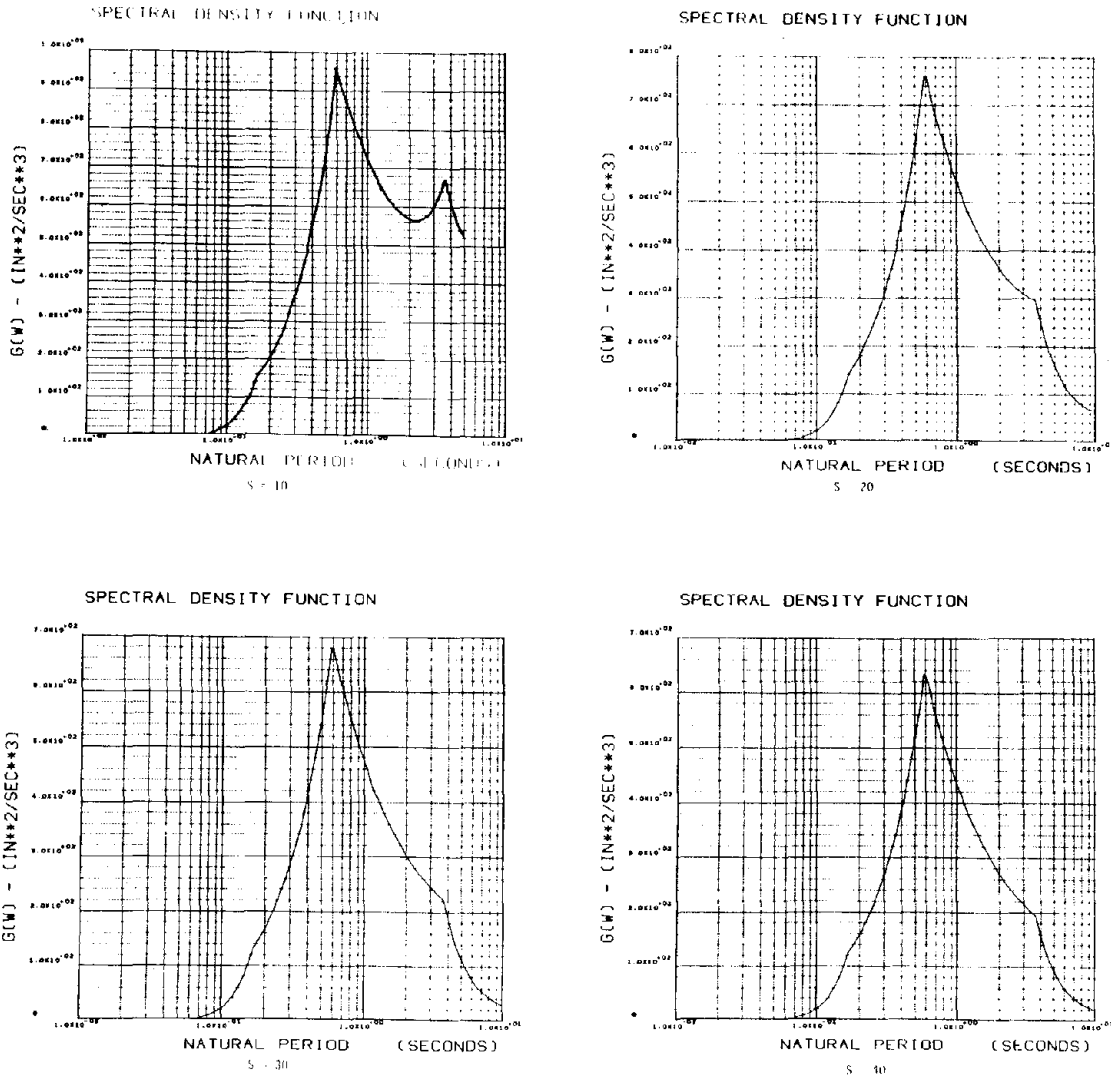


FIG. 4.1 - POWER SPECTRAL DENSITY FUNCTIONS FOR  
 $S = 10, 20, 30, 40$  SECONDS

$m = 2$  and  $S_0 \approx 0.15S$ .

Moreover, for non-stationary SDOF response, a fictitious time-dependent damping parameter  $\zeta_t$  is used (22):

$$\zeta_t = \frac{\zeta}{1 - e^{-2\zeta\omega_n t}} \quad (4-3)$$

Both of the above-mentioned modifications with regard to non-stationalities of the response were incorporated in this study. Eq. (2-25) now becomes

$$d = \delta \left\{ \ln [1 - \exp (\mu_a S_0)] - \ln (- \ln P) \right\} \quad (4-4)$$

where  $d$  is the amount of inelastic displacement with probability  $P$  of not being exceeded.

#### 4.2.2 Expected Inelastic Peak Displacement

With the PSD's as in Fig. 4.1, it is possible to predict the inelastic displacement for a probability level  $P$  of not being exceeded. 50% was used as the probability level in this study. For a given natural period and ductility demand of SDOF elasto-plastic systems, the corresponding resistance function  $R_m$  can be determined directly from the results of time history analysis. With this information, a backfigured value can be computed from the random vibration analysis. The back-figured  $\delta$  value is denoted as  $\delta^*$ . From Eq. (4-1), the original  $\delta$  value can also be calculated for the same system. By comparing the two  $\delta$  values, namely  $\delta$  and  $\delta^*$ , information of the  $r$ -dependent relationship of inelastic response can be obtained.

A set of systems has been selected for this study. It comprises ten natural periods varying from 0.1 to 7.0 seconds. Each natural period has four different levels of resistance functions corresponding to  $\mu = 2, 3, 4$  and  $5$ . In other words, a total of 40 systems subjected to four motions with different strong ground motion durations were studied. Since results for  $S = 20, 30,$  and  $40$  seconds are quite similar, only results for  $S = 10$  and  $20$  seconds are presented and compared.

The values of  $\delta^*$  can be normalized to  $\delta$ . The resulting relationships between  $\delta^*/\delta$  and  $r$  are plotted in Fig. 4.2. As shown in the figure, the two variables,  $r$  and  $\delta^*/\delta$ , are significantly correlated. Note that results for  $S = 10$  seconds are generally greater than those corresponding to  $S = 20$  seconds. However, the results do tend to suggest a unique relationship between  $\delta^*/\delta$  and  $r$ . Since  $\delta$  equals  $\sigma_y/2r$ , values of the corresponding ratio  $\delta^*/\sigma_y$  can be plotted versus  $r$ . The relationships are shown in Fig. 4.3. The results of simulation studies for white noise Gaussian excitations by Yanev (26) are also shown in the figure. Notice that these data are on the high side compared with the time-history-based simulated results in this study.

A linear relationship between  $\delta^*/\delta$  and  $r$  was first assumed. This implies a lack of dependence of  $\delta^*$  on  $r$  since  $\delta$  is inversely proportional to  $r$ . A fitted straight line with slope 0.4 in Fig. 4.2 (dash line) was tested. This corresponds to a constant  $\delta^*$  value in Fig. 4.3. A different fit leads to a quadratic relationship in Fig. 4.2 (solid line), which implies a linear relationship between  $\delta^*$  and  $r$  in Fig. 4.3. Based on either of these relationships, inelastic deformation can be predicted. The results are quite satisfactory in both cases and will be presented in the next section. The constant  $\delta^*/\sigma_y$  relationship tends to overestimate inelastic response when  $r$  is large, but it is somewhat simpler. Therefore, both relationships are proposed as reasonable approximations for use in inelastic one-degree response prediction:

$$\delta^* = 0.2 \sigma_y \quad (4-5)$$

$$\delta^* = (0.25 - 0.03r) \sigma_y \quad (4-6)$$

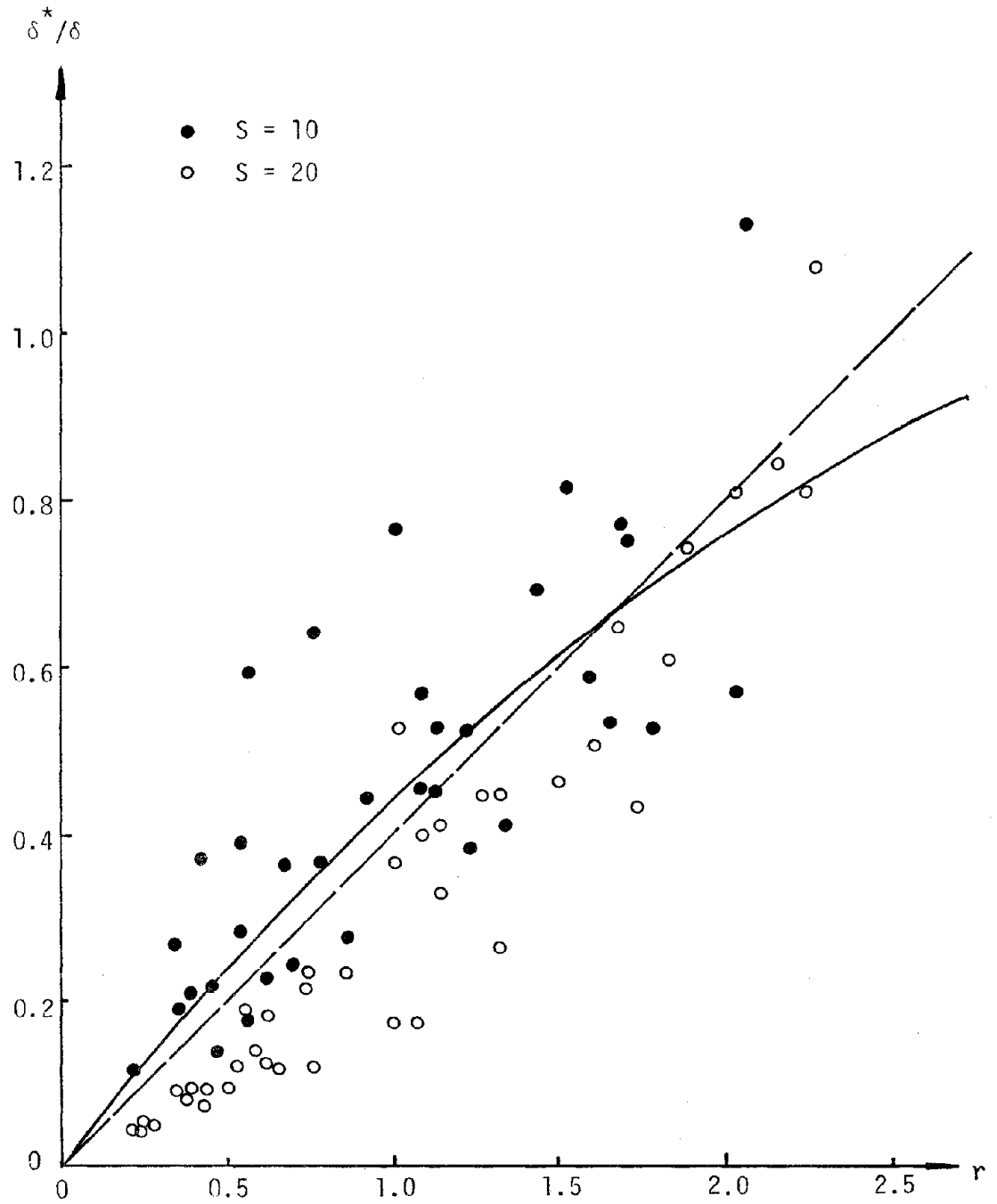


FIG. 4.2 - COMPARISON OF SIMULATED AND THEORETICAL VALUES FOR AVERAGE AMOUNT OF INELASTIC DISPLACEMENT VERSUS THRESHOLD LEVELS  $r$ .

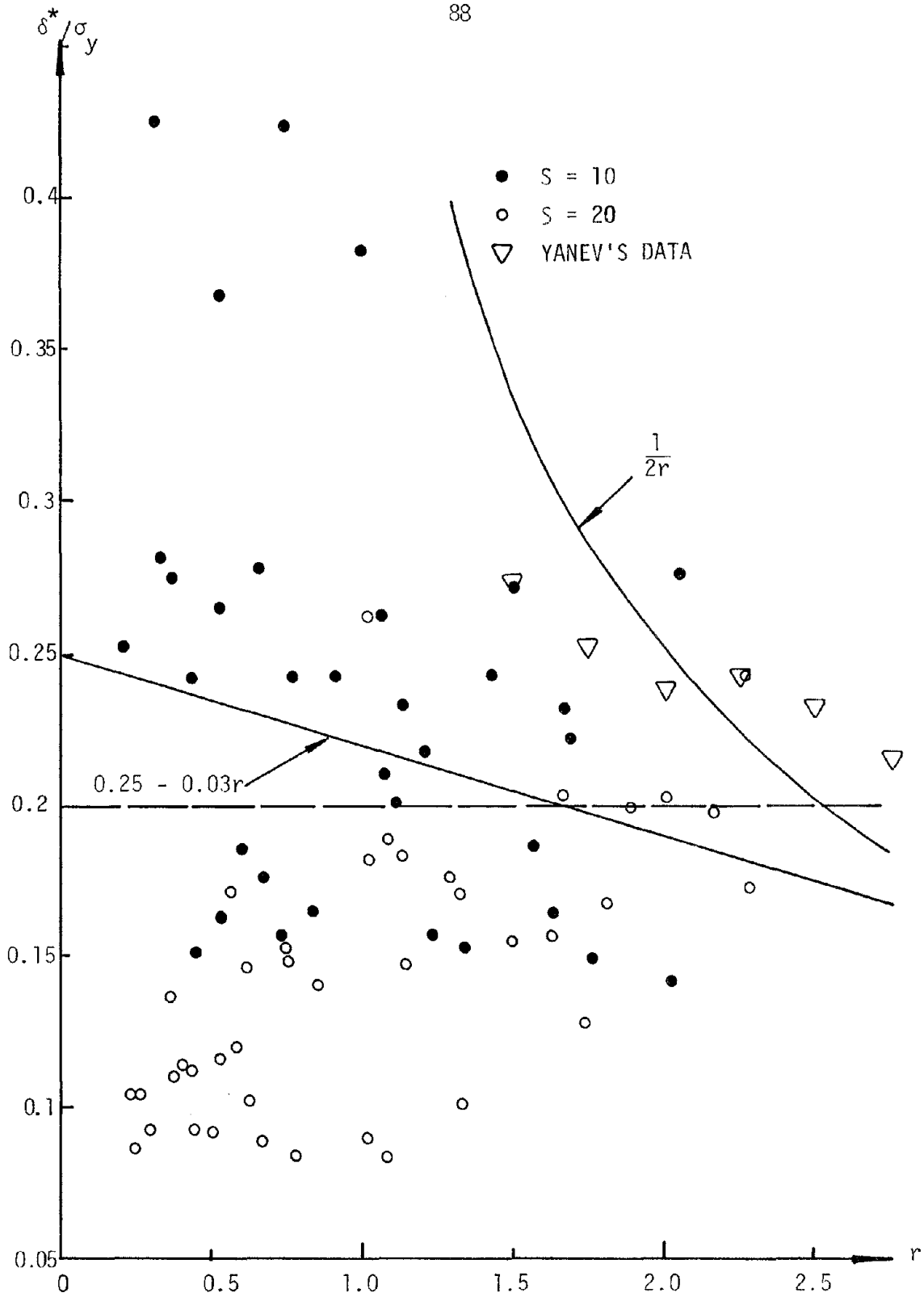


FIG. 4.3 - COMPARISON OF SIMULATED AND THEORETICAL VALUES FOR  $\delta^*/\sigma_y$  VERSUS THRESHOLD LEVELS  $r$

Eq. (4-4) becomes

$$d = \delta^* \left\{ \ln [1 - \exp (\mu_a S_0)] - \ln (- \ln P) \right\} \quad (4-7)$$

The relationship of Eq. (4-1) is also plotted in Fig. 4-3. Notice that when  $r$  is large, the value of  $\delta^*/\sigma_y$  calculated by Eq. (4-6) is approaching that predicted by Eq. (4-1) within the range of the data. Hence, this semi-empirical relationship is not incompatible with the original relationship as expressed in Eq. (4-1) for higher thresholds.

### 4.3 RESULTING INELASTIC RESPONSE RATIOS

Based on the modifications mentioned in the previous section, inelastic response ratios can be calculated for different strong motion durations. The resulting inelastic response ratios of displacement for  $S = 20$  seconds are shown in Fig. 4.4. Notice that the ratios decrease with increasing ductility factors. The abrupt changes of the ratios in the figure are due to the abrupt changes in the power spectral density function which corresponds to the Newmark elastic response spectrum.

Comparison with the mean inelastic displacement response ratios obtained from time history analysis indicates that the results by random vibration are generally very satisfactory. This is also true for mean inelastic acceleration response ratios, which, as shown next, can be approximately derived from the inelastic displacement response ratios.

Fig. 4.5 shows a typical force-displacement relationship for elasto-plastic SDOF systems. The inelastic response ratio for displacement can be expressed as:

$$\text{displacement ratio} = \frac{U_e^*}{U_{\max}} = \frac{U_e^*}{\mu U_e} \quad (4-8)$$

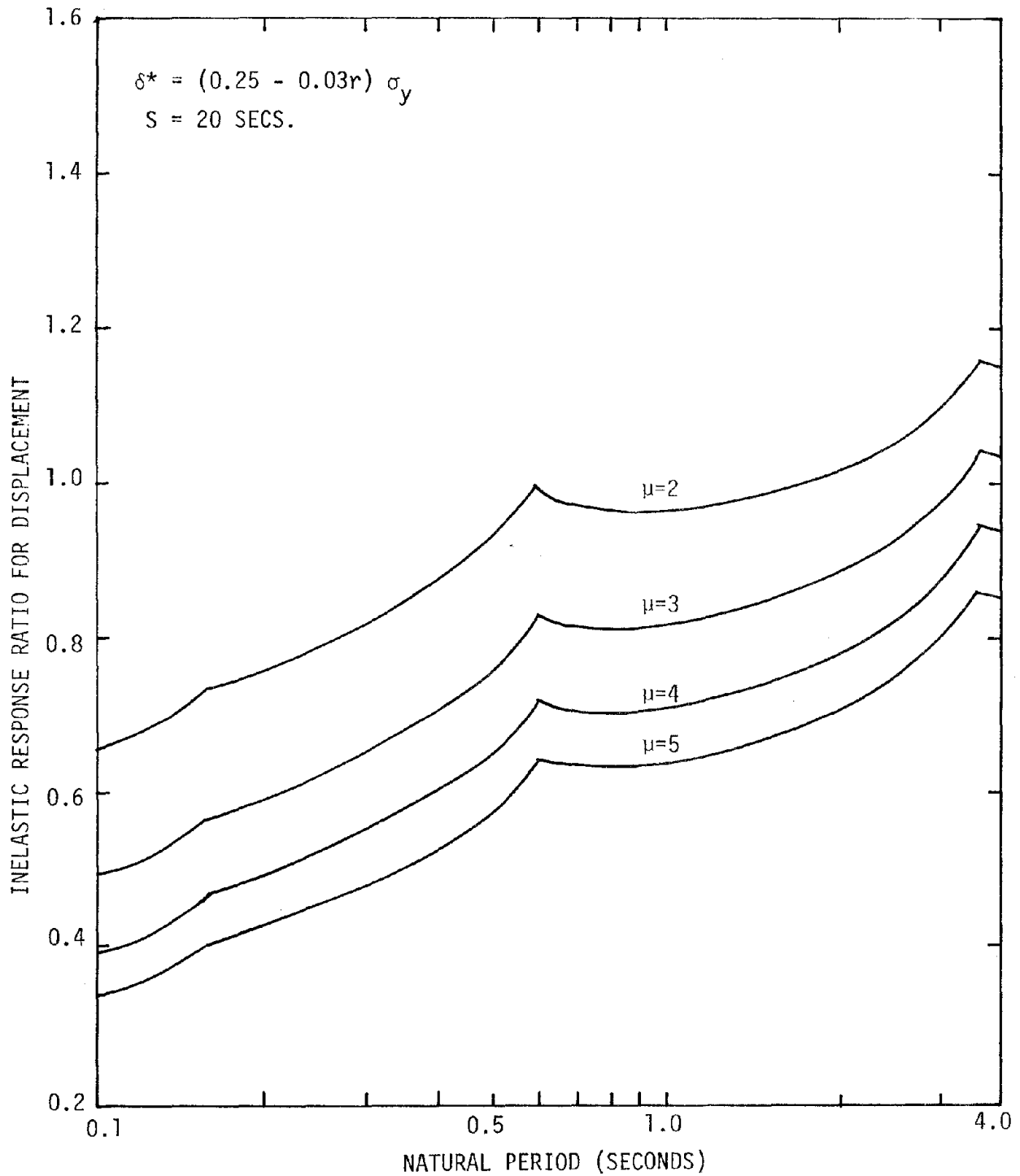


FIG. 4.4 - INELASTIC RESPONSE RATIOS FOR DISPLACEMENT PREDICTED BY  
RANDOM VIBRATION ( $\zeta = 0.05$ ,  $S = 20$ )

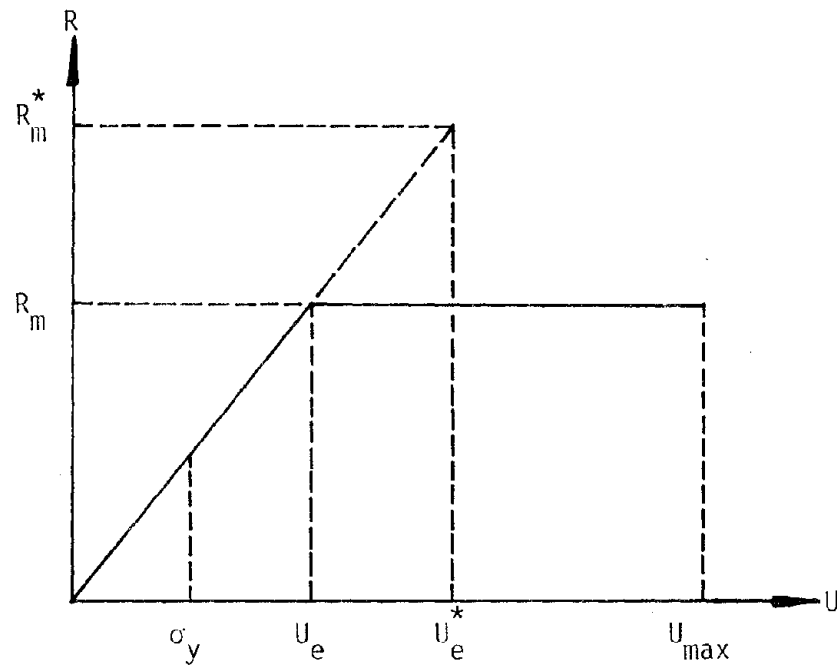


FIG. 4.5 - RELATIONSHIP BETWEEN INELASTIC RESPONSE RATIOS  
FOR DISPLACEMENT AND ACCELERATION

where  $U_{\max}$  is the maximum relative inelastic displacement,  $U_e$  is the yielding displacement, and  $U_e^*$  is the maximum elastic displacement of the associated linear elastic system.

From the basic motion equation (Eq.2 -1), the maximum absolute acceleration of the SDOF elasto-plastic response can be derived as follows:

$$M\ddot{U} + C\dot{U} + KU = -M\ddot{y}_s$$

$$\ddot{y} = \text{absolute acceleration} = \ddot{U} + \ddot{y}_s$$

which leads to

$$\ddot{y} = \frac{-(KU + C\dot{U})}{M}$$

and therefore

$$\left| \ddot{y}_{\max} \right| = \left| \frac{R_m + C\dot{U}}{M} \right| \quad (4-9)$$

Generally, the damping term is small. The maximum absolute acceleration is approximately equal to the maximum spring resistance function  $R_m$  (assuming unit mass). Hence, the elastic response ratio for acceleration can be expressed as:

$$\text{acceleration ratio} = \frac{|\ddot{y}_{\max}^*|}{|\ddot{y}_{\max}|} \approx \frac{R_m^*}{R_m} = \frac{U_e^*}{U_e} \quad (4-10)$$

where  $R_m^*$  is the maximum spring force for the associated elastic system as shown in Fig. 4-5.

From Eqs. (4-8 and 4.10), one can conclude that the inelastic response ratio for acceleration approximately equals the ductility factor times the inelastic response ratio for displacement.

Fig. 4.6 shows the resulting inelastic response ratios of acceleration for  $S = 20$  seconds. With increasing ductilities, the discrepancies between the calculated ratios and those by the Newmark approach (Sec. 3.4.1) increase. This again indicates that the Newmark procedure in constructing the inelastic response spectra is unconservative for larger ductility.

In Eq. (4-7) it is quite clear that the inelastic responses will increase with increasing strong ground motion duration. This is especially true when  $\mu_a S_0$  is large. For example, the inelastic response for  $S = 30$  seconds will be somewhat greater than those corresponding to  $S = 20$  seconds.

#### 4.4 CONCLUSIONS

For the purpose of improving random vibration predictions of inelastic response, simulation studies of SDOF elasto-plastic systems were performed. Semi-empirical modifications were suggested. As shown in this

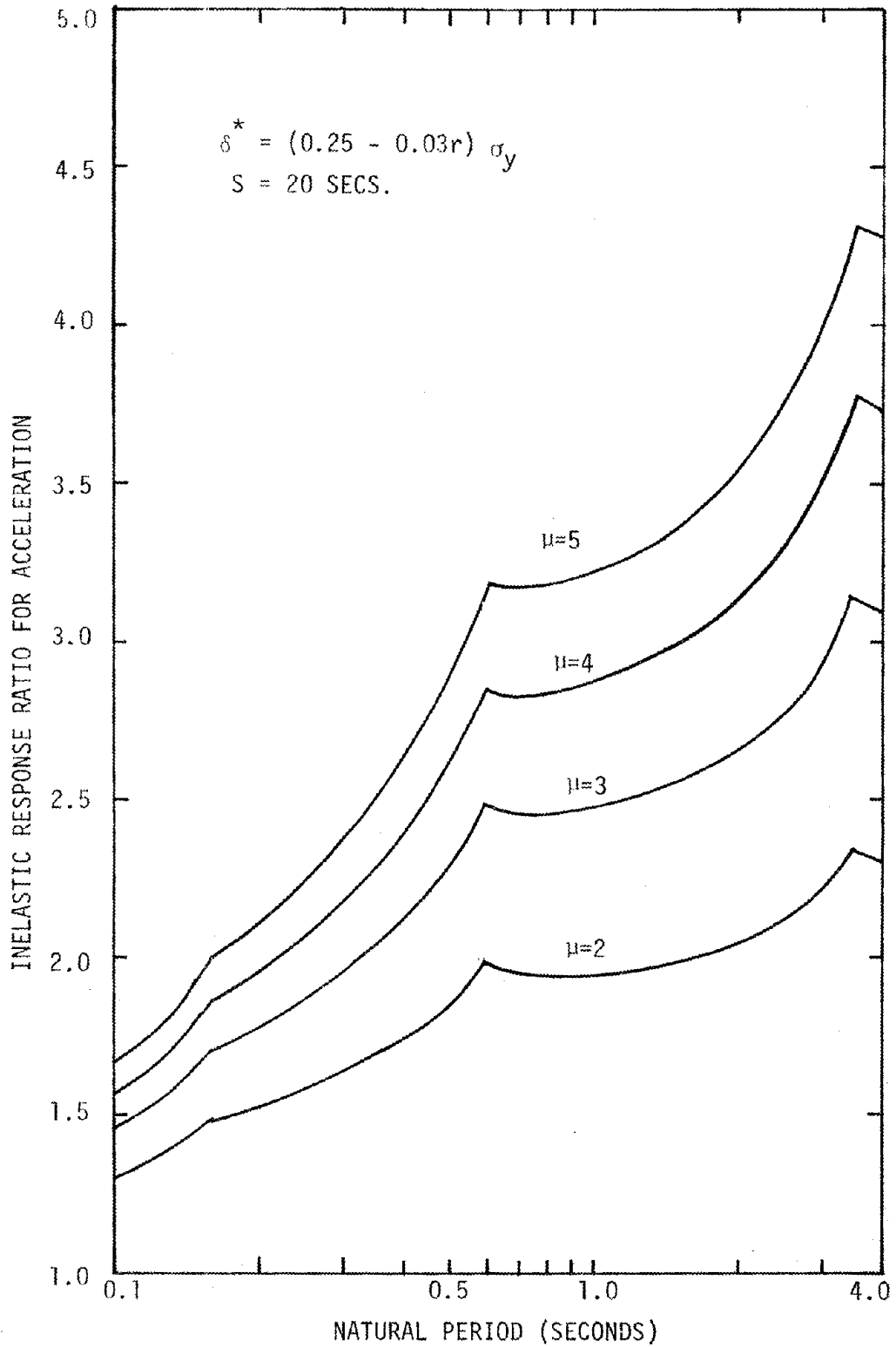
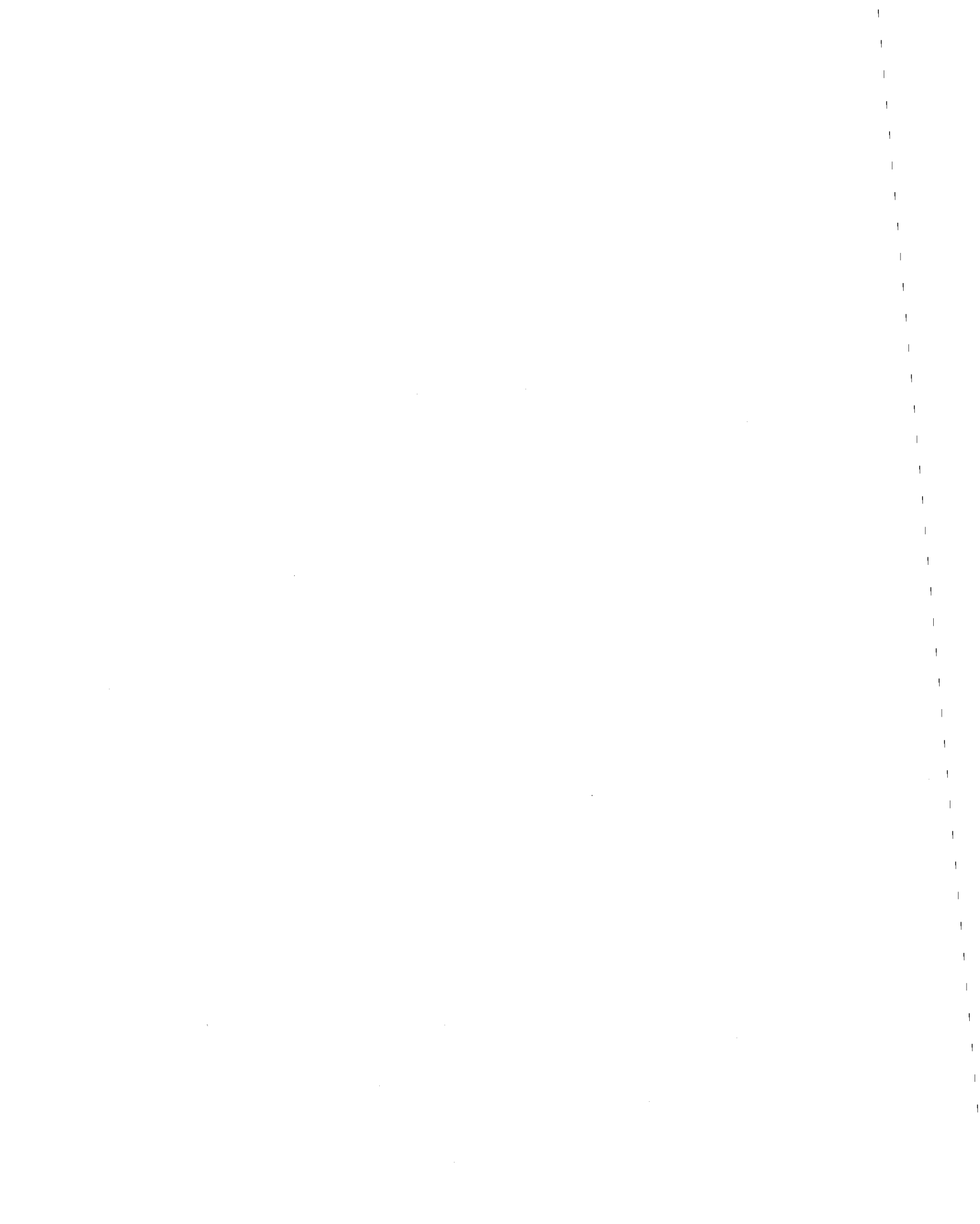


FIG. 4.6 - INELASTIC RESPONSE RATIOS FOR ACCELERATION PREDICTED BY RANDOM VIBRATION ( $\zeta = 0.05$ ,  $S = 20$ )

Chapter, the new random vibration model is more dependent on the strong motion duration. In general, the results of the new random vibration approach are quite compatible with those of the time history analyses. This will permit probabilistic prediction of inelastic action in terms of ductility factor or maximum inelastic displacement.

In comparison with the time history analysis, it is quite clear that the random vibration model used in this study is much simpler and less expensive to implement. Although the results presented herein are only for SDOF inelastic systems, the potential of the approach to deal with MDOF inelastic systems is considerable.



# CHAPTER 5

## INELASTIC RESPONSE FOR STRUCTURAL FRAMES

### 5.1 INTRODUCTION

Based upon the new inelastic response spectra as presented in Chapter 3, it is of great interest to investigate the applicabilities of the response-spectra-based modal analysis inelastic design procedure for structural frames. In this Chapter, brief descriptions of modal analysis are first presented. The modal-analysis-based inelastic design procedure is then tested for a simple shear beam model. This is followed by general descriptions of the structural frames used in this study. For a specified ductility level, the required member strength of the frames can be determined from modal analysis using inelastic response spectra. The actual ductility distributions of the so-designed frames can be obtained by time history analysis. By comparing this actual ductility and the design ductility, the adequacy of the modal-analysis-based inelastic design procedure can be assessed. Results corresponding to the new proposed inelastic response spectra and the Newmark inelastic response spectra are also compared.

A very powerful method that can be used to determine the dynamic response of complicated structural problems is known as the method of modal analysis. The response of each normal mode of vibration for a

MDOF system is computed, and the total response of the system is obtained by superimposing the responses of the contributing modes. The decomposition of the motion equation into a set of close-coupled elastic modal equations is based on the following equation:

$$\left[ [K]_L - \omega_n^2 [M]_D \right] \{\phi_n\} = 0 \quad (5-1)$$

where  $[K]_L$  is the total lateral stiffness matrix,  $[M]_D$  is the diagonal lumped mass matrix,  $\{\phi_n\}$  is the mode shape, and  $\omega_n$  is the natural frequency for mode n.

Because of the use of modal superposition, the method is theoretically limited to linear-elastic systems. However, due to its straightforwardness, the modal analysis using the inelastic response spectra has been applied to inelastic systems. The modal relative displacement  $\{U_n\}$  and absolute acceleration  $\{A_n\}$  of the inelastic responses are expressed as:

$$\begin{aligned} \{U_n\} &= \Gamma_n S_d \{\phi_n\} \\ \{A_n\} &= \Gamma_n S_a \{\phi_n\} \end{aligned} \quad (5-2)$$

where

$$\Gamma_n = \frac{\{\phi_n\}^T [M]_D \{\phi_n\}}{\{\phi_n\}^T [M]_D \{\phi_n\}} = \text{modal participation factor.}$$

$S_d$  and  $S_a$  are the ordinates of the inelastic response spectra for displacement and acceleration corresponding to  $\omega_n$  respectively. Note that for elastic response spectra,  $S_a$  equals  $\omega_n^2 S_d$ .

The maximum response of the system can be approximately predicted by superimposing individual maximum mode responses. Various methods of modal superposition have been proposed. The method of "the square root of the sum of the squares" (SRSS) has been considered the best prediction

for the maximum structural response. Hence, the SRSS method of modal superposition was employed in this study.

## 5.2 INELASTIC RESPONSE OF SIMPLE SHEAR BEAM MODEL

### 5.2.1 Simple Shear Beam Model

In order to study the applicability of inelastic design procedure based on modal analysis using the inelastic response spectra, a simple shear beam model was first employed. The purpose in using a shear beam model was to simplify the problem. Properties of the uncoupled shear beam system were selected to simulate those of the 10-story steel building as described later in this Chapter. Except for the first story, the stiffnesses of the story shear springs were assumed to vary linearly with height. 5% damping was used for the system. The values of story masses and stiffnesses are tabulated in Table 5-1. The interstory heights are 12 feet, except for the first story, which is 15 feet as shown in Fig. 5.1.

In this Chapter, all the artificial motions were scaled to have 0.33G peak ground acceleration. Hence, the proposed inelastic response spectra were also scaled to 1/3 of the original values. Since the design ductility level used was 4, the proposed inelastic response spectra shown in Fig. 3.21 ( $\mu=4$ ,  $\zeta=0.05$ ) were used.

Based on modal analysis using the proposed inelastic acceleration response spectrum, the maximum forces in the story shear springs were computed by the program APPLE PIE (20). Since the gravity load effects cannot readily be included in a shear beam model, they have been neglected. Hence, the maximum story resistances are set equal to the maximum shear

TABLE 5-1 - PROPERTIES OF THE SIMPLE  
SHEAR BEAM MODEL

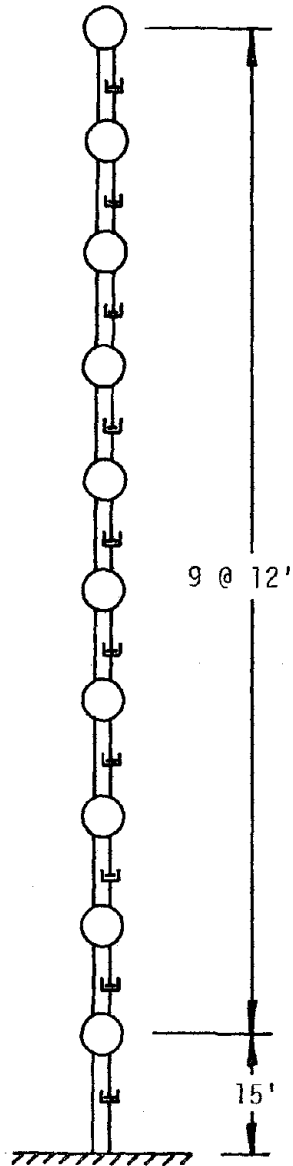


FIG. 5.1 - SIMPLE SHEAR  
BEAM MODEL

STORY	MASS	STIFFNESS	STORY STRENGTH	
			NEWMARK	PROPOSED
10	0.256	20	17.4	23.4
9	0.262	40	23.8	30.7
8	0.262	60	29.4	37.4
7	0.262	80	33.8	43.0
6	0.262	100	38.3	48.0
5	0.262	120	41.9	52.1
4	0.262	140	45.0	56.2
3	0.262	160	48.6	61.2
2	0.262	180	52.0	66.0
1	0.262	220	54.0	68.8

forces obtained from modal analysis. The maximum story resistance corresponding to the Newmark inelastic acceleration response spectrum ( $\mu=4$ ) was also computed by modal analysis. The values of the maximum story resistances based on the proposed inelastic response spectrum and those of the Newmark spectrum are tabulated in Table 5-1. Note that the story resistance forces corresponding to the proposed inelastic response spectrum are on the average 27% greater than those based on the Newmark response spectrum. Since higher modes are not very important in the determination of story forces, only the first four modes have been included in the analyses. The natural periods of the four modes are 1.922, 0.834, 0.531 and 0.388 seconds, respectively. The modal shapes of the first four modes are tabulated in Table A-1 in the Appendix.

### 5.2.2 Resulting Story Ductility and Displacement Distributions

The program STAVROS (1) was used to compute the time history responses of the simple shear beam modal described previously. The responses are measured by the ductility factors  $\mu$ , where  $\mu$  is defined as the maximum relative horizontal displacement divided by the yield displacement of each story.

Five artificial strong ground motions scaled to 0.33G peak ground acceleration, with  $S = 20$  seconds, were used for the analyses. The mean and standard deviations of the maximum story ductilities for the shear beam system subjected to different motions can be calculated. Fig. 5.2 shows the distributions of the mean and mean  $\pm$  one standard deviation of the maximum story ductilities. The mean ductility factors corresponding to the system with story strength determined from the proposed inelastic

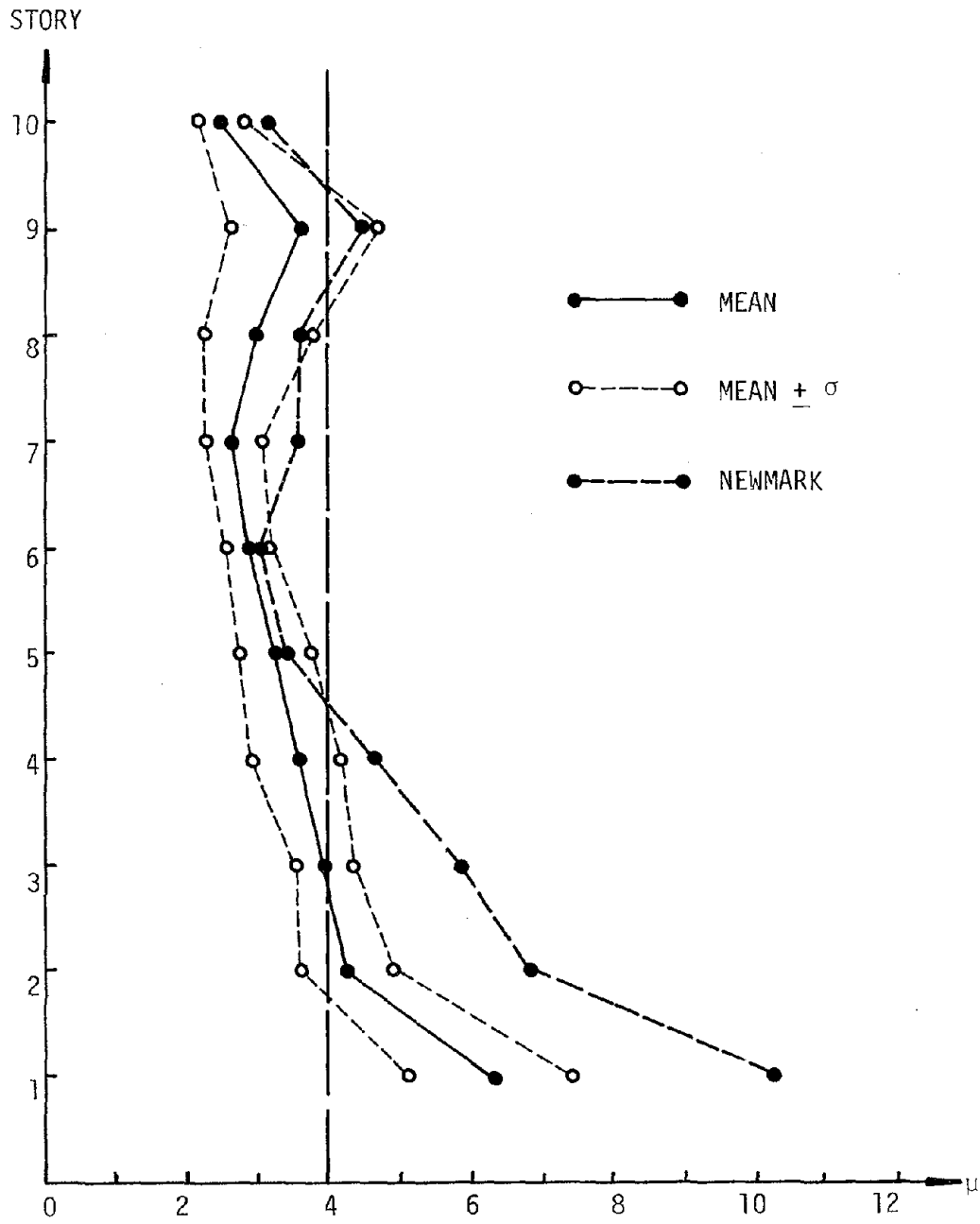


FIG. 5.2 - DUCTILITY DISTRIBUTION FOR SIMPLE SHEAR BEAM MODEL

acceleration response spectrum are shown in solid lines on the figure. They are greater than the design ductility ( $\mu=4$ ) in the first two stories and smaller than that in the upper stories.

For the system with story strength determined by the Newmark inelastic acceleration response spectrum, the mean story ductilities are shown as dash lines in Fig. 5.2. Note that the mean story ductilities corresponding to the Newmark inelastic acceleration response spectrum are greater than those of the proposed spectrum in all stories. In fact, the story ductilities are approximately 60% greater at the first two stories and 5 ~ 45% for other stories. On the average, the mean story ductilities of the system design based on the Newmark inelastic response spectrum are 30% greater than those by the proposed spectrum. In comparison with the design ductility level, it can be concluded that the system with story strength determined by the proposed inelastic acceleration response spectrum performs better than the system corresponding to the Newmark spectrum.

From the time history analyses, information concerning maximum story displacement can also be obtained. The resulting mean maximum story displacements for the set of strong ground motions are plotted in Fig. 5.3. Based on the inelastic displacement response spectrum ( $\mu=4$ ,  $\zeta=0.05$ ), the maximum story displacement can be directly predicted by the modal analysis. The mean maximum story displacements predicted by the SRSS method of modal superposition using the Newmark inelastic displacement response spectrum and the proposed one are also plotted in Fig. 5.3.

The results in Fig. 5.3 can be summarized as follows:

- 1) For the results of time history analyses, the mean maximum story displacements of the system with story resistances determined by the

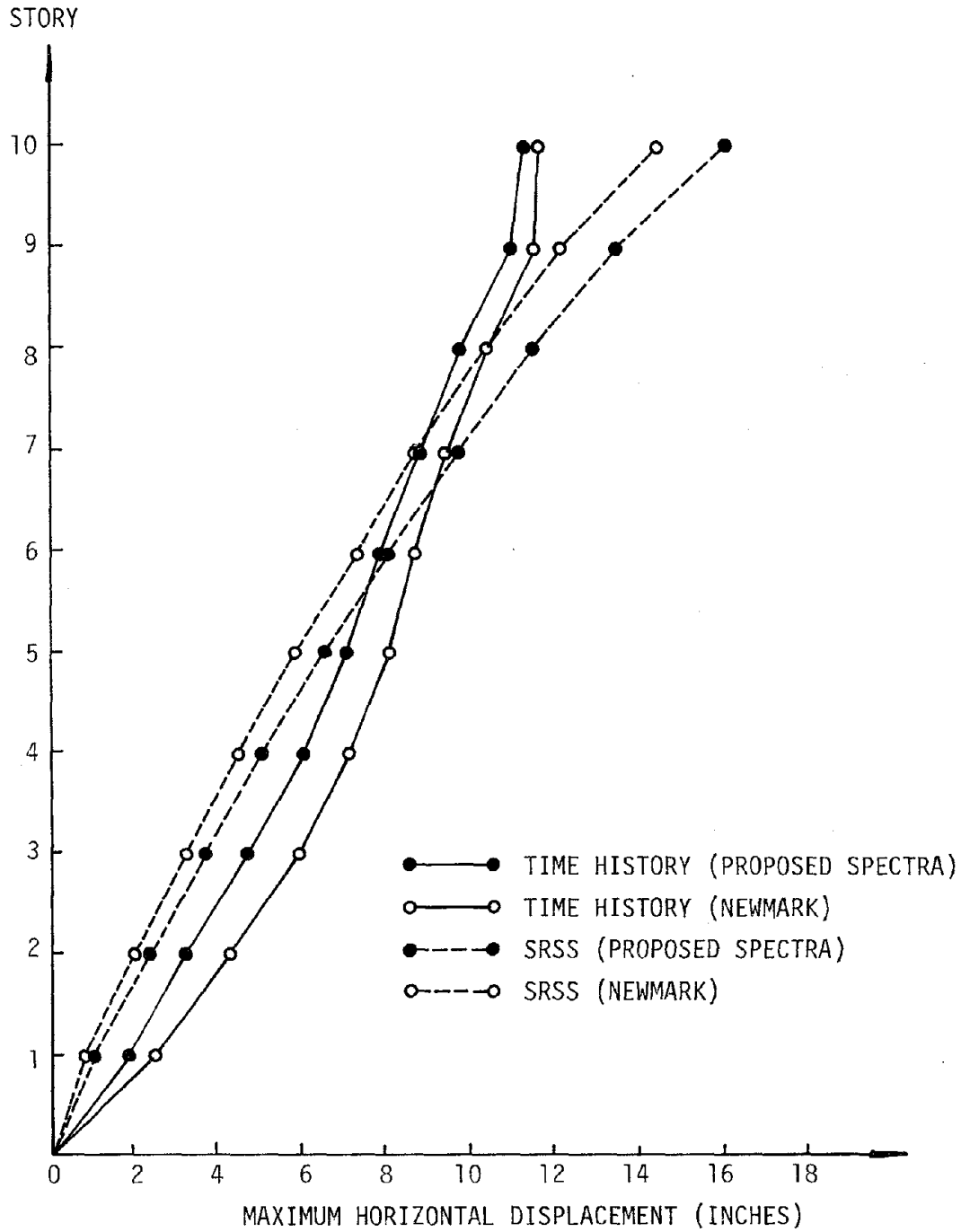


FIG. 5.3 - MAXIMUM RELATIVE DISPLACEMENTS OF SIMPLE SHEAR BEAM MODEL ( $\zeta = 0.05$ )

Newmark inelastic acceleration response spectrum are greater than those corresponding to the proposed spectrum for all stories.

- 2) In comparison with the results of time history analyses, the maximum story displacements predicted directly by the SRSS method of modal superposition using inelastic "displacement" response spectra are conservative at the top stories and unconservative at the lower stories.
- 3) The negative contribution of the second mode for story displacement is significant in the upper stories. Hence, the prediction of the maximum story displacement directly from the inelastic displacement response spectrum by the SRSS method of modal superposition is not adequate for inelastic systems. Better prediction of the response can be made by adding numerically the responses of the first two modes.

Based upon the above-mentioned analyses, it can be concluded that the proposed inelastic response spectra yield better predictions of the inelastic structural responses than the Newmark inelastic response spectra. Further investigations of the applicabilities for the inelastic design procedure based on modal analysis to actual structural frames are presented in the following sections.

### 5.3 DESCRIPTION OF BUILDING FRAMES INVESTIGATED

#### 5.3.1 Basic Frames

Three steel moment-resisting frames, i.e., 4-, 10-, and 16-story, were used extensively in this study. The frames were designed according to the Uniform Building Code Specifications (1973) by Piqué (18). The design of the frames was based on the maximum effect of the following static loading combinations: i)  $D + L$  in all spans, ii)  $D + L$  in alternate spans (maximum positive moment), iii)  $D + L$  in two adjacent spans

(maximum negative moment), and iv)  $3/4 (D + L + EQK)$ . Shear and deflection restraints were checked for girder designs. Total drift limitation for wind was  $1/350$ , and  $1/500$  for earthquake. The dead load (D) was 80 psf for all frames.

Plans and elevations of the three steel frames used in this study are shown in Figs. 5.4 - 5.7. In coping with the current design practice of minimizing the variation for member sections, the column sections were kept the same for two stories, while the girder sections were kept the same across all spans. The dimensions of the 4-story frame were selected to represent a typical low-rise apartment. As shown in the elevation view of the 4-story frame in Fig. 5.5, the story heights are 10 feet, with exterior span 20 feet and interior span 15 feet.

The 10- and 16-story frames represent typical commercial office buildings. As shown in the elevation views of the 10- and 16-story frames in Figs. 5.6 and 5.7, the story heights are 12 feet, except for the first story, which is 15 feet. Both exterior and interior spans are 20 feet. The inter-frame spacing is 20 feet for all frames, as shown in Fig. 5.4. All frames were assumed to have adequate bracing systems to resist out-of-plane motion. Torsional effects have been neglected in all of the following analyses.

Based on member properties of the frames described previously, modal analyses using inelastic response spectra were performed. From the results, the frames were re-designed by determining new strength in the members. Detailed discussions of the determination of member strength are presented next.

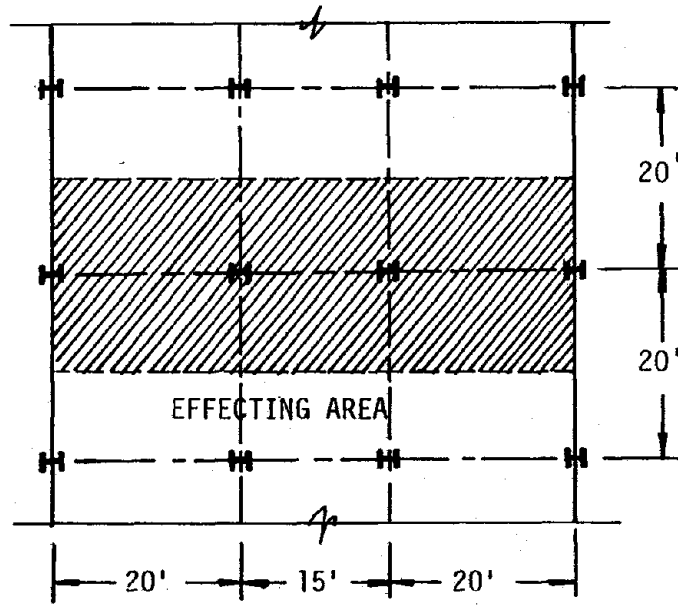


FIG. 5.4 - 4-STORY BUILDING PLAN

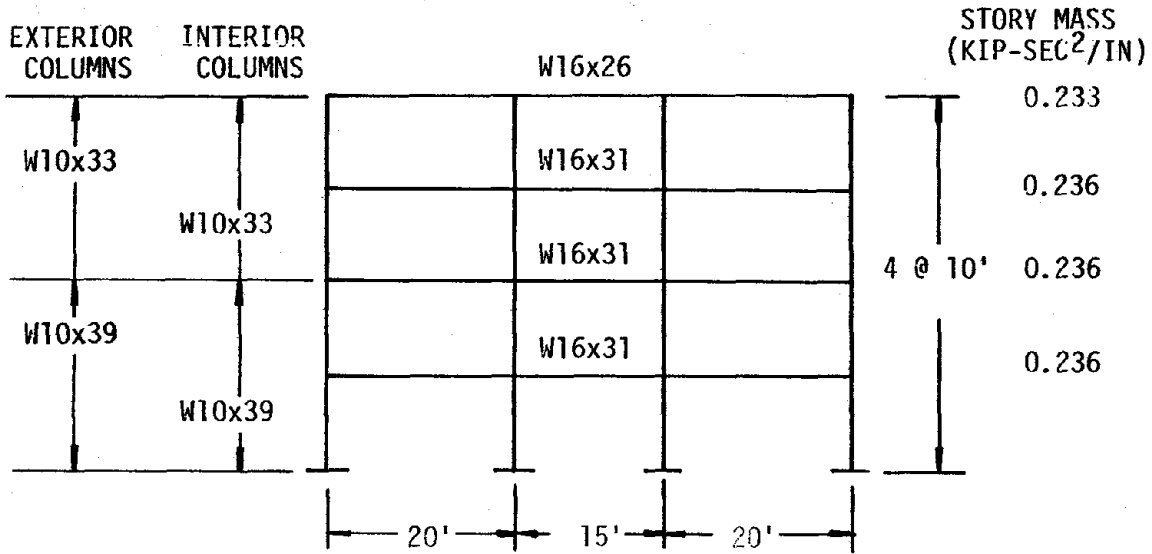


FIG. 5.5 - 4-STORY BUILDING ELEVATION  
(Redrawn from Ref. 18)

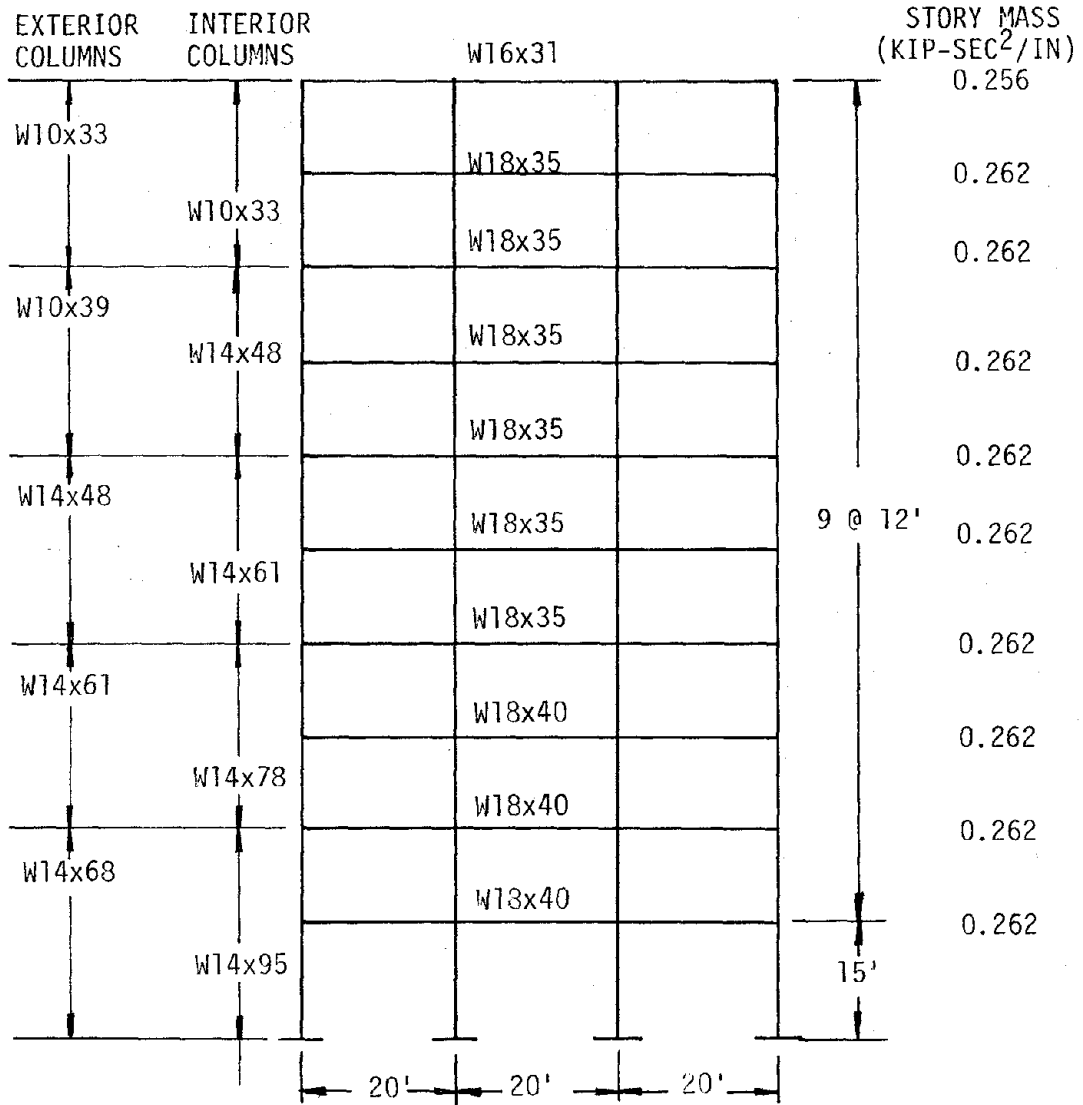


FIG. 5.6 - 10-STORY BUILDING ELEVATION  
(Redrawn from Ref. 18 )

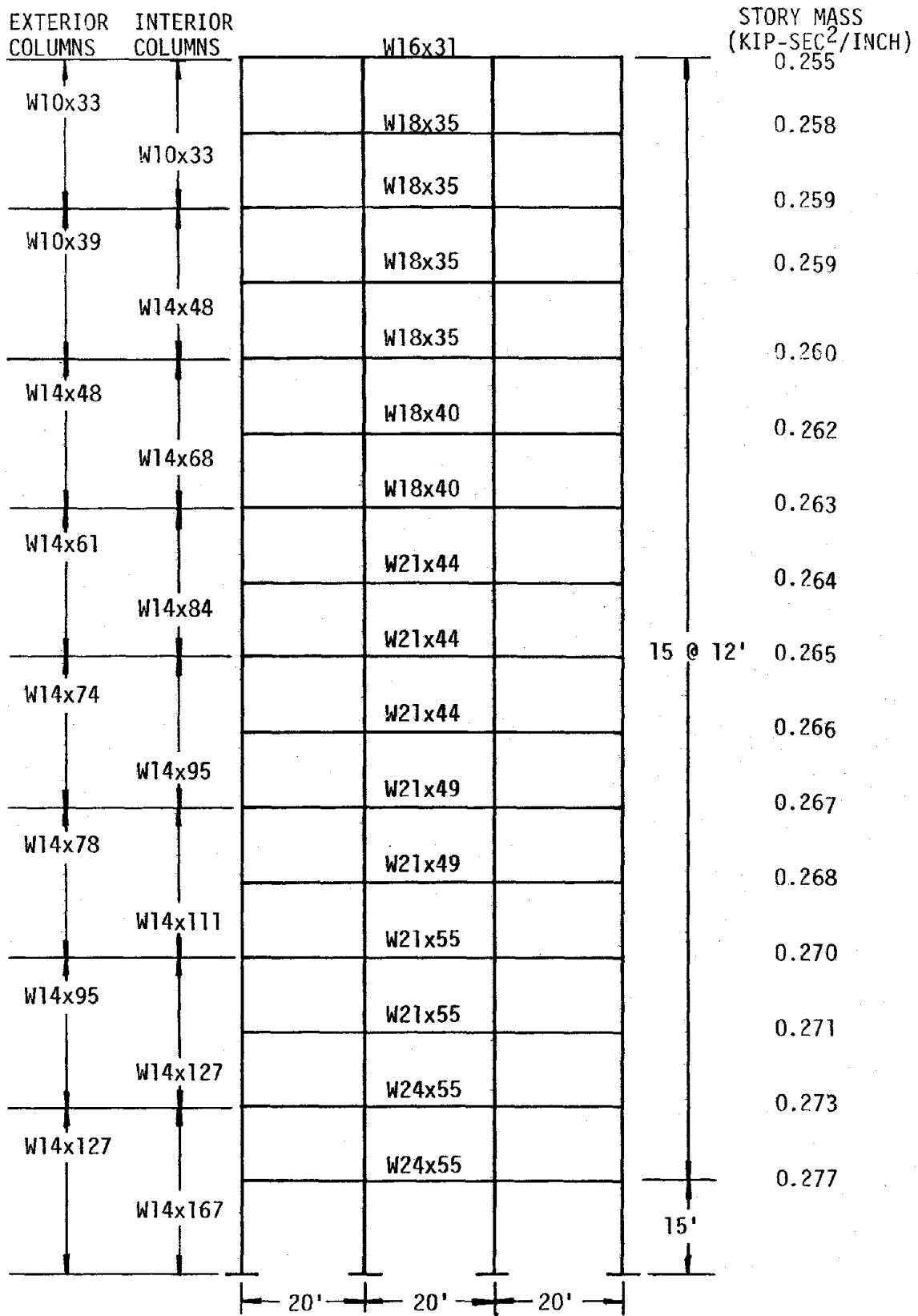


FIG. 5.7 - 16-STORY BUILDING ELEVATION (Redrawn from Ref. 18).

### 5.3.2 Determination of Member Strength

In the determination of member strength, the method proposed by Luyties et al. (15) and modified by Haviland et al. (12) was used. Strain hardening effects, shear deformations, buckling in compression members, and axial forces in the girders were not considered in this study.

Girder moment capacities were determined according to the following expression:

$$M_y = \max \{M_{EQ} \text{ or } w\ell^2/8\} \quad (5-3)$$

where  $M_{EQ}$  was the average of the end moments due to earthquake. The end moments were computed by modal analysis using inelastic acceleration response spectra as discussed in Section 5.1. The second criterion,  $w\ell^2/8$ , was to insure against the undesirable formation of plastic hinge at girder midspan due to the gravity load.  $w = 80$  psf is the uniform dead load for the frames.

For the 4-story frame, the second criterion controls the moment capacities of the upper-three-story exterior girders and the top-story interior girder. For the 10-story frame, the  $w\ell^2/8$  criterion controls the moment capacities of all girders from the 4<sup>th</sup> to the top story. For the 16-story frame, the criterion controls the moment capacities of the upper-seven-story exterior girders and the upper-five-story interior girders. The above-mentioned results were computed based on the modal analysis using the proposed inelastic acceleration response spectrum as shown in Fig. 3.21 ( $\mu=4$ ,  $\zeta=0.05$ ). The member moment capacities for all three frames are tabulated in Tables A-5 - A-7 in the Appendix.

Column moment capacities were determined based upon the AISC axial-flexural interaction formula: (AISC 2.4-3)

$$\frac{P}{P_y} + \frac{M}{1.18 M_y} \leq 1.0 \quad ; \quad M \leq M_y \quad (5-4)$$

With the assumption that the ratio of plastic modulus  $Z$  to area  $A$  is equal to 6 for all the column sections in this study (12, 15, 19), Eq. (5-4) becomes

$$\begin{aligned} M_y &\geq 6P + M/1.18 \quad ; \quad M_y \geq M \\ P_y &= M_y/6 \end{aligned} \quad (5-5)$$

where  $P = P_{EQ} + P_{GR}$  = maximum axial force in the columns due to earthquake and gravity loads.  $M$  is the maximum applied design moment defined as follows:

$$M = \max \{M_{EQ} \text{ or } M_{GR}\} \quad (5-6)$$

where  $M_{EQ}$  is the average of the two column end moments due to earthquake, and  $M_{GR}$  is the average of the two column end moments due to the gravity load.

For all three frames analyzed in this study, the column design moments are controlled by the earthquake load except for the top story exterior columns. The column moment capacities for the frames are also tabulated in Tables A-5 - A-7 in the Appendix.

## 5.4 INELASTIC DYNAMIC ANALYSIS FOR FRAMES

### 5.4.1 Program FRIEDA

The program FRIEDA (Frame Inelastic Earthquake Dynamic Analysis) was used to compute the time history inelastic responses of frames. It was originally developed by Aziz (4) and subsequently modified by Luyties et al. (15). Only brief descriptions of the program are presented here.

In performing the time history analysis of plane frame structures, the program neglects shear deformation, axial deformation in the girders, soil-structure interaction, P- $\Delta$  effect, etc. Masses are lumped at the floor levels. The member moment-rotational relationship is modelled by the dual-component point hinge model. It is comprised of an elastic component and an elasto-plastic component. The superposition of the two components leads to a bilinear moment-deformation relationship. In this study, 5% of the initial member stiffness was taken as the second slope of the bilinear model.

The axial-flexural interaction as in Eq. (5-4) has been incorporated in the program to compute the new yield moment due to the change of axial force in the member. Further discussions of this updating process are presented in the following paragraphs.

#### 5.4.2 Ductility Measures

Two different ductility factors were used to measure the inelastic response of frames in this study. Brief descriptions of the two ductilities, namely, rotational ductility and moment ductility, are first presented. The detailed discussions of the two factors based on time history results are presented later in this section.

The rotational ductility, denoted as  $\mu_{\theta}$ , is defined as follows: (7)

$$\mu_{\theta} = \frac{\theta_i}{\theta_y} + 1 \quad (5-7)$$

where  $\theta_y = M_y L / 6EI$  is the yield rotation corresponding to the yield moment  $M_y$  for an anti-symmetric deformed shape.  $\theta_i$  is the maximum additional plastic rotation at the member end. The relationship is illus-

trated in Fig. 5.8.

The moment ductility, denoted as  $\mu_M$ , is defined as follows: (2)

$$\mu_M = \frac{\theta_m}{\theta_y} = 1 + \frac{M_f - M_y}{p M_y} \quad (5-8)$$

As shown in Fig. 5.9,  $\theta_m$  is the total maximum member rotation,  $p$  is the ratio of the second slope to the initial stiffness of the bilinear moment-rotational relationship,  $M_f$  is the maximum member end moment, and  $M_y$  is the yield moment.

The main difference between the two ductilities is that the moment ductility will change with varying axial force in the member. This is because the yield moment,  $M_y$ , will decrease with increasing member axial force, while for rotational ductility,  $M_y$  is a selected constant for individual members. Therefore, Haviland et al. (12) suggested the moment ductility might be better in measuring inelastic action since the yield curvature was not denoted by a constant as in the case of rotational ductility ( $M_y L/6EI$ ). Furthermore, they argued that in the presence of gravity load, the unsymmetrical end restraints or irregular geometry would decrease the accuracy of the assumed anti-symmetrical deformed shape of rotational ductility. In summary, Haviland et al. concluded that the moment ductility was superior to the rotational ductility. However, from the results of time history analysis in this study, it has been found that the above-mentioned argument is true for girders, but is inadequate for columns. The detailed discussions of the relationship between moment ductility and rotational ductility for columns are presented in the following paragraphs.

Assuming yielding has occurred in a column, the corresponding moment-

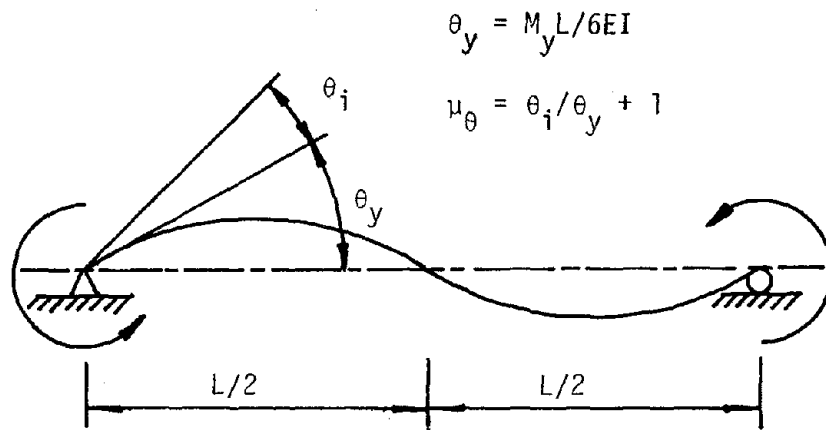


FIG. 5.8 - DEFINITION FOR ROTATION DUCTILITY

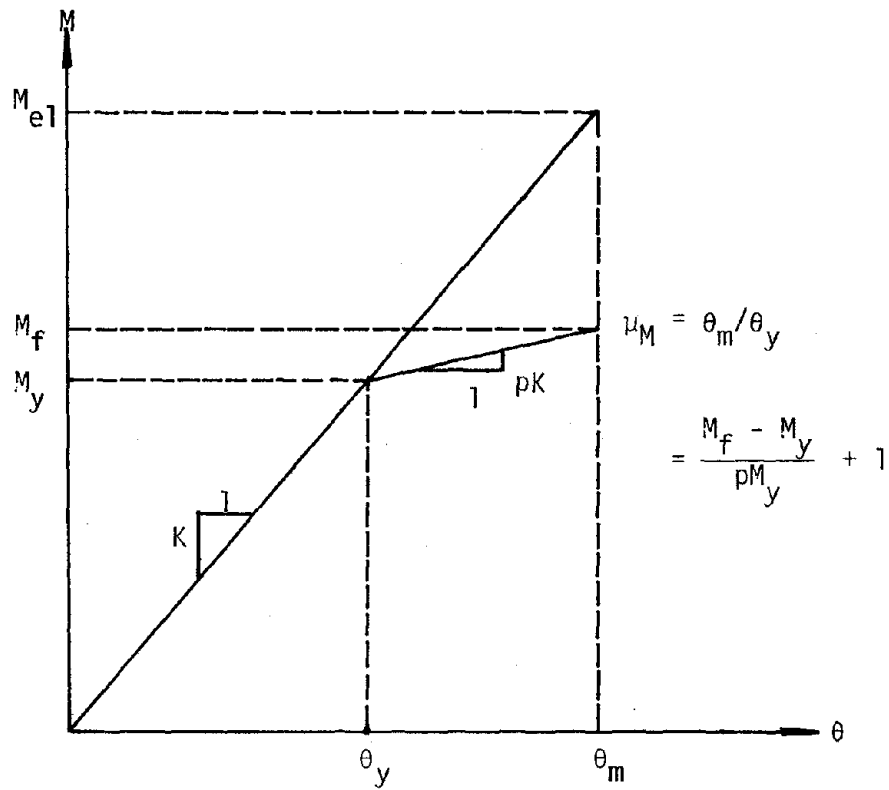


FIG. 5.9 - DEFINITION FOR MOMENT DUCTILITY

rotational relationship is shown in Fig. 5.10. The column has a total rotation  $\theta$ , yield rotation limit  $\theta_y$  and acting end moment  $M_f$ . The corresponding ductility factor is  $\theta/\theta_y$ , denoted by  $\mu_\theta$  regardless of different ductility definitions. If the axial force in the column changes, assuming  $M_f$  remains the same, the moment ductility will vary. This raises the question: supposing the change of axial force in the column does not result in any further yielding action, can the corresponding change of moment ductility be justified? In order to answer the question, two approximate models were postulated. The first model assumes the column rotation  $\theta$  will change with varying axial force. The second model assumes that the rotation will remain the same. The detailed discussion of the two models are presented herein.

a) Varying  $\theta$

With an increase of axial force, the yield moment  $M_y$  of the column will decrease to  $M_y^*$ , as shown in Fig. 5.10. The yield rotation limit decreases from  $\theta_y$  to  $\theta_y^*$  accordingly. Based on the bilinear moment-rotational relationship, the corresponding total column rotation will increase to  $\theta^*$  for the same end moment  $M_f$ . Hence, the new moment ductility, denoted as  $\mu_M^*$ , becomes  $\theta^*/\theta_y^*$ , as shown in Fig. 5.10. The relationship between  $\mu_M^*$  and the original ductility  $\mu_\theta$  can be expressed as follows:

$$\mu_\theta = \frac{\theta}{\theta_y} = \frac{M_f - M_y}{pM_y} + 1$$

$$\mu_M^* = \frac{\theta^*}{\theta_y^*} = \frac{M_f - M_y^*}{pM_y^*} + 1$$

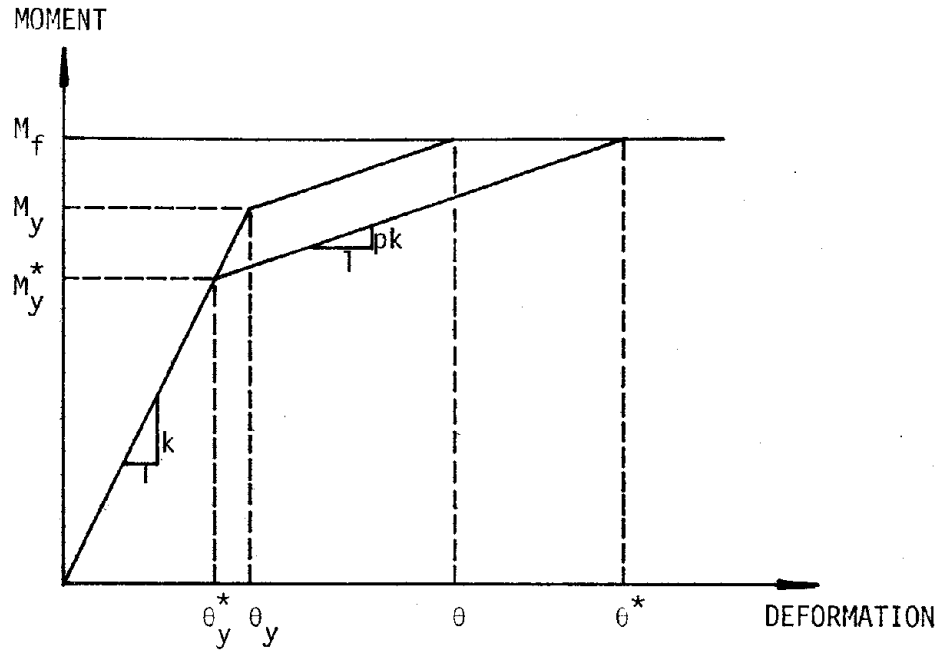


FIG. 5.10 - MOMENT-DEFORMATION RELATIONSHIP FOR ROTATIONAL AND MOMENT DUCTILITIES

$$\frac{\mu_M^*}{\mu_\theta} = \frac{M_y}{M_y^*} + \frac{(1-p)(M_y - M_y^*)}{p M_y^* \mu_\theta} \quad (5-9)$$

where  $p$  is the ratio of the second slope to the initial stiffness in the moment-rotational relationship. In this study  $p$  is taken to be 0.05.

Based on Eq. (5-9), the value of  $\mu_M^*/\mu_\theta$  can be predicted for a given change of axial force in the column.

b) Constant  $\theta$

This model assumes the column rotation remains the same for small changes of axial force. This means no further inelastic action for the column. Based on definition, the moment ductility  $\mu_M^*$ , now becomes  $\theta/\theta_y^*$ . The relationship between  $\mu_M^*$  and  $\mu_\theta$  can be expressed as follows:

$$\mu_{\theta} = \frac{\theta}{y}, \mu_M^* = \frac{\theta}{\theta_y^*}$$

$$\frac{\mu_M^*}{\mu_{\theta}} = \frac{\theta_y}{\theta_y^*} = \frac{M_y}{M_y^*} \quad (5-10)$$

Therefore, the value of  $\mu_M^*/\mu_{\theta}$  can also be predicted based on the second model for a given small change of axial force in the columns.

In order to investigate the relationship between moment ductility and rotational ductility, the 10-story frame was designed based upon the procedure described in Section 5.3.2. The moment capacities,  $M_y$ 's, and the axial force capacities,  $P_y$ 's, for the exterior columns are tabulated in Table 5-2. The static axial forces due to the gravity load, denoted by  $P_{GR}$ , are also listed. By using the program FRIEDA, the time history responses of the 10-story frame subjected to an artificial strong ground motion can be computed. The results for exterior columns are tabulated. In Table 5-2,  $P_{GR} + EQ$  represents the maximum axial force of the column due to earthquake and gravity loads. Note that the additional axial force due to earthquake is about 44% of the axial force due to gravity load at the first story.  $(M_y)_{GR}$  and  $(M_y)_{GR}^* + EQ$  are the reduced moment capacities corresponding to  $P_{GR}$  and  $P_{GR} + EQ$ , respectively. Both were determined from the axial-flexure interaction formula (Eq. (5-4)).  $\mu_{\theta}$  is the maximum local rotational ductility. Note that in the program FRIEDA,  $\mu_{\theta}$  is calculated based on the reduced yield moment  $(M_y)_{GR}$ . This means that in the determination of column rotational ductility, the axial-flexure interaction has been incorporated only for gravity load.

Based upon the above-mentioned results, the ratio of  $\mu_M^*/\mu_{\theta}$  corresponding to  $P_{GR} + EQ$  can be approximately predicted by the two models described earlier. The results are tabulated in Table 5-2.

TABLE 5-2 ROTATIONAL DUCTILITIES VS. MOMENT DUCTILITIES FOR 10-STORY BUILDINGS

STORY	$P_y$	$P_{GR}$	$P_{GR+EQ}$	$M_y$	$(M_y)_{GR}$	$(M_y)_{GR+EQ}^*$	$\mu_\theta$	$\mu_M^*$	$\mu_M^*/\mu_\theta$ (predicted)	
									a	b
10	68	15	16	408	376	369	4.759	0.926	1.09	1.020
9	95	31	36	570	454	421	4.500	1.043	1.415	1.080
8	103	47	57	619	397	326	5.420	1.454	1.981	1.218
7	133	63	79	795	494	381	4.009	1.434	2.703	1.297
6	169	79	102	1015	541	403	5.541	1.276	2.524	1.344
5	196	95	126	1176	713	495	5.350	1.128	3.005	1.440
4	222	111	151	1326	779	502	3.545	2.242	4.515	1.553
3	253	128	177	1518	889	542	4.227	1.511	4.520	1.640
2	279	143	203	1674	960	542	3.490	1.722	5.979	1.772
1	349	159	229	2092	1343	851	3.649	2.390	4.591	1.578

Note that the first model always predicts greater values than the second one. The actual ratios of moment ductility versus rotational ductility from the time history analyses are also tabled. As shown in the Table, the ratios predicted by the constant- $\theta$  model are much better in matching the actual ratios. This suggests that the additional inelastic member rotation is not very pronounced when the axial force in the column changes. Hence, the use of moment ductility for columns cannot be justified; instead, the rotational ductility should be employed.

In this study, rotational ductility was used for all columns, and moment ductility was used for all girders to measure the inelastic responses of structural frames. The results of the time history analysis are presented next.

## 5.5 RESULTS OF INELASTIC DYNAMIC ANALYSIS FOR FRAMES

### 5.5.1 Ductility Distribution

Based upon the modal analysis using inelastic acceleration response spectra, all three steel moment-resisting frames were designed for a ductility level of 4. The inelastic responses of each frame were then computed by the program FRIEDA. The results for story maximum local ductilities are first presented. Comparisons between the resulting ductility distributions corresponding to the new proposed inelastic acceleration response spectrum and those of the Newmark response spectrum are also included. Then, the results of maximum story displacement are reported and discussed.

#### 5.5.1.1 4-story Frame

Five artificial motions scaled to 0.33 G peak acceleration with  $S = 10$  seconds were used for time history analyses. The member strength of the frame was determined based on the proposed inelastic acceleration response spectrum. The spectrum used has been scaled to 1/3 of the original spectrum (Fig. 3.21). Fig. 5.11 shows the mean maximum ductility factors for columns and girders of the 4-story frame. The mean ductilities are the average of five maximum local ductilities corresponding to the different artificial strong ground motions. Rotational ductility was used for columns, whereas moment ductility was used for girders.

As shown in the figure, the mean maximum ductilities of the first two stories for exterior columns are approximately equal to the design ductility level. But the top two stories show larger maximum story ductilities than the design level. For interior columns, the mean maximum story ductilities are quite satisfactory in matching the design ductility level with the height. The moment ductilities for girders are also shown in Fig. 5.11. For exterior girders, except for the first floor, all the upper floors have smaller mean maximum local ductilities than the design ductility. This is not surprising, since the moment capacities of the upper-three-floor exterior girders are controlled by the criterion  $w\ell^2/8$ . (Remember the criterion was to ensure against the undesirable formation of plastic hinge at girder midspan.) These moment capacities are greater than the needed capacities based on earthquake and gravity loads. Hence, smaller local ductility factors have resulted. In interior girders, all maximum ductilities are smaller than the design ductility. Since only the top floor girder is controlled by the  $w\ell^2/8$  criterion, this may sug-

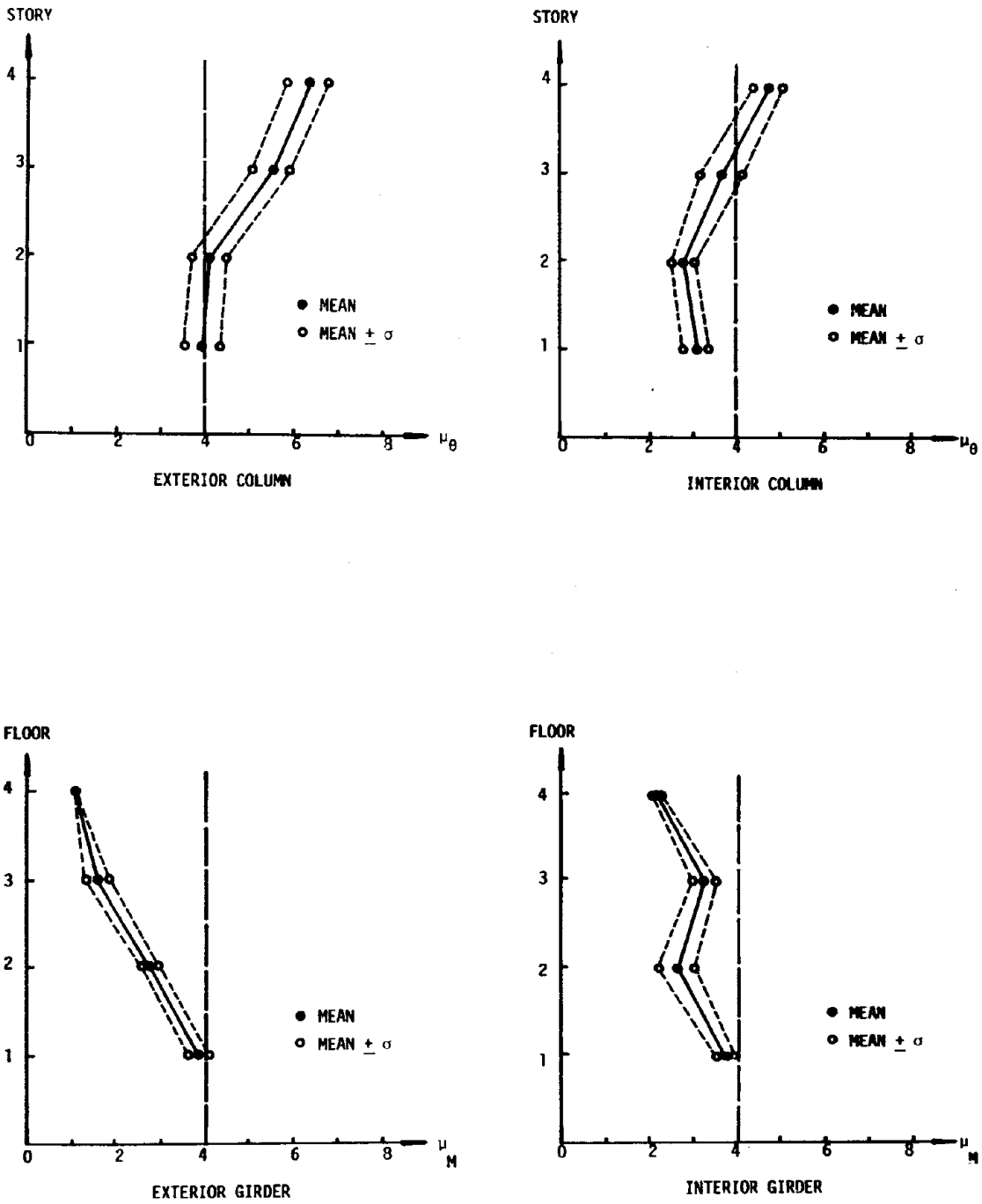


FIG. 5.11 - MAXIMUM DUCTILITY FACTORS FOR 4-STORY BUILDING  
(PROPOSED SPECTRA,  $\zeta = 0.05$ )

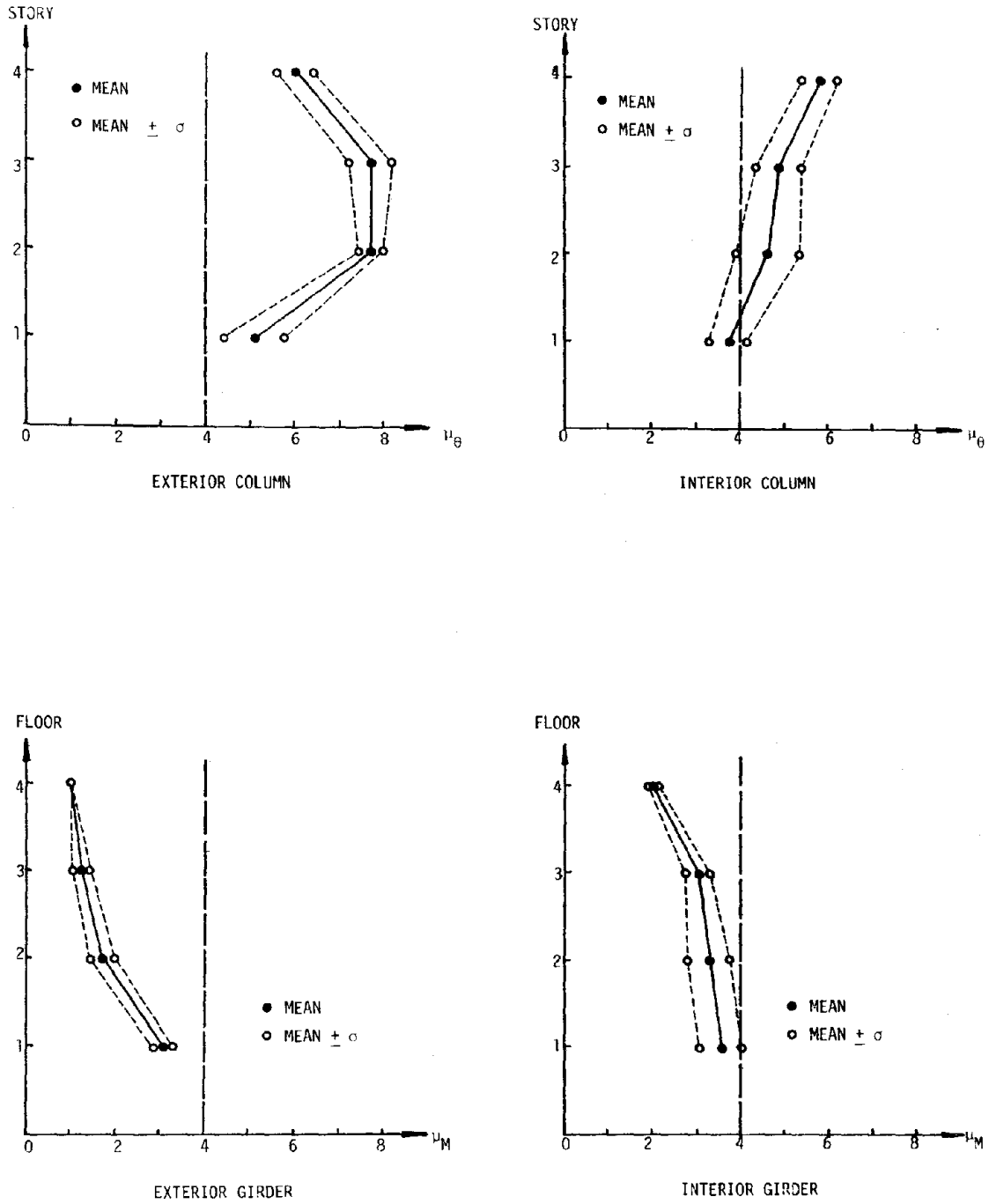


FIG. 5.12 - MAXIMUM DUCTILITY FACTORS FOR 4-STORY BUILDING  
(NEWMARK,  $\zeta = 0.05$ )

gest that the inelastic design procedure yields conservative interior girders.

The above-mentioned results are for the system with member strength determined by the modal analysis method using the proposed inelastic acceleration spectrum. The system with member strength determined by the Newmark inelastic acceleration response spectrum has also been analyzed. The moment capacities for girders and columns corresponding to the Newmark spectrum are tabulated in Table A-8 in the Appendix.

Fig. 5.12 shows the mean maximum local ductilities of the 4-story frame corresponding to the Newmark inelastic response spectrum. For exterior columns, the ductilities are much greater than the design ductility for all stories. In comparison with the results shown in Fig. 5.11, the results corresponding to the Newmark inelastic spectrum are much more conservative. For interior columns, the mean maximum ductilities are also greater than the design ductility except for the first story. In exterior and interior girders, the ductilities are all smaller than the design ductility. This is again due to the criterion of insuring against undesirable formation of plastic hinges at member midspans.

The results reported herein are summarized in Section 5.5.1.4.

#### 5.5.1.2 10-story Frame

Five artificial strong ground motions with  $S = 20$  seconds were used to calculate time history inelastic responses for the 10-story building. As shown in Fig. 5.13, the resulting mean maximum story ductilities for exterior columns are greater than the design ductility at upper stories. For interior columns, the ductilities are quite compatible with the

design ductility level for all stories. Fig. 5.14 shows the mean maximum story ductilities for exterior and interior girders. Due to the criterion  $w\ell^2/8$  mentioned earlier, the local ductilities are smaller than the design ductility for the upper six floors. Note that the standard deviations of maximum ductilities at lower floors are relatively large.

Figs. 5.15 and 5.16 show the results of mean ductilities for the system designed by modal analysis using the Newmark inelastic acceleration response spectrum. The member moment capacities are tabulated in Table A-9 in the Appendix. For exterior columns, the mean maximum story ductilities are greater than those in Fig. 5.13. The ductilities for the interior columns match nicely with the design ductility. For exterior girders, the mean ductilities are much greater than the design ductility level in lower floors, as shown in Fig. 5.16. For interior girders, the ductilities are smaller than the design ductility at the upper seven floors. This is again due to the criterion insuring against undesirable formation of plastic hinges at girder midspans.

Note that the differences between the results based on the proposed inelastic acceleration response spectrum and that of the Newmark spectrum are less pronounced for the 10-story frame than for the 4-story frame. This can be related to the different natural periods of the frames. The fundamental natural period for the 4-story frame is 0.97 second, whereas for the 10-story frame is 2.32 seconds. As shown in Fig. 3.21, the discrepancy between the proposed inelastic acceleration response spectrum and that of Newmark is more pronounced for 0.97 second than for 2.32 seconds. Although the inelastic response of a frame is not necessarily dominated by the first mode, this is a clear indication of the dependency

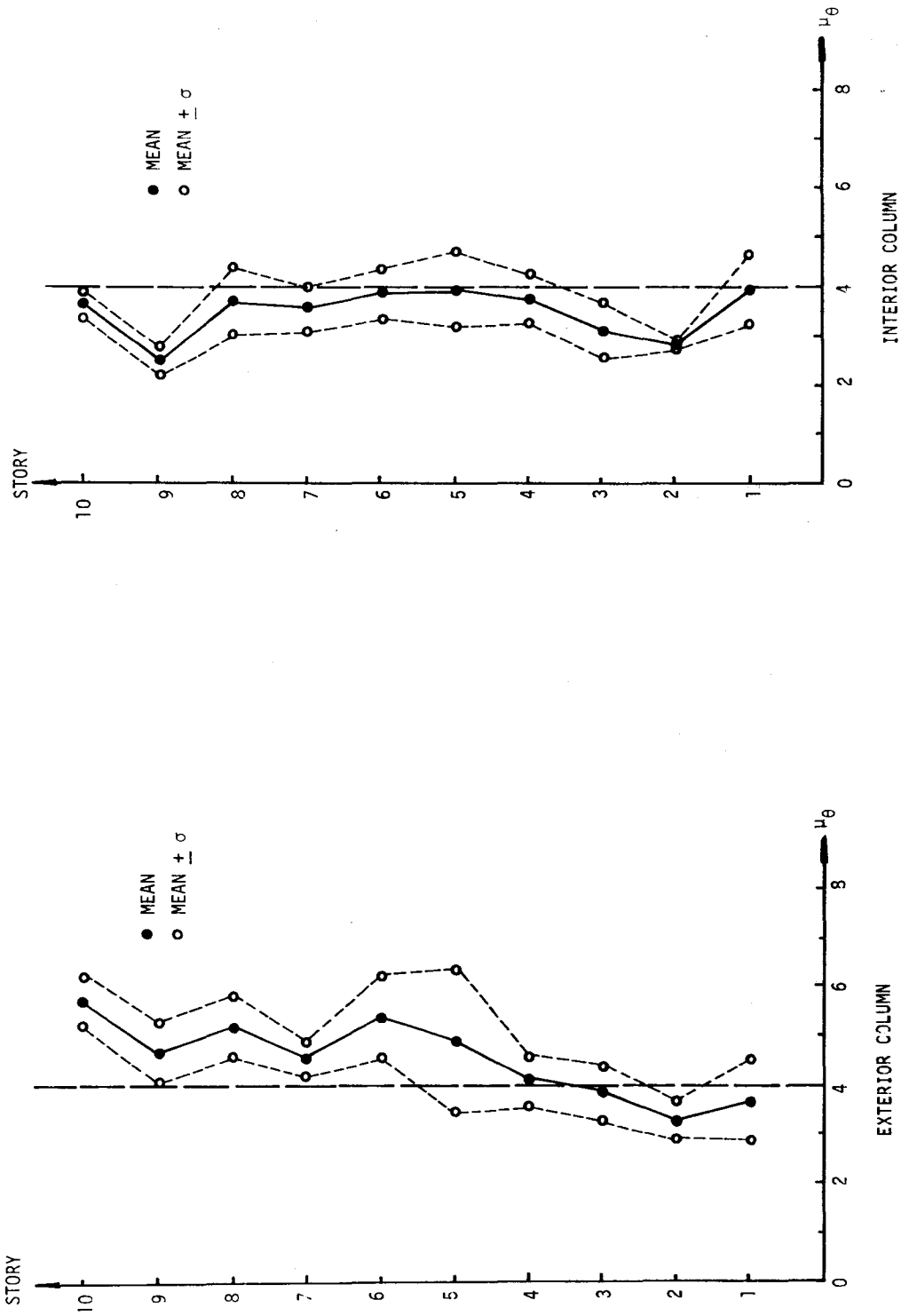


FIG. 5.13 - MAXIMUM COLUMN DUCTILITY FACTORS FOR 10-STORY BUILDING (PROPOSED SPECTRA,  $\zeta = 0.05$ )

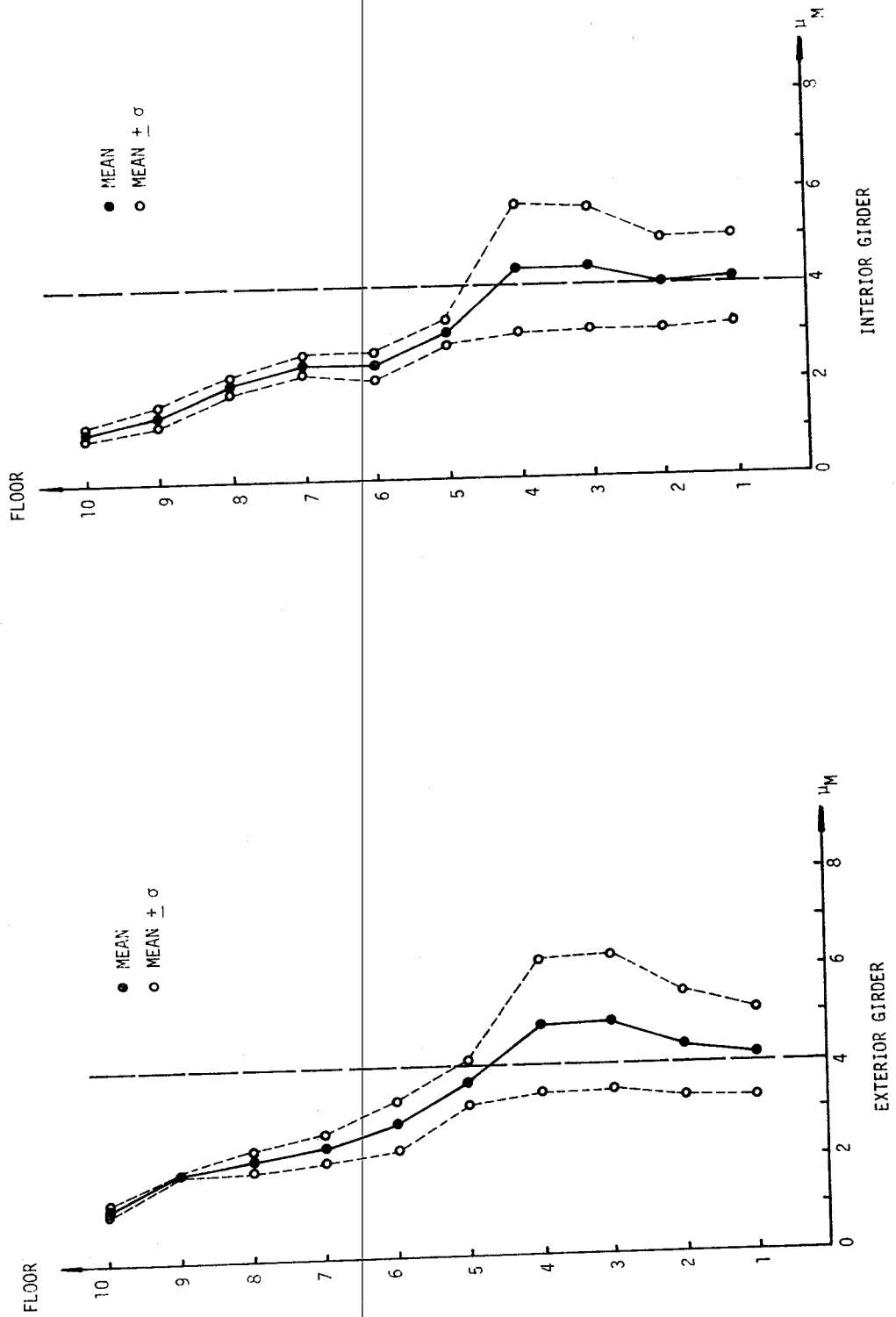


FIG. 5.14 - MAXIMUM GIRDER DUCTILITY FACTORS FOR 10-STORY BUILDING (PROPOSED SPECTRA,  $\zeta = 0.05$ )

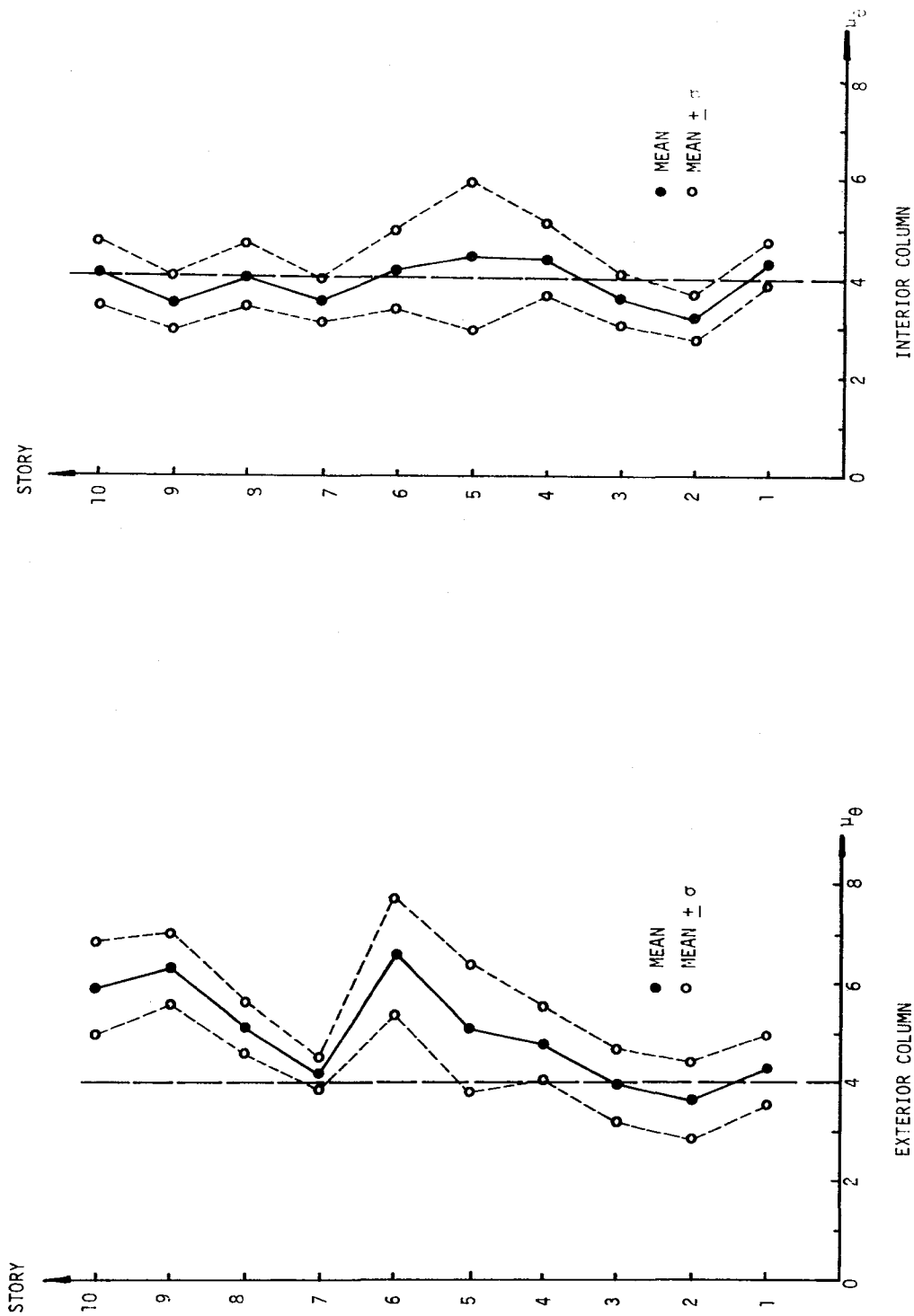


FIG. 5.15 - MAXIMUM COLUMN DUCTILITY FACTORS FOR 10-STORY BUILDING (NEWMARK,  $\zeta = 0.05$ .)

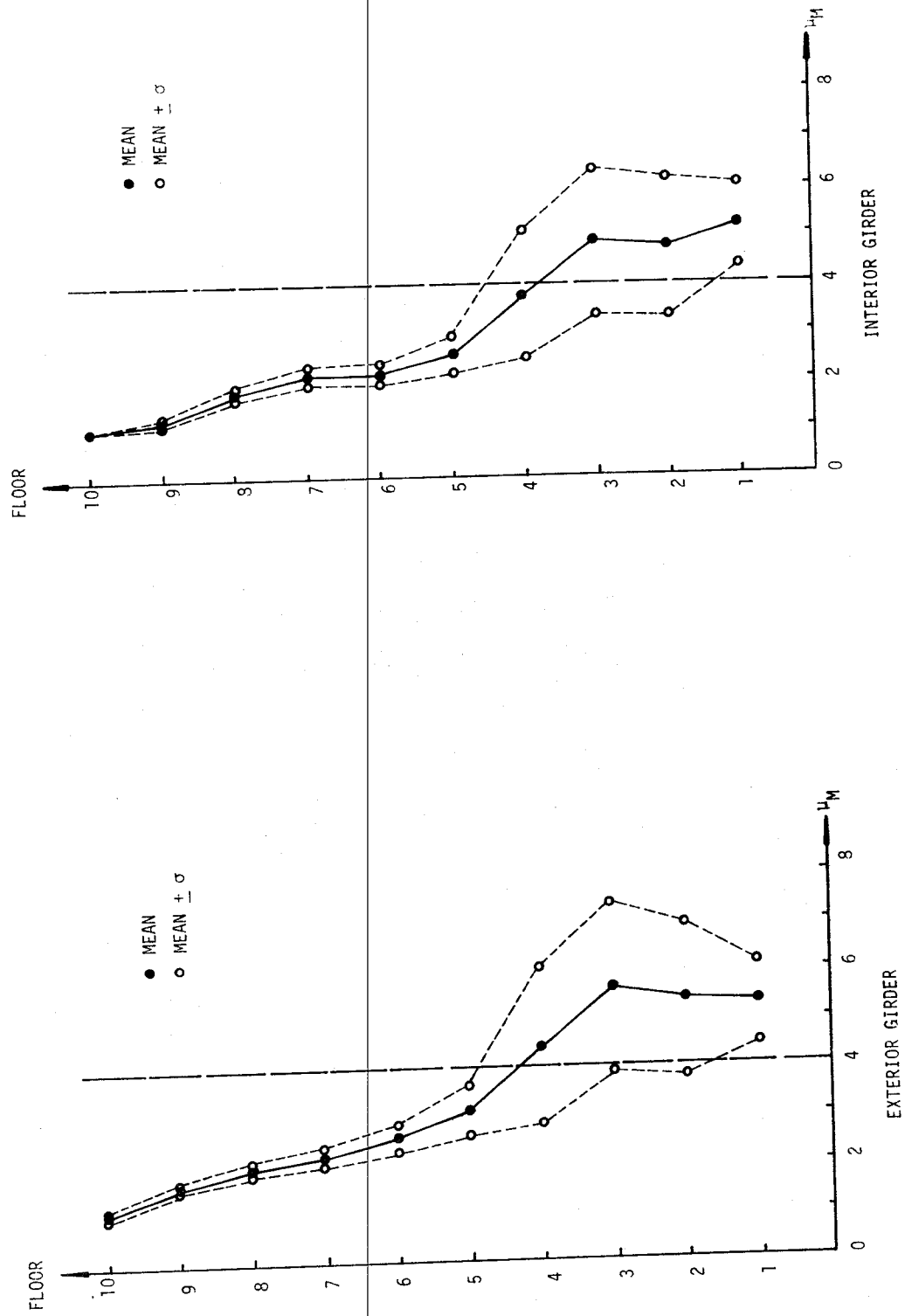


FIG. 5.16 - MAXIMUM GIRDER DUCTILITY FACTORS FOR 10-STORY BUILDING (NEWMARK,  $\zeta = 0.05$ )

of the inelastic response on the inelastic response spectrum.

#### 5.5.1.3 16-story Frame

The same set of artificial motions as for the 10-story frame was used for the 16-story frame. The resulting mean maximum story ductilities of the system with member strength determined by the proposed inelastic response spectrum are shown in Figs. 5.17 and 5.18. For the exterior columns, the mean maximum ductilities are less than the design level except for the top stories. The ductilities for interior columns are all smaller than the design ductility. This suggests the inelastic-response-spectrum-based modal analysis yields conservative interior column design. For exterior girders, the mean ductilities are quite compatible with the design ductility level as shown in Fig. 5.18. For interior girders, the ductilities are smaller than the design level except for the first floor. Since the moment capacities of the upper-seven-floor exterior girders and the upper-five-floor interior girders are controlled by the  $w\ell^2/8$  criterion, the corresponding mean story ductilities are all smaller than the design ductility.

The fundamental natural period of the frame is 2.94 seconds. From Fig. 3.21, the proposed inelastic acceleration response is only 17% greater than those of Newmark for  $T = 2.94$  seconds. Therefore, for economy, the expensive time history analysis for the system design based on the Newmark inelastic response spectrum was not performed.

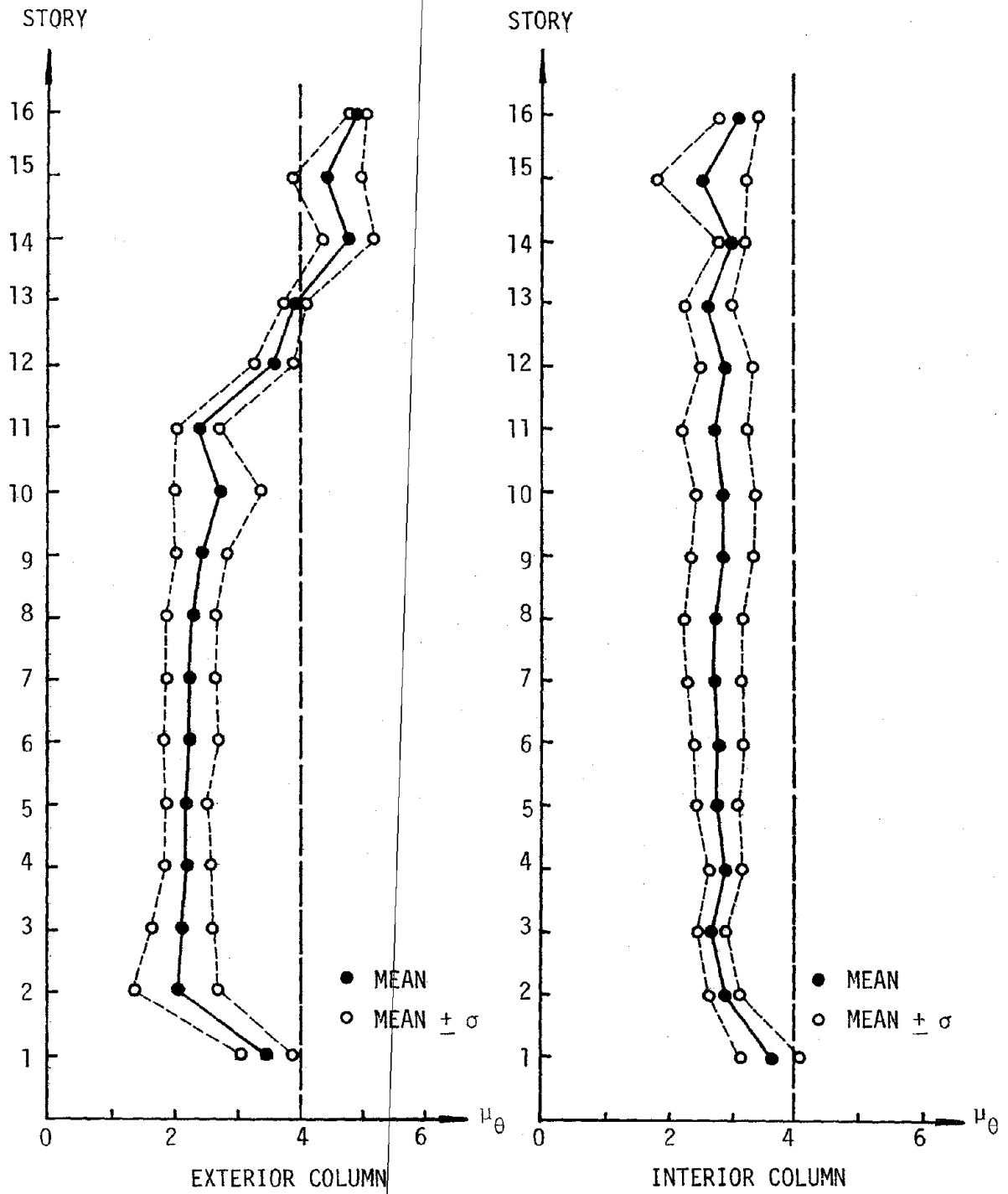


FIG. 5.17 - MAXIMUM COLUMN DUCTILITY FACTORS FOR 16-STORY BUILDING  
(PROPOSED SPECTRA,  $\zeta = 0.05$ )

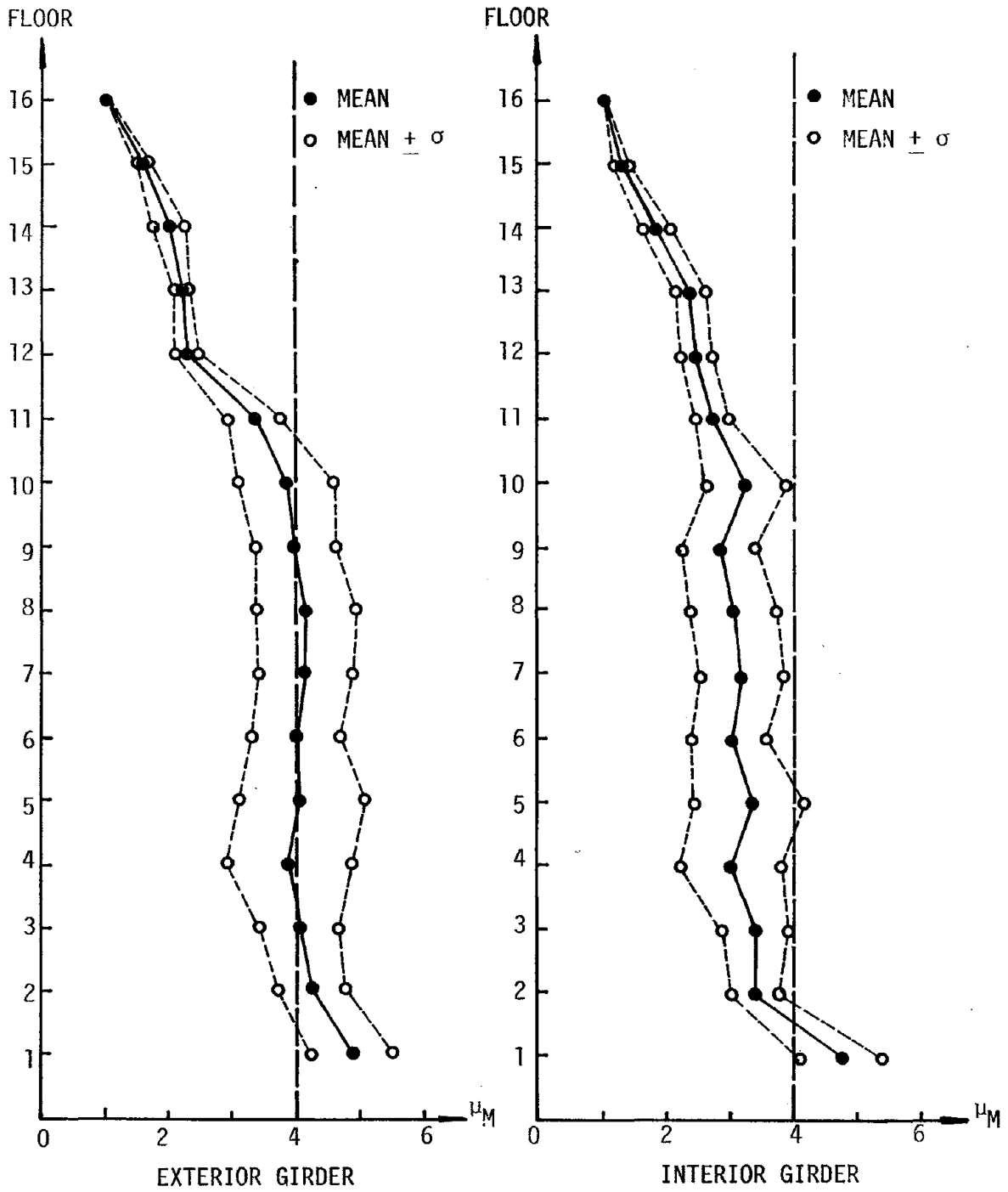


FIG. 5.18 - MAXIMUM GIRDER DUCTILITY FACTORS FOR 16-STORY BUILDING  
(PROPOSED SPECTRA,  $\zeta = 0.05$ )

#### 5.5.1.4 Summary

The above-mentioned results for the three steel moment-resisting frames analyzed in this study can be summarized as follows:

- 1) The system designed by modal analysis using the proposed inelastic acceleration response spectrum performs better in matching the design ductility level than the system corresponding to the Newmark response spectrum.
- 2) The mean maximum ductilities for interior columns are generally smaller than the design ductility, whereas the mean ductilities for exterior columns are greater than the design ductility at upper stories. This leads to the conclusion that the design of interior columns is generally conservative, whereas the design of exterior columns for the upper stories is unconservative.
- 3) When the girder moment capacity is controlled by the  $w\ell^2/8$  criterion to insure against the undesirable formation of midspan plastic hinge, the corresponding maximum local ductility is much smaller than the design ductility.
- 4) The mean maximum ductilities for exterior girders corresponding to the proposed inelastic acceleration response spectrum are quite compatible with the design ductility level. The ductilities for interior girders are generally a little smaller than the design ductility.
- 5) The standard deviations of the maximum local ductilities for girders are relatively larger than those for the columns.

#### 5.5.2 MAXIMUM STORY DISPLACEMENT

From time history analyses (FRIEDA,1), the information concerning maximum story relative displacement can be obtained. Based upon the inelastic response spectrum, the maximum story displacement can also be

directly predicted by modal analysis (APPLE PIE, 20). The results of maximum story displacements for both approaches are reported herein. Comparisons between the results corresponding to the new proposed inelastic response spectrum and those based on the Newmark response spectrum are also included.

#### 5.5.2.1 4-story Frame

As mentioned in Section 5.5.1.1, five artificial motions with  $S = 10$  seconds were used in the time history analyses for the 4-story frame. The resulting mean maximum relative displacements for the system designed according to the proposed inelastic acceleration response spectrum ( $\mu=4$ ,  $\zeta=0.05$ ) are shown in Fig. 5.19. The displacements for the system corresponding to the Newmark response spectrum are also plotted in the figure. Note that the differences between the two sets of maximum displacements are not significant. For example, the mean maximum displacement at the top for the system based on the proposed spectrum is 4.78 inches, whereas the mean displacement is 4.94 inches for the system corresponding to the Newmark spectrum.

By using the inelastic displacement response spectrum, the maximum story displacement can be directly calculated by modal analysis. The results from using the SRSS method of modal superposition are also plotted in Fig. 5.19. As expected, the maximum story displacements corresponding to the proposed inelastic displacement spectrum are greater than those from the Newmark response spectrum. For example, the maximum story displacements are 7.24 inches versus 6.09 inches at the top. Since the proposed inelastic response spectrum was derived from the smoothed inelastic displacement

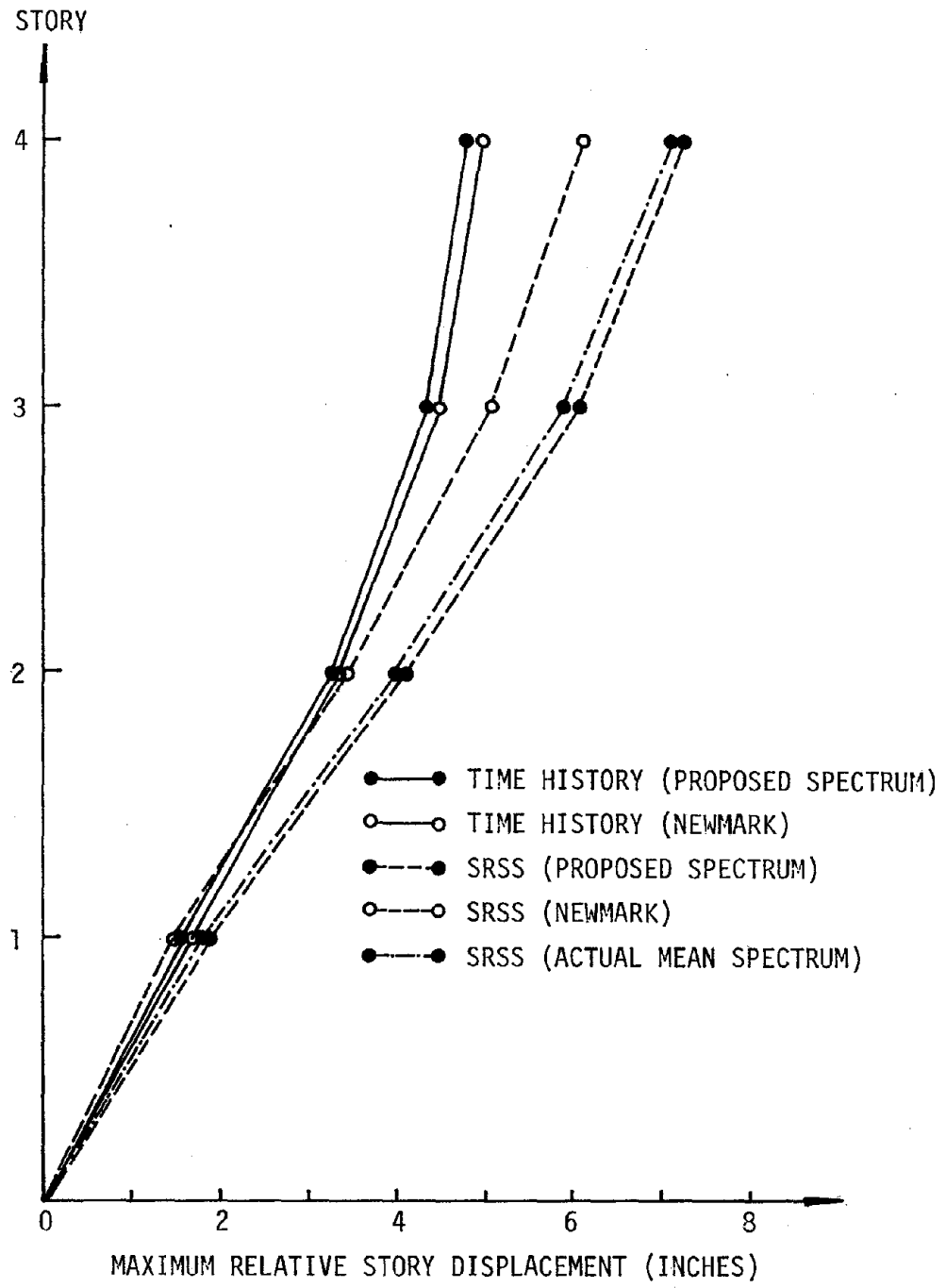


FIG. 5.19 - MAXIMUM RELATIVE STORY DISPLACEMENTS FOR 4-STORY BUILDING

response ratios, it is of interest to examine the maximum story displacements predicted by the original mean inelastic response ratios (Fig. 3.10). The results are not very different from those of the proposed spectrum. For example, the maximum top displacement is 7.12 inches.

The discussions presented herein are summarized in Section 5.5.2.4.

#### 5.5.2.2 10-story Frame

Five artificial motions with  $S = 20$  seconds were used for the time history analyses of the 10-story frame. Fig. 5.20 shows the resulting maximum story relative displacements predicted by all the different approaches. The general trends of the results are quite similar to those of the 4-story frame. For example, the mean maximum displacement at the top is 11.6 inches for the system corresponding to the proposed inelastic acceleration response spectrum, and it is 11.7 inches for the system based on the Newmark spectrum. The top displacement predicted by the SRSS-modal analysis using the proposed inelastic displacement response spectrum is 16.9 inches, and it is 15.7 inches for the Newmark spectrum. Based on the actual mean inelastic response ratio (Fig. 3.10), the top displacement predicted by SRSS modal analysis is 14.7 inches, which is much smaller than the one corresponding to the proposed inelastic displacement response spectrum. This reflects the conservatism introduced in proposing the smoothed inelastic displacement response spectrum.

#### 5.5.2.3 16-story Frame

The same set of artificial motions for the 10-story frame were used for 16-story frames. Fig. 5.21 shows the maximum story displacements

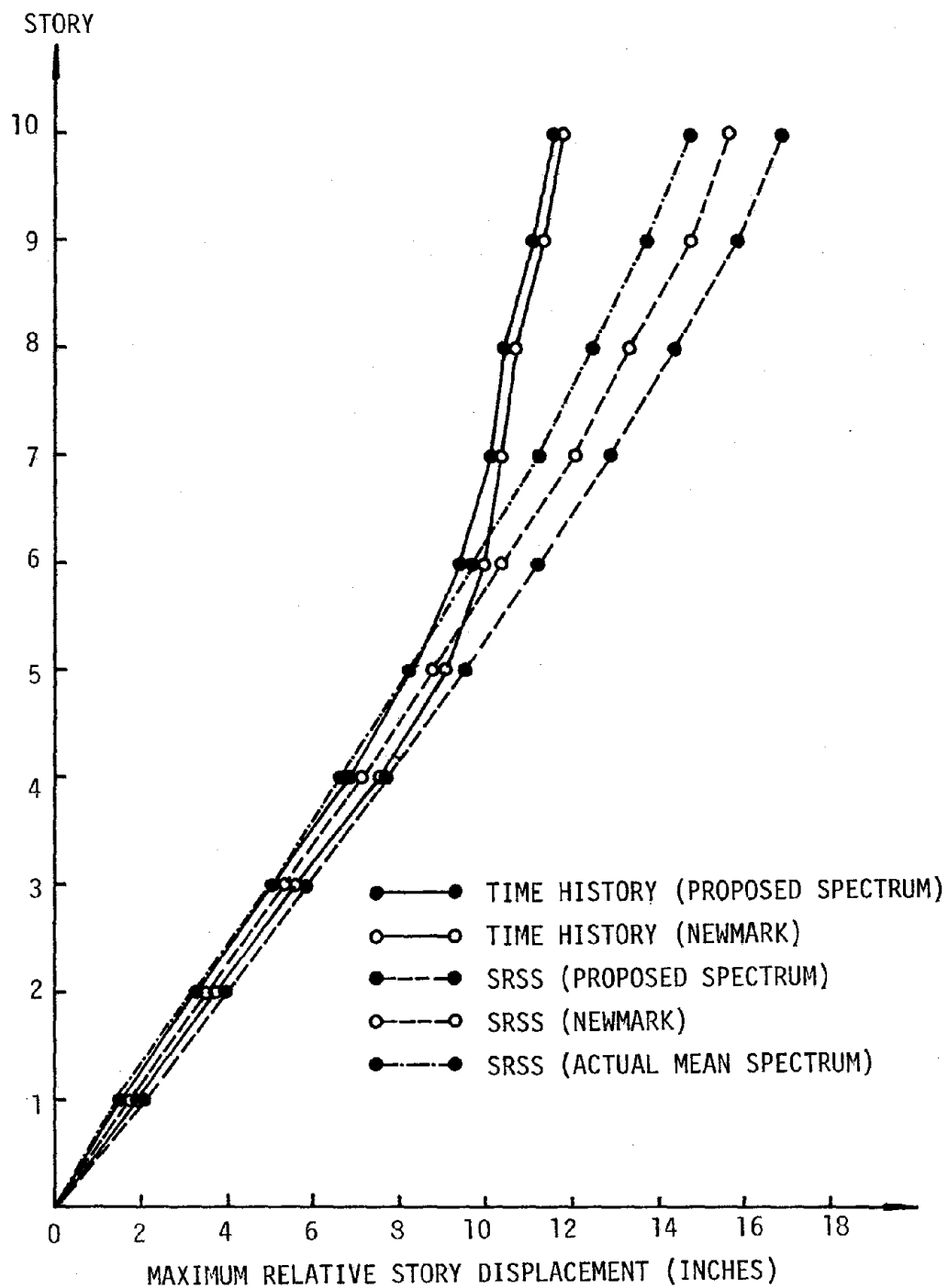


FIG. 5.20 - MAXIMUM RELATIVE STORY DISPLACEMENTS FOR  
10-STORY BUILDING

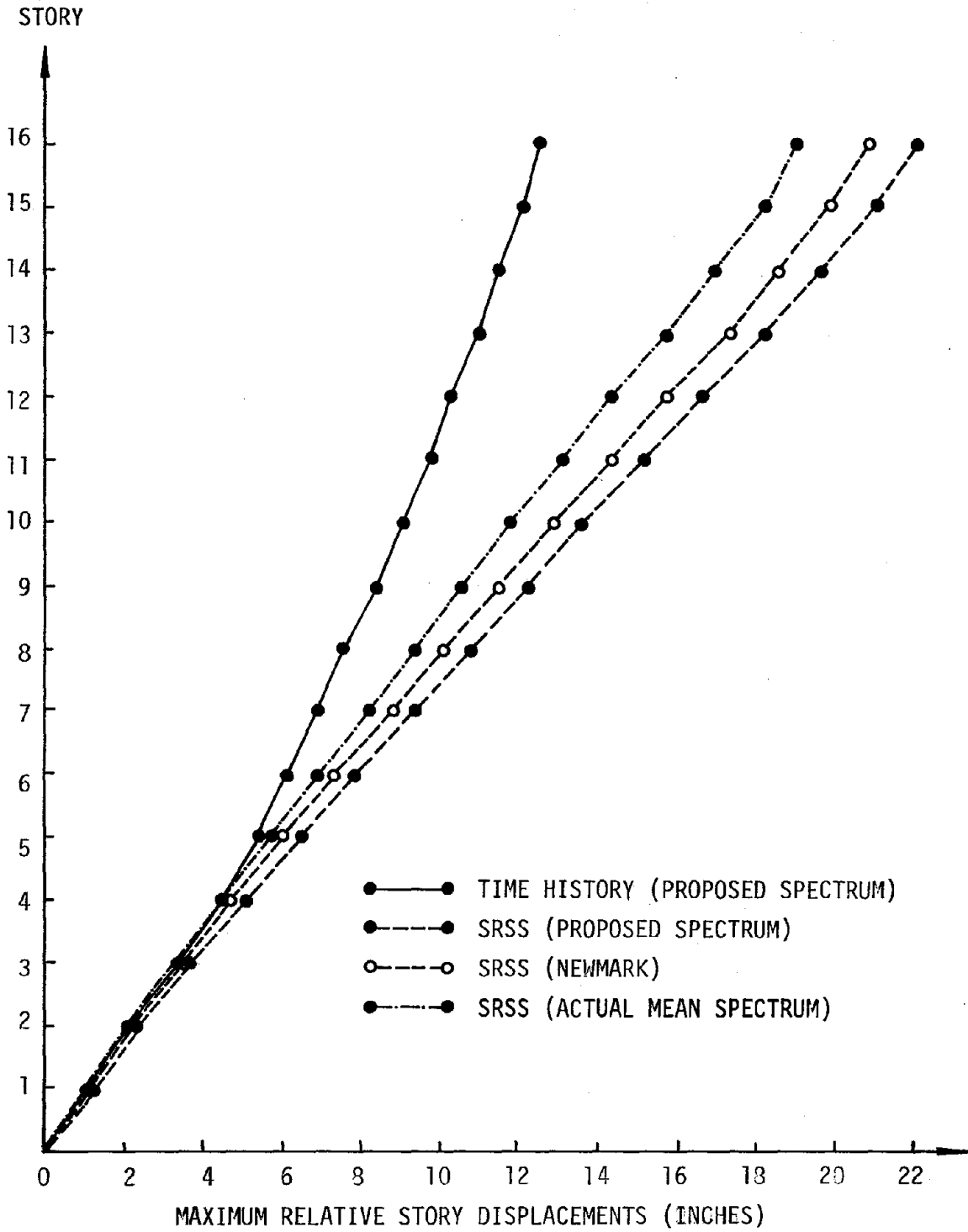


FIG. 5.21 - MAXIMUM RELATIVE STORY DISPLACEMENTS FOR 16-STORY BUILDING

resulting from different approaches, as mentioned earlier. Note that for economy, the expensive time history analysis of the system designed by the Newmark inelastic acceleration response spectrum was not performed. As shown in the figure, the general trends of the results are quite compatible with those of the 10-story frame. The mean maximum top story displacement based on the proposed inelastic acceleration response spectrum is 12.7 inches. The top displacement predicted by the SRSS-modal analysis using the proposed inelastic displacement spectrum is 22.3 inches, and it is 21.0 inches for the Newmark spectrum. From the actual mean inelastic displacement ratios, the predicted top story displacement is 19.3 inches, as shown in Fig. 5.21.

#### 5.5.2.4 Summary

The above-mentioned results of the maximum story displacement for steel frames can be summarized as follows:

- 1) The maximum story displacement of the system with member strength determined by modal analysis using the proposed inelastic acceleration response spectrum is smaller than those corresponding to the Newmark spectrum.
- 2) Comparing with the results of time history analysis, the maximum story displacement predicted by the SRSS-modal analysis using the inelastic displacement response spectrum is too conservative. The conservatism is much greater for the upper stories.
- 3) The conservatism introduced when proposing the smoothed inelastic displacement response spectrum in Section 3.6.1 is quite pronounced in higher natural period ranges for 5% damped system.
- 4) Since the negative contributions of the second mode for the maximum story displacement are considerable, this indicates the SRSS method

of modal superposition is not adequate for predicting the maximum displacement directly from the inelastic displacement response spectrum. Numerical addition of the responses of the first two modes appears to be a better prediction.

In comparison with the results summarized in Section 5.2.2, the above-mentioned conclusions are quite consistent with those of the simple shear beam model.

## 5.6 CONCLUSION

Haviland et al. (12) and Robinson (19) have all concluded that the inelastic frame design procedure based on modal analysis using the Newmark inelastic response spectrum is unconservative. They suggested the use of a "spectral strength factor" to adjust the member strength so as to properly control the inelastic behavior of frames. Robinson has also observed that the unconservatism of the inelastic seismic design procedure is considerably less for 2% damping than for the 5% damping system.

As concluded in Chapter 3, the widely accepted Newmark inelastic response spectra predict unconservative inelastic responses for 5% damped systems and conservative responses for 2% damped systems. This is quite consistent with what Haviland et al. and Robinson have argued concerning the inelastic frame responses. The new proposed inelastic response spectra as described in Section 3.6 have corrected the unconservatism or the conservatism associated with the Newmark spectra. Hence, the frame design procedure based on modal analysis using the proposed inelastic response spectrum yields better results in terms of the maximum local ductility distribution.

From the results presented in this chapter, the following conclusions can be reached:

- 1) The inelastic frame design procedure based upon modal analysis using the proposed inelastic acceleration response spectrum yields much better frame design than that corresponding to the Newmark inelastic spectrum.
- 2) The proposed inelastic-response-spectrum-based design procedure will result in conservative design for interior columns, and unconservative design for upper story exterior columns. The procedure will also yield competent design for exterior girders and conservative design for interior girders.
- 3) The SRSS modal analysis of using the inelastic displacement response spectrum will predict conservative maximum story displacements. The conservatism is quite pronounced at top stories.
- 4) Since the negative contributions of higher modes for story displacement are considerable, this indicates that the SRSS method of modal superposition is not adequate for predicting the maximum displacement directly from the inelastic displacement response spectrum.
- 5) As the conclusions mentioned for structural frames are quite consistent with those of the simple shear beam model, it can be concluded that the applicability of the inelastic frame design procedure using the modal analysis is not significantly related to the gravity load.

# CHAPTER 6

## CONCLUSIONS AND RECOMMENDATIONS

### 6.1 CONCLUSIONS

The objectives of the study were: i) to investigate the sources of variability of inelastic response spectra, i.e., strong ground motion duration, ductility level, and viscous damping ratio; and ii) to assess the validity of the inelastic frame design procedure based on modal analysis using inelastic response spectra. From the results presented in previous Chapters, the following conclusions were reached:

- 1) For a specified ductility level, the inelastic time history responses of maximum relative displacement and absolute acceleration for the elasto-plastic system are not significantly dependent on the strong ground motion duration. However, this conclusion is valid only when the duration-dependent strong ground motions are compatible with the same prescribed elastic response spectra.
- 2) The traditional ductility factor reveals only information about maximum inelastic structural response. The suggested "cumulative yielding ductility," on the other hand, indicates the effect of motion duration on the amount of energy dissipation in an inelastic system. Therefore, it is a pertinent and probably superior indicator of structural damage.

- 3) "Inelastic response ratios" are useful measures for investigating the variability of inelastic response spectra, especially when comparison with the Newmark inelastic response spectra is desired.
- 4) Newmark's procedure for predicting the inelastic response of a 5% damped elasto-plastic system is unconservative. It becomes more unconservative when the level of ductility increases. In 2% damped elasto-plastic systems, the Newmark approach predicts a conservative inelastic response. The conservatism decreases with increasing ductility factor.
- 5) In the longer natural period range, the maximum relative elasto-plastic displacement is smaller than the elastic displacement of the associated linear-elastic system. This suggests that the principle of energy conservation is not valid for higher natural period systems.
- 6) The inelastic responses of elasto-plastic systems subjected to real ground motions are quite compatible with those of the artificial motions. Hence, it appears that conclusions based on artificial motions can be applied to real strong ground motions.
- 7) Based upon the simulation studies, semi-empirical modifications for the random vibration model were suggested. The probabilistic prediction of inelastic response from the new random vibration model is quite consistent with those computed by the time history analysis.
- 8) The inelastic frame design procedure based on modal analysis using the new proposed inelastic "acceleration" response spectrum yields a better frame design than that based on the Newmark spectrum.
- 9) The proposed inelastic response spectrum frame design procedure will result in conservative design for interior columns and girders, and unconservative design for upper story exterior columns. The inelastic design procedure will also yield reliable design for exterior girders.

- 10) The maximum story displacement directly predicted by the SRSS modal analysis using the inelastic "displacement" response spectrum is conservative. The conservatism is quite significant for upper stories. This leads to the conclusion that the SRSS method of modal superposition is not adequate for predicting the maximum story displacement directly from the inelastic displacement response spectrum.

## 6.2 RECOMMENDATIONS FOR FURTHER RESEARCH

Further research is necessary for a better understanding of the applicability of the inelastic frame design procedure based on modal analysis using inelastic response spectra. The recommendations for this endeavor are outlined as follows:

- 1) Investigate further the dependence of inelastic response spectra on motion duration for a larger set of real strong ground motions.
- 2) Assess the potential of using "cumulative yielding ductility" to measure structural damage due to seismic action.
- 3) Extend the modified random vibration model of SDOF elasto-plastic systems to predict inelastic response of MDOF systems.
- 4) Study the adequacy of using either moment ductility or rotational ductility to measure inelastic response.
- 5) Incorporate the P- $\Delta$  effect and soil-structure interaction in the time history frame analysis.
- 6) Evaluate the validity of using the SRSS method of modal superposition in predicting maximum story displacement.
- 7) Determine the member strength by computing the actual ratio of plastic modulus  $Z$  to area  $A$  for each member, instead of assuming it equals 6.

- 8) Consider the possible buckling of the column in the determination of maximum column axial capacity. For example, together with the axial-flexural interaction formula, the following restraint should be met.

$$\frac{P}{P_{cr}} + \frac{C_m M}{\left(1 - \frac{P}{P_e}\right) M_y} \leq 1.0 \quad (\text{AISC 2.4-2})$$

where

$$P_{cr} = 1.7 A F_a$$

$$P_e = \frac{\pi^2 EA}{\left(K \ell_b / r_b\right)^2}$$

$C_m$  = coefficient depending on member end moments.

- 9) Apply the inelastic frame design procedure based on modal analysis and the use of inelastic response spectra to reinforced concrete structures.

## REFERENCES

1. Anagnostopoulos, S.A., "Non-linear Dynamic Response and Ductility Requirements of Building Structures Subjected to Earthquakes," M.I.T. Department of Civil Engineering Research Report R72-54, Order No. 349, September, 1972.
2. Anderson, J.C. and Bertero, V.V., "Seismic Behavior of Multistory Frames Designed by Different Philosophies," Earthquake Engineering Research Center Report No. EERC 69-11, University of California, Berkeley, California, October, 1969.
3. Applied Technology Council, An Evaluation of a Response Spectrum Approach to Seismic Design of Buildings, A Study Report for Center for Building Technology, Institute of Applied Technology, National Bureau of Standards, September, 1974.
4. Aziz, T.S., "Inelastic Dynamic Analysis of Building Frames," M.I.T. Department of Civil Engineering Research Report R76-37, Order No. 554, August, 1976.
5. Biggs, J.M., Introduction to Structural Dynamics, McGraw-Hill, New York, 1964.
6. C.I.T. Earthquake Engineering Research Laboratory, "Strong-Motion Earthquake Accelerograms--Digitized and Plotted Data," Vol. II, 1971.
7. Clough, R.W., "Inelastic Earthquake Response of Tall Buildings," Proceedings of the Third World Conference on Earthquake Engineering, Vol. II, New Zealand, 1965.
8. Crandall, S.H. and Mark, W.D., Random Vibration in Mechanical Systems, Academic Press, New York, 1973.
9. Drake, A.W., Fundamentals of Applied Probability Theory, McGraw-Hill, New York, 1967.
10. Gasparini, D.A. and Vanmarcke, E.H., "Simulated Earthquake Motion Compatible with Prescribed Response Spectra," M.I.T. Department of Civil Engineering Research Report R76-4, Order No. 527, January, 1976.
11. Gazetas, G., "Random Vibration Analysis of Inelastic Multi-Degree-of-Freedom Systems Subjected to Earthquake Ground Motions," M.I.T. Department of Civil Engineering Research Report R76-39, Order No. 556, August, 1976.
12. Haviland, R.W., Biggs, J.M., Anagnostopoulos, S.A., "Inelastic Response Spectrum Design Procedures for Steel Frames," M.I.T. Department of Civil Engineering Research Report R76-40, Order No. 557, September, 1976.

13. Karnopp, D. and Scharton, T.D., "Plastic Deformation in Random Vibration," Journal of the Acoustical Society of America, Vol. 39, No. 6, June, 1966.
14. Lai, S.P., "SIMQKE: A Program for Artificial Motion Generation, User's Manual and Documentation," Internal Study Report, M.I.T. Department of Civil Engineering, November, 1976.
15. Luyties, W.H., Anagnostopoulos, S.A., Biggs, J.M., "Studies on the Inelastic Dynamic Analysis and Design of Multistory Frames," M.I.T. Department of Civil Engineering Research Report R76-29, Order No. 548, July, 1976.
16. Newmark, N.M., Blume, J.A., and Kapur, K.K., "Design Response Spectra for Nuclear Power Plants," Journal of the Power Division, ASCE, November, 1973.
17. Newmark, N.M. and Hall, W.J., "Procedures and Criteria for Earthquake Resistant Design," Building Practices for Disaster Mitigation, Building Science Series 46, National Bureau of Standards, February 1973.
18. Piqué, J.R., "On the Use of Simple Models in Nonlinear Dynamic Analysis," M.I.T. Department of Civil Engineering Research Report R76-43, Order No. 559, September, 1976.
19. Robinson, J.H., "Inelastic Dynamic Design of Steel Frames to Resist Seismic Loads," M.I.T. Department of Civil Engineering Research Report R77-23, Order No. 574, July, 1977.
20. Roesset, J.M., Unpublished Users' Guide for the Computer Program APPLE PIE, M.I.T., Cambridge, Massachusetts.
21. Vanmarcke, E. H., "First Passage and Other Failure Criteria in Narrow-Band Random Vibration: A Discrete State Approach," M.I.T. Department of Civil Engineering Research Report R69-68, October, 1969.
22. Vanmarcke, E.H., Chapter 8 of Seismic Risk and Engineering Decisions, Lomnitz, C. and Rosenblueth, E., Editors, Elsevier Publishing Co., 1977.
23. Vanmarcke, E.H. and Lai, S.P., "Strong-Motion Duration of Earthquakes," M.I.T. Department of Civil Engineering Research Report R77-16, Order No. 569, July 1977.
24. Vanmarcke, E.H. and Veneziano, D., "Probabilistic Seismic Response of Simple Inelastic Systems," Proceedings of the 5th World Conference on Earthquake Engineering, Vol. II, Italy, 1973.

25. Veletsos, A.S., Newmark, N.M. and Chelapati, C.V., "Deformation Spectra for Elastic and Elastoplastic Systems Subjected to Ground Shock and Earthquake Motions," Proceedings of the Third World Conference on Earthquake Engineering, Vol. II, New Zealand, 1965.
26. Yanev, P.I., "Response of Simple Inelastic Systems to Random Excitation," S.M. Thesis, M.I.T., June, 1970.



# APPENDIX

TABLE A-1 MODAL PROPERTIES OF SIMPLE SHEAR BEAM MODEL

STORY	1ST	2ND	3RD	4TH
	MODAL SHAPE T=1.922	MODAL SHAPE T=0.834	MODAL SHAPE T=0.531	MODAL SHAPE T=0.388
10	1.090	1.251	0.931	-0.496
9	0.941	0.343	-0.738	1.171
8	0.800	-0.239	-0.896	-0.008
7	0.669	-0.567	-0.453	-0.785
6	0.548	-0.708	0.086	-0.693
5	0.435	-0.716	0.486	-0.143
4	0.331	-0.633	0.671	0.397
3	0.235	-0.496	0.653	0.665
2	0.147	-0.329	0.488	0.614
1	0.067	-0.154	0.242	0.334

TABLE A-2 MODAL PROPERTIES OF 4-STORY FRAME

STORY	1ST	2ND	3RD	4TH
	MODAL SHAPE T=0.967	MODAL SHAPE T=0.32	MODAL SHAPE T=0.186	MODAL SHAPE T=0.134
4	1.432	-1.213	-0.826	-0.297
3	1.201	0.249	1.397	0.883
2	0.805	1.337	-0.084	-1.340
1	0.350	0.968	-1.266	1.255

TABLE A-3 MODAL PROPERTIES OF 10-STORY FRAME

STORY	1ST	2ND	3RD	4TH
	MODAL SHAPE T = 2.322	MODAL SHAPE T=0.835	MODAL SHAPE T=0.496	MODAL SHAPE T=0.339
10	0.939	-0.993	0.892	-0.744
9	0.891	-0.653	0.121	0.482
8	0.809	-0.135	-0.696	0.880
7	0.728	0.251	-0.858	0.199
6	0.626	0.579	-0.544	-0.669
5	0.524	0.752	-0.025	-0.799
4	0.411	0.789	0.496	-0.244
3	0.303	0.701	0.760	0.436
2	0.196	0.511	0.714	0.764
1	0.095	0.265	0.419	0.556

TABLE A-4 MODAL PROPERTIES OF 16-STORY FRAME

STORY	1ST	2ND	3RD	4TH
	MODAL SHAPE T=2.935	MODAL SHAPE T=1.112	MODAL SHAPE T=0.659	MODAL SHAPE T=0.469
16	-0.812	-0.868	-0.836	0.753
15	-0.780	-0.688	-0.406	0.033
14	-0.731	-0.401	0.189	-0.669
13	-0.682	-0.151	0.532	-0.734
12	-0.621	0.114	0.696	-0.359
11	-0.563	0.313	0.649	0.105
10	-0.502	0.471	0.446	0.496
9	-0.444	0.571	0.182	0.646
8	-0.387	0.619	-0.095	0.546
7	-0.330	0.624	-0.339	0.268
6	-0.273	0.589	-0.516	-0.084
5	-0.219	0.522	-0.597	-0.384
4	-0.167	0.430	-0.585	-0.562
3	-0.119	0.326	-0.494	-0.577
2	-0.074	0.212	-0.345	-0.452
1	-0.036	0.105	-0.178	-0.247

TABLE A-5 MOMENT CAPACITIES FOR 4-STORY FRAME  
(PROPOSED SPECTRA)

STORY	COLUMN $M_p$ 'S (K-in)		GIRDER $M_p$ 'S (K-in)	
	EXTERIOR	INTERIOR	EXTERIOR	INTERIOR
1	1100	1524	965	899
2	794	1333	960*	839
3	597	964	960*	602
4	419	582	960*	540*

NOTE: \* Controlled by  $w\ell^2/8$

TABLE A-6 MOMENT CAPACITIES FOR 10-STORY FRAME  
(PROPOSED SPECTRA)

STORY	COLUMN $M_p$ 'S (K-in)		GIRDER $M_p$ 'S (K-in)	
	EXTERIOR	INTERIOR	EXTERIOR	INTERIOR
1	2092	3216	1034	1002
2	1674	2778	1028	1017
3	1518	2465	984	974
4	1326	2230	960*	960*
5	1176	1971	960*	960*
6	1015	1713	960*	960*
7	795	1513	960*	960*
8	619	1249	960*	960*
9	570	865	960*	960*
10	408	547	960*	960*

NOTE: \* Controlled by  $w\ell^2/8$

TABLE A-7 MOMENT CAPACITIES FOR 16-STORY FRAME  
(PROPOSED SPECTRA)

STORY	COLUMN $M_p$ 'S (K-in)		GIRDER $M_p$ 'S (K-in)	
	EXTERIOR	INTERIOR	INTERIOR	INTERIOR
1	3289	4669	1552	1486
2	2778	4239	1560	1544
3	2613	3939	1407	1419
4	2398	3681	1353	1400
5	2207	3423	1227	1307
6	2019	3199	1214	1295
7	1877	2941	1124	1199
8	1693	2714	1076	1174
9	1509	2475	1042	1156
10	1338	2236	960*	1010
11	1183	1999	960*	999
12	1024	1747	960*	960*
13	814	1523	960*	960*
14	636	1275	960*	960*
15	590	886	960*	960*
16	432	547	960*	960*

NOTE: \* Controlled by  $wl^2/2$

TABLE A.8 MOMENT CAPACITIES FOR 4-STORY FRAME (NEWMARK SPECTRA)

STORY	COLUMN $M_p$ 'S (K-in)		GIRDER $M_p$ 'S (K-in)	
	EXTERIOR	INTERIOR	EXTERIOR	INTERIOR
1	909	1304	960*	666
2	661	1121	960*	623
3	488	801	960*	540*
4	415	467	960*	540*

Note: \*Controlled by  $w\ell^2/8$

TABLE A.9 MOMENT CAPACITIES FOR 10-STORY FRAME (NEWMARK SPECTRA)

STORY	COLUMN $M_p$ 'S (K-in)		GIRDER $M_p$ 'S (K-in)	
	EXTERIOR	INTERIOR	EXTERIOR	INTERIOR
1	1967	3051	1034	1002
2	1594	2665	1028	1017
3	1451	2383	984	974
4	1262	2152	960*	960*
5	1108	1889	960*	960*
6	945	1627	960*	960*
7	733	1413	960*	960*
8	587	1139	960*	960*
9	484	760	960*	960*
10	405	455	960*	960*

Note: \* Controlled by  $w\ell^2/8$

